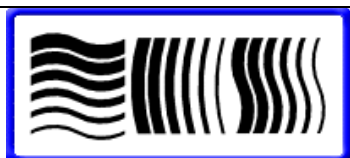


# **Monte Carlo Treatment Planning**

## **An Introduction**

**NEDERLANDSE COMMISSIE VOOR STRALINGSDOSIMETRIE**

**Report 16 of the Netherlands Commission on Radiation Dosimetry**



**Netherlands Commission on Radiation Dosimetry**  
**Subcommission Monte Carlo Treatment Planning**  
**June 2006**

# **Monte Carlo Treatment Planning**

## **An Introduction**

**NEDERLANDSE COMMISSIE VOOR STRALINGSDOSIMETRIE**

**Report 16 of the Netherlands Commission on Radiation Dosimetry**

### **Authors:**

**N. Reynaert**

**S. van der Marck**

**D. Schaart**

**W. van der Zee**

**M. Tomsej**

**C. van Vliet- Vroegindeweyj**

**J. Jansen**

**M. Coghe**

**C. De Wagter**

**B. Heijmen**

**Netherlands Commission on Radiation Dosimetry**

**Subcommission Monte Carlo Treatment Planning**

**June 2006**

## Preface

The Nederlandse Commissie voor Stralingsdosimetrie (NCS, Netherlands Commission on Radiation Dosimetry) was officially established on 3 September 1982 with the aim of promoting the appropriate use of dosimetry of ionizing radiation both for scientific research and practical applications. The NCS is chaired by a board of scientists, installed upon the suggestion of the supporting societies, including the Nederlandse Vereniging voor Radiotherapie en Oncologie (Netherlands Society for Radiotherapy and Oncology), the Nederlandse Vereniging voor Nucleaire Geneeskunde (Netherlands Society for Nuclear Medicine), the Nederlandse Vereniging voor Klinische Fysica (Netherlands Society for Clinical Physics), the Nederlandse Vereniging voor Radiobiologie (Netherlands Society for Radiobiology), the Nederlandse Vereniging voor Stralingshygiëne (Netherlands Society for Radiological Protection), the Nederlandse Vereniging voor Medische Beeldvorming en Radiotherapie (Netherlands Society for Medical Imaging and Radiotherapy), the Nederlandse Vereniging voor Radiologie (Netherlands Society for Radiology) and the Belgische Vereniging voor Ziekenhuisfysici/Société Belge des Physiciens des Hôpitaux (Belgian Hospital Physicists Association).

To pursue its aims, the NCS accomplishes the following tasks: participation in dosimetry standardisation and promotion of dosimetry intercomparisons, drafting of dosimetry protocols, collection and evaluation of physical data related to dosimetry. Furthermore the commission shall maintain or establish links with national and international organisations concerned with ionizing radiation and promulgate information on new developments in the field of radiation dosimetry.

Current members of the board of the NCS:

S. Vynckier, chairman

B.J.M. Heijmen, vice-chairman

E. van Dijk, secretary

J. Zoetelief, treasurer

A.J.J. Bos

A.A. Lammertsma

J.M. Schut

F.W. Wittkämper

D. Zweers

## Monte Carlo Treatment Planning: An Introduction

This report was prepared by a subcommittee of the Netherlands Commission on Radiation Dosimetry (NCS), consisting of Belgian and Dutch scientists.

Members of the subcommittee:

N. Reynaert, chairman  
S. van der Marck  
D. Schaart  
W. van der Zee  
M. Tomsej  
C. Van Vliet-Vroegindewey  
J. Jansen  
M. Coghe  
C. De Wagter  
B. Heijmen

Monte Carlo Treatment Planning: An Introduction

Report 16 of the Netherlands Commission on Radiation Dosimetry (NCS)

June 2006

NCS, Delft, The Netherlands

ISBN 90-78522-01-1

For more information on this and other NCS Reports, see <http://www.ncs-dos.org>

## User guide

This report presents an overview of the literature for physicists in radiotherapy departments who intend to buy/use/customise a Monte Carlo treatment planning system for electron and/or photon therapy. The report focuses on commissioning, selection of treatments requiring Monte Carlo, variance reduction techniques, accelerator head modelling, patient modelling (conversion of CT Hounsfield units), hardware requirements and the required knowledge to operate an MCTP system. In addition an overview of existing Monte Carlo dose engines and MCTP systems is given.

The report consists of three main parts.

The first part provides insight in the Monte Carlo method for dose calculations. An overview of general purpose Monte Carlo codes, used in the field of electron and photon dosimetry, is given. An extensive description of modelling of electron and photon transport and the usage of cross sections is presented.

The second part deals with MCTP specific topics such as CT conversion, linac head modelling, scoring, variance reduction, Monte Carlo based treatment planning (optimisation), and 4D planning.

The third and final part focuses on practical aspects. It provides an overview of Monte Carlo dose engines used for Monte Carlo treatment planning, an overview of commercial MCTP systems, and guidelines on benchmarking of these systems (focussing on MC specific benchmarks).

# Contents

PREFACE.....	I
USER GUIDE.....	III
CONTENTS.....	IV
SUMMARY .....	1
ABBREVIATIONS .....	3
1 INTRODUCTION.....	5
PART I: INTRODUCTION TO MONTE CARLO .....	6
2 MONTE CARLO FOR SOLVING NUMERICAL PROBLEMS .....	7
2.1 COMPARISON WITH ANALYTICAL AND NUMERICAL APPROACHES .....	7
2.2 MONTE CARLO DOSE CALCULATIONS.....	7
2.3 EXAMPLE: AN 8 MEV ELECTRON HITTING THE LINAC TARGET.....	8
3 BASIC ELEMENTS OF A MONTE CARLO CODE FOR DOSE CALCULATIONS	11
3.1 PHYSICS MODELS .....	11
3.2 INTERACTION DATA TABLES.....	11
3.3 RANDOM NUMBER GENERATOR .....	12
3.4 GEOMETRY .....	12
3.5 MATERIAL COMPOSITION.....	12
3.6 SOURCE DEFINITION.....	12
3.7 SCORING .....	13
3.8 VARIANCE REDUCTION AND APPROXIMATIONS .....	13
4 A BRIEF HISTORY .....	14
4.1 GENERAL PURPOSE CODES .....	15
5 GENERAL PURPOSE MONTE CARLO CODES IN RADIOTHERAPY.....	17
5.1 EGS.....	17
5.2 MCNP .....	19
5.3 PENELOPE.....	20
5.4 GEANT .....	21
6 RATIONALE FOR MONTE CARLO TREATMENT PLANNING.....	23
6.1 REQUIREMENTS ON UNCERTAINTY IN TREATMENT PLANNING.....	23
6.2 WHY MONTE CARLO TREATMENT PLANNING .....	24
6.3 PHANTOM EXPERIMENTS.....	25
6.4 COMPARISONS FOR CLINICAL CASES.....	28
6.5 CONCLUSIONS.....	38

PART II: FUNDAMENTALS OF MONTE CARLO .....	40
7      MODELLING OF PARTICLE TRANSPORT .....	41
7.1    PHOTON TRANSPORT .....	41
7.2    ELECTRON TRANSPORT .....	43
7.3    INTERACTION DATA TABLES .....	48
8      GEOMETRY AND MATERIAL SPECIFICATION .....	59
8.1    VOLUMES .....	59
8.2    VOXELISED PHANTOMS .....	59
8.3    CONVERSION OF CT NUMBERS INTO TISSUE PARAMETERS .....	59
9      ACCELERATOR MODELLING .....	66
9.1    GENERAL ASPECTS .....	66
9.2    MODELLING OF THE LINAC HEAD .....	67
9.3    VIRTUAL SOURCE MODEL .....	68
9.4    BEAM MODIFIERS .....	71
10     DOSE SCORING .....	75
10.1   DOSE DETERMINATION .....	75
10.2   SCORING GRIDS .....	76
10.3   SPATIAL RESOLUTION .....	77
10.4   CONVERSION OF MONTE CARLO RESULTS TO DOSE TO WATER .....	78
11     VARIANCE REDUCTION TECHNIQUES AND APPROXIMATIONS .....	80
11.1   INTRODUCTION .....	80
11.2   VARIANCE OF A MONTE CARLO CALCULATION .....	81
11.3   VARIANCE REDUCTION TECHNIQUES .....	81
11.4   RISKS OF VARIANCE REDUCTION .....	89
11.5   DENOISING .....	91
12     MONTE CARLO TREATMENT PLANNING .....	96
13     4D MONTE CARLO DOSE CALCULATIONS .....	101
 PART III: MONTE CARLO TREATMENT PLANNING IN PRACTICE .....	106
14     MONTE CARLO DOSE CALCULATION ENGINES FOR TREATMENT PLANNING .....	107
14.1   PIONEERING WORK .....	107
14.2   DPM .....	109
14.3   MCDOSE/ MCSIM .....	110
14.4   VMC, XVMC, VMC++ .....	110

14.5	PEREGRINE.....	112
14.6	MACRO MONTE CARLO (MMC).....	113
14.7	DOSE ENGINES SERVING AS COMMISSIONING TOOL .....	114
15	AVAILABLE COMMERCIAL MCTP SYSTEMS.....	116
16	MONTE CARLO SPECIFIC ISSUES OF COMMISSIONING .....	118
16.1	INTRODUCTION.....	118
16.2	PARTICLE SOURCE AND BEAM MODIFIERS .....	119
16.3	SEGMENTATION .....	120
16.4	NORMALIZATION / MU DETERMINATION .....	120
16.5	VARIANCE REDUCTION.....	121
16.6	LITERATURE DATA ON MCTP VERIFICATION .....	121
16.7	CONCLUSION .....	126
17	RECOMMENDATIONS .....	127
17.1	COMPARISON OF DIFFERENT DOSE ENGINES .....	127
17.2	COMMISSIONING .....	128
17.3	CT CONVERSION .....	129
17.4	CONVERSION OF DOSE TO MEDIUM TO DOSE TO WATER .....	129
17.5	VARIANCE REDUCTION TECHNIQUES AND APPROXIMATIONS .....	129
17.6	DENOISING.....	130
18	CONCLUSION .....	131
	REFERENCES.....	133
	APPENDICES .....	159
	APPENDIX A. AN EXAMPLE TO ILLUSTRATE DIFFERENCES BETWEEN THE MONTE CARLO TECHNIQUE AND ANALYTICAL AND NUMERICAL APPROACHES.....	160
A.1	ANALYTICAL TECHNIQUE .....	160
A.2	NUMERICAL TECHNIQUE .....	161
A.3	MONTE CARLO TECHNIQUE .....	162
A.4	SUMMARY.....	164
	APPENDIX B: RANDOM NUMBERS IN MONTE CARLO .....	165
B.1	RANDOM NUMBERS IN COMPUTERS .....	165
B.2	RANDOM NUMBER GENERATORS .....	166



## Summary

The accuracy of dose calculation engines used for treatment planning in radiotherapy has increased steadily, ranging from calculations based on measurements, to pencil beam algorithms and superposition/convolution algorithms. Currently, Monte Carlo dose calculation engines are implemented in commercial treatment planning software as it is believed that the Monte Carlo method can provide an accuracy within 2-3 %. It is important that clinical physicists have insight in these systems, when introducing them into the clinic. This report tackles this acute problem by providing extensive information on:

- general purpose Monte Carlo codes for photon and electron dosimetry applications
- modelling of particle transport
- cross sections
- MCTP (Monte Carlo Treatment Planning) specific issues such as linac modelling, CT conversion, variance reduction techniques, scoring grids
- Recent developments such as 4D applications and MCTP optimisation

An important question is whether the added value of MCTP is clinically relevant. To answer this question an extensive overview of the literature is provided. The main conclusion is that the MC method has important added value when compared to pencil beam algorithms. More information is needed when comparing MC to superposition/convolution algorithms, although the first experiments (comparing accurate Monte Carlo dose calculation engines to superposition/convolution algorithms) demonstrate that the MC method will become very important in clinical treatment planning.

As the Monte Carlo method is, by its nature, very time consuming, a number of approximations have been included in commercial Monte Carlo dose calculation engines for treatment planning. This leads to a reduction in calculation time of several

orders of magnitude. The impact on the dosimetrical accuracy however is not well known yet. This report provides an overview of existing Monte Carlo dose calculation engines, focussing on applied approximations. An overview of commercial MCTP systems that are already available or are currently being developed is given. As benchmarking remains as important as for any other treatment planning system, a paragraph is devoted to quality control. Commercial MCTP systems can be benchmarked by measurements but also by comparison with accurate Monte Carlo dose calculation engines containing only a few approximations.

## Abbreviations

3D	Three-Dimensional
4D	Four-Dimensional
AAPM	American Association of Physicists in Medicine
ASCII	American Standard Code for Information Interchange
BEAM	an EGS4/PRESTA or EGSnrc/PRESTAll Monte Carlo user code
CERN	European Organization for Nuclear Research
CSDA	Continuous Slowing Down Approximation
CPU	Central Processing Unit
CT	Computed Tomography
CTV	Clinical Target Volume
DOSXYZ	an EGS4/PRESTA Monte Carlo user code
DPM	Dose Planning Method (MC algorithm for photons and electrons)
DVH	Dose-Volume Histogram
EGS	Electron Gamma Shower (a Monte Carlo code)
ENIAC	Electronic Numerical Integrator And Computer
EPID	Electronic Portal Imaging Device
EPL	Equivalent Path Length
ESTRO	European Society for Therapeutic Radiology and Oncology
ETRAN	Electron TRANsport (a Monte Carlo code)
FORTRAN	FORmula TRANslation (programming language)
FWHM	Full Width at Half Maximum
GEANT	GEometry ANd Tracking (a Monte Carlo code)
ICRU	International Commission on Radiation Units and Measurements
IMRT	Intensity-Modulated Radiation Therapy
ITS	Integrated Tiger Series (a Monte Carlo code package)
KEK	National Laboratory for High Energy Physics (Japan)
LANL	Los Alamos National Laboratory
MC	Monte Carlo
MCDOSE	an EGS4/PRESTA Monte Carlo user code
MCNP3	Monte Carlo Neutron Photon (a Monte Carlo code)
MCNP4	Monte Carlo N-Particle (a Monte Carlo code)
MCTP	Monte Carlo Treatment Planning
MLC	Multi-Leaf Collimator
MMC	Macro Monte Carlo (MC algorithm for electrons)
MORTRAN	Fortran pre-processor (used for EGS)
MRI	Magnetic Resonance Imaging
MU	Monitor Unit
NIST	National Institute of Standards and Technology
NCS	Netherlands Commission on Radiation Dosimetry
NRC	National Research Council of Canada
NTCP	Normal Tissue Complication Probability
PB	Pencil Beam
PC	Personal Computer
PENELOPE	PENetration and Energy LOss of Positron and Electrons (MC code)

PET	Positron Emission Tomography
PRESTA	Parameter Reduced Electron Stepping Algorithm
PTV	Planning Target Volume
RBE	RadioBiological Effectiveness
QA	Quality Assurance
SLAC	Stanford Linear Accelerator Center
SPECT	Single Photon Emission Computed Tomography
TPS	Treatment Planning System
TRUS	TransRectal UltraSound
TCP	Tumor Control Probability
VISED	Visual Editor (graphical interface for MCNP)
VMC	Voxel Monte Carlo (MC algorithm for electrons)
VMC++	MC algorithm based on VMC and XVMC
XVMC	MC algorithm for photons based on VMC

# 1 Introduction

In the past decades, the sophistication of dose calculation models implemented in clinical radiotherapy treatment planning systems has gradually improved, together with available computing power in hospitals. This evolution, going from rather simple scatter- and inhomogeneity corrections to pencil beams and superposition/convolution models has resulted in continuous improvements in the accuracy of predicted patient doses. In superposition/convolution models, pre-determined Monte Carlo results are used. Full Monte Carlo dose calculations would therefore seem the next logical step.

For many years it has been realised that full Monte Carlo simulations of the radiotherapy dose delivery process should further improve calculation accuracy. Due to limitations in computing power, however, this was never a realistic option in a clinical setting. Recently, vendors of clinical treatment planning systems have nevertheless started to offer Monte Carlo dose calculations. However, available computing power may still not allow for full Monte Carlo simulations in clinical practice. Approximations and simplifications to speed up the calculations may therefore be necessary, possibly (partially) jeopardising the advantages of full Monte Carlo dose calculations.

The aim of this NCS report is to provide potential users of a clinical treatment planning system with an introduction in the Monte Carlo technique. Apart from providing an explanation of fundamental and practical aspects specific to Monte Carlo treatment planning, recommendations (although limited) for potential users and vendors are included. This report only covers external photon and electron beam therapy using conventional linear accelerators. Brachytherapy, hadron therapy, tomotherapy, robotic radiotherapy, etc., are beyond the scope of this report.

## ***Part I: Introduction to Monte Carlo***

## 2 Monte Carlo for solving numerical problems

### 2.1 *Comparison with analytical and numerical approaches*

The main difference between the Monte Carlo technique on one hand and analytical and numerical approaches on the other is the use of a random number generator and a set of probability distributions to sample parameter values for calculating a possible solution to the problem for a single “case” or “event”. By simulating many “cases” or “events,” reliable average values can be obtained. Since the result is an average, it is associated with a standard deviation that expresses the uncertainty due to the fact that the simulated number of events is less than infinite.

This source of uncertainty is not present when analytical methods are used. Of course, the answer obtained with analytical methods is still associated with an uncertainty, arising from the common sources such as uncertainties in the input parameters and possible systematic errors in the model. A possible disadvantage of analytical methods is that solutions may be difficult to obtain for complex problems. (Minor) changes in the relationship between parameters, or the introduction of a new parameter, may create a major problem in finding a new analytical solution.

Numerical methods are generally less sensitive to such changes. If, for instance, a relationship changes, the numerical algorithm can stay the same, because it only uses the *values* of the function at certain points. In Appendix A, the example of calculating the area of a circle with radius 1 is used to demonstrate some differences between the different techniques.

### 2.2 *Monte Carlo dose calculations*

In a Monte Carlo dose calculation, the track of each individual ionizing particle (in radiotherapy generally photons and electrons) through the volume of interest is simulated. Along its way, the particle may interact with the matter through which it is passing, e.g. through Compton scattering (for photons) or Coulomb scattering (for electrons). Using a random number generator and probability distributions for the different types of interaction, the program samples the distance  $l$  to the ‘next’ interaction for a particle at a given position and with velocity vector  $\mathbf{v}$  in a certain

direction. The particle is then propagated with velocity  $v$  over the distance  $l$  to the interaction location. Next, the program chooses the type of interaction that will take place. For a dose calculation, one extra step is needed. The dose is defined as the amount of energy deposited per unit of mass ( $\text{J/kg} = \text{Gy}$  in SI units). Therefore, for each interaction that is simulated, the program calculates the energy balance: the energy of the 'incoming' particle(s) minus the energy of the 'outgoing' one(s). To calculate the dose in a particular volume (voxel), one adds the contributions from all interactions taking place inside the volume, and divides this by the mass in the volume.

### *2.3 Example: An 8 MeV electron hitting the linac target*

To illustrate some of the principles of Monte Carlo dose calculations, the simulation of a photon that is generated in a linac head when an 8 MeV electron hits the target is described. The energy distribution of the photons generated is depicted in the left panel of Figure 2.1. The photon energy can be determined in two ways. The first one is the so-called hit-or-miss method. For this method, two random numbers are generated, one of which, designated "x", is uniformly distributed between 0.01 and 8 (photon energy), the other, "y" is uniformly distributed between 0 and 1.2 (probability density of a photon with that energy). The value of 1.2 is chosen to be equal to the maximum of the energy probability distribution (left panel of Figure 2.1), or slightly above that. The point "x,y" is now plotted in this probability distribution. If it is above the curve "the target was missed", the point is rejected, and a next point is randomly generated. If it is below, the point is accepted, and the photon energy is "x" MeV.



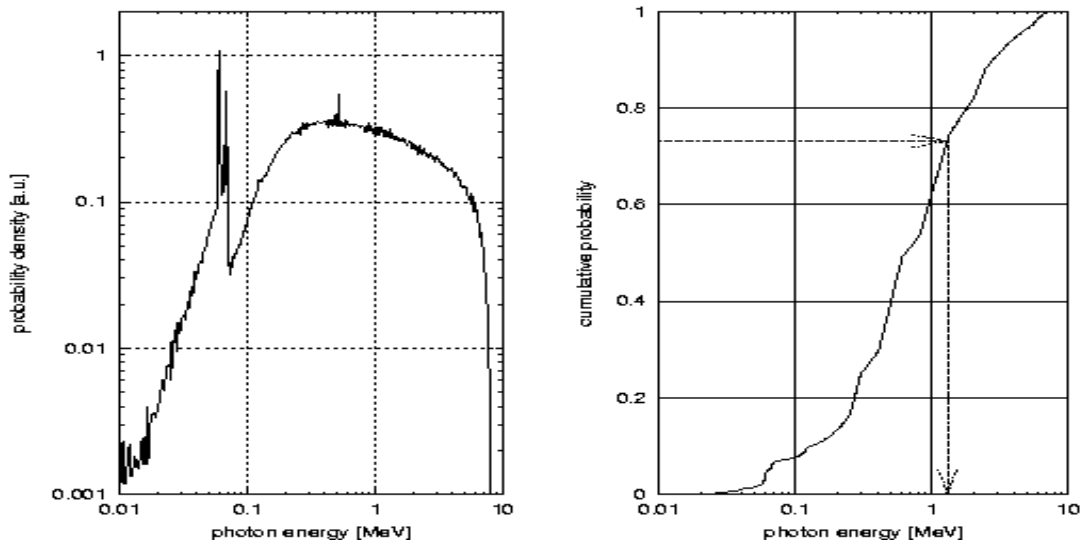


Figure 2.1 Left panel: energy probability distribution for photons that are generated when an 8 MeV electron hits a linac target. Right panel: cumulative probability distribution generated from the left panel. The cumulative probability at a certain energy is the probability to generate a photon at or below that energy.

At first glance, it may seem that there is a reasonable chance that a chosen point “x,y” will end up below the curve, yielding the hit-or-miss method rather efficient. However, the probability density in Figure 2.1 is plotted on a log-scale. Therefore, a large number of points will be rejected.

A more efficient method for selecting photon energies is based on the cumulative probability distribution (right panel of Figure 2.1). For this method, values for the cumulative probability are randomly selected, using a single random number, uniformly distributed between 0 and 1. Figure 2.1 shows an example for a selected value of 0.732. The corresponding energy, in this case 1.3 MeV, is selected. This algorithm is very efficient because only one random number is needed, and each value results in the selection of a photon energy, i.e. there is never a “miss.”

Apart from the photon energy, the angles  $\varphi$  and  $\vartheta$  between the directions of the incoming electron and the created photon have to be selected. Also for these angles, probability distributions are known. Therefore, the Monte Carlo program can generate values for  $\vartheta$  and  $\varphi$  in exactly the same way as for the energy. Once the energy and angles of the photon are known, the distance to the first interaction site can be

selected, using the *attenuation coefficient*  $\mu$  ( $[m^{-1}]$ ), which is the product of the atomic cross sections ( $[m^2]$ ) of the materials that the photon encounters, and the atom density of these materials ( $[m^{-3}]$ ). The probability that the photon will travel a distance  $l$  without undergoing any interactions is then given by  $\exp(-\mu l)$ , and  $\mu dl$  is the probability to interact in the interval  $dl$ . So, the probability for an interaction between  $l$  and  $l+dl$  is given by  $\mu \exp(-\mu l)dl$ . Similar as for the selection of the photon energy (Figure 2.1), a cumulative probability curve  $P(l)$  can now be constructed for selection of the (first) interaction site:

$$P(l) = \int_0^l \mu e^{-\mu s} ds = \dots = 1 - e^{-\mu l} \quad (1.1)$$

From this cumulative probability distribution of distances, the travel length  $l$  for a random number  $r$  in the range  $[0,1]$  can now be expressed analytically:

$$r = 1 - e^{-\mu l} \quad \Rightarrow \quad l = -\frac{1}{\mu} \ln(1-r) = -\frac{1}{\mu} \ln(r') \quad (1.2)$$

Here,  $1-r$  is again a random number that is uniformly distributed between 0 and 1; in the final step it has been replaced by a new random number,  $r'$ .

With the travel distance  $l$  to the first interaction site known, the position of the photon can be updated, and the type of interaction that will take place can be selected, based on the cross section data for the different interactions. Subsequently, the energies and angles of the particles that are produced in the interaction are generated, and the whole process is repeated until all particle energies are below a pre-defined cut-off energy.

### **3 Basic elements of a Monte Carlo code for dose calculations**

#### *3.1 Physics models*

The physics models are usually hard-coded in the Monte Carlo software. Photons are transported in a way that is analogue to reality. For electrons, the simulation of each individual interaction is very time consuming and impractical for radiotherapy applications. Therefore, so-called condensed history techniques have been introduced (section 7.2). These techniques are approximations of the “real physics”, and implementation differences exist between different codes. This may lead to different results, which is the main reason why these codes need to be thoroughly benchmarked. Even with condensed history techniques, electron transport often remains the most time-consuming part of radiotherapy Monte Carlo simulations.

The user may be able to manipulate the physics modelling via a number of so-called transport parameters. For example, the user may enable/disable certain interactions and/or set the values of parameters that determine e.g. cut-off energies or electron step lengths. Such parameters may significantly influence a simulation. For example, when a particle’s energy decreases below the cut-off energy, it is discarded and the remaining energy is deposited locally. Obviously, increasing this parameter will increase the calculation speed, but accuracy might be lost. See sections 7.1 and 7.2 for details.

#### *3.2 Interaction data tables*

Data tables with interaction probabilities for each type of interaction for each element are usually provided together with a Monte Carlo program. Each of the Monte Carlo programs has its own format for these tables, therefore interchanging data tables between the various Monte Carlo programs is a non-trivial task. However, since these data tables are so closely linked to the Monte Carlo program, the installation of the program will typically also include installation of the data tables (see section 7.3).

### 3.3 *Random number generator*

By its nature, the Monte Carlo method requires a random number generator for sampling the probability distributions. In computer codes, this is generally solved by implementing a recurrence relation. Properties such as uniformity of distribution and random number sequence length are crucial for the reliability of the Monte Carlo code. This topic is addressed in more detail in Appendix B.

### 3.4 *Geometry*

The geometry is to be specified by the user. Depending on the code, different geometric structures can be defined: planes, cylinders, spheres, cones, and sometimes even more complicated structures, see section 8.1. In some general purpose Monte Carlo codes, an (additional) scoring geometry has to be introduced in regions where the dose distribution is to be calculated.

### 3.5 *Material composition*

All materials present in a simulation must be specified by the user. In most programs, the materials are specified in terms of their elemental composition and density (see chapter 8). Sometimes additional information is required to enhance the accuracy of modelling.

### 3.6 *Source definition*

The tracking of particles starts at a position (or range of positions) where the energy and angular distributions of the particles are known with some confidence. For instance, in a linac the energy and angular distributions of electrons hitting the target are fairly well known. Accelerator modelling is described in more detail in chapter 9.

### 3.7 *Scoring*

To extract the absorbed dose distribution from the particle transport simulation, one has to define a so-called tally or scoring function. More details on this topic are provided in chapter 10.

### 3.8 *Variance reduction and approximations*

To increase the efficiency of Monte Carlo calculations, approximations and variance reduction techniques have been introduced. Examples of approximations are the already mentioned condensed history technique for electron transport, and the use of cut-off energies. Variance reduction techniques are statistical methods that enhance the efficiency of a calculation. Theoretically, these techniques result in identical expectation values as without variance reduction, whilst the calculation speed is increased. In practice, however, care should be taken and each of these techniques should be benchmarked. More details are given in chapter 11.

## 4 A brief history

The technique of random sampling to solve mathematical problems is quite old. One of the earliest documentations is by Comte de Buffon in 1770. In the early nineteen-thirties, using a mechanical adding machine, Fermi already applied statistical sampling techniques for radiation transport calculations related to neutron diffusion (Metropolis 1987, Wood 1986). The statistical techniques were, however, considered impractical as they were time-consuming and tedious. During the second world war Mauchly and colleagues developed the first electronic digital computer named ENIAC, Electronic Numerical Integrator And Computer, containing around 18.000 double triode vacuum tubes in a system with half a million solder joints (Cooper 1989). Development of the ENIAC was inspired by the labor- and time-intensive ballistic computations for generation of firing-tables. The system was realised in late 1946, and in 1947 it was moved to its permanent home at the Ballistics Research Laboratory in Maryland, USA. Very soon it was realised that the ENIAC offered new opportunities for statistical sampling techniques. The first tests were on a variety of problems in neutron transport. One of the collaborators, N. Metropolis, named the mathematical method “Monte Carlo”, after the city with its famous casinos (Metropolis 1987, Cooper 1989).

As computers gained speed and memory, the Monte Carlo codes became more sophisticated. The first version was written in machine code, but by the early 1960s programming languages such as FORTRAN (FORmula TRANslation released in 1957 by IBM -International Business Machines- and standardised in 1966, 1977 and 1990) got into use. The fast developments in computer hardware and software and in statistics were of great influence on the application of Monte Carlo techniques. These Monte Carlo methods on the other hand helped to improve the hard- and software, and became one of the most important tools of the statisticians.

At first, the development of dedicated coupled photon electron transport codes for each specific problem required a lot of effort. Today, this is no longer necessary due to the availability of general purpose codes, like ETRAN, ITS, MCNP, EGS, GEANT, and PENELOPE. Most Monte Carlo systems dedicated to radiotherapy are (partially) based on these codes. Therefore, a short history of the most important

general purpose codes is given in the following section. The introduction of Monte Carlo into radiotherapy treatment planning is discussed in detail in section 14.1.

#### *4.1 General purpose codes*

The ETRAN (Electron TRANsport) code, developed and maintained at the National Institute of Standards and Technology (NIST), Gaithersburg, Maryland, USA, contains the basic algorithms for simulating the tracks of electrons and photons travelling through matter (Seltzer 1988). The code was originally developed as a tool for solving electron transport problems involving energies up to a few MeV. Later, the production and propagation of secondary bremsstrahlung was added, to extend the calculation to higher energies. The methods used to generate electron trajectories go back to a paper of Berger (1963), describing the sampling from multiple-scattering distributions. In the early 1970's, at Sandia National Laboratories, the ETRAN code was made more user friendly, especially regarding the specification of the problem geometry, and extensions were made to lower energies by including more elaborate ionization and relaxation models. The combined software was designated the Integrated TIGER Series (ITS) system (Halbleib et al 1988). The Los Alamos National Laboratory (LANL) integrated the electron transport algorithms of ITS 3.0 into their MCNP3 (Monte Carlo Neutron Photon) code, yielding the MCNP4 (Monte Carlo N-Particle) system, which was first released in 1990 (Briesmeister 2000). Based on this code, a different group at LANL developed MCNPX, which can be used to simulate many additional types of particle (Waters 2002).

During the early 1960's, Nagel wrote his Ph.D. thesis at the Rheinischen Friedrich-Wilhelms-Universität in Bonn on electron-photon Monte Carlo. The in-house developed Fortran code was a very practical (freeware) tool for experimental physicists during the mid 1960's. Electrons and positrons could be simulated from 1 GeV down to 1.5 MeV, and photons were followed down to 0.25 MeV. The code was limited in geometry handling. From 1972 to 1978, Ford and Nelson from Stanford Linear Accelerator Center (SLAC) collaborated to revamp Nagel's program and make it more user friendly. In addition, special attention was given to allow for easy future enhancements. The resulting EGS3 code (Electron Gamma Shower) was introduced

in 1978. Nelson (SLAC) and Hirayama (National Laboratory for High Energy Physics, KEK) extended the flexibility of EGS in general, and for high energy accelerators in particular. Rogers and colleagues (National Research Council of Canada, NRC) extended the code to low energies. These efforts were pooled together in 1985, and EGS4 was introduced (Nelson et al 1985). In 1990, PRESTA (Parameter Reduced Electron Stepping Algorithm) was introduced in EGS4 (Bielajew and Rogers 1987). In 2000, Kawrakow and Rogers released the EGSnrc code as the successor to EGS4, with further improvements in the modelling of electron transport (Kawrakow and Rogers 2000).

PENELOPE (PENetration and Energy LOSS of Positrons and Electrons) was developed by Universitat de Barcelona and Institut de Tècniques Energètiques, Universitat Politècnica de Catalunya in Barcelona, Spain, and Universidad Nacional de Cordoba, Argentina (Salvat et al 2003). It was first released in 1996. PENELOPE performs Monte Carlo simulation of electron-photon showers in arbitrary materials. Initially, it was devised to simulate the penetration and energy loss of positrons and electrons in matter; photons were introduced later. Large efforts were made to make the simulation of electron transport as accurate as possible, especially in the low energy region.

The first version of GEANT (GEometry ANd Tracking) was written in 1974 as a bare framework, which initially emphasised tracking of a few particles per event through relatively simple detectors. The code was developed as a simulation tool for high energy physics experiments. From 1993 to 1998, the FORTRAN based GEANT3 simulation program was entirely redesigned as an object-oriented program written in C++, designated GEANT4 (Agostinelli et al 2003). This code is a collaboration of many international research groups under supervision of CERN (Conseil Européen pour la Recherche Nucléaire / European Organization for Nuclear Research). It is a very versatile code, useful for many different types of particles over a wide energy range and capable of handling complex geometries. GEANT4, includes a low-energy electromagnetic physics package, which makes it useful for radiotherapy applications. Recently, an implementation of the PENELOPE electromagnetic physics has also been added to the code.



## 5 General purpose Monte Carlo codes in radiotherapy

At present, four general purpose Monte Carlo systems are in use for radiotherapy dose calculation. These systems are EGS (Nelson et al 1985, Kawrakow and Rogers 2000), MCNP (Briesmeister 2000, Waters 2002), PENELOPE (Salvat et al 2003), and GEANT (Agostinelli et al 2003).

EGS and PENELOPE simulate the coupled transport of photons and electrons (and positrons), while other particles such as neutrons or protons are not taken into account. This has the advantage that during the development of these codes all attention has been focused on the particles of interest for radiotherapy dose planning. On the other hand, in high energy photon beams (18 MV and higher) the production of neutrons and protons in the accelerator head may impact (the biological effect of) the physical dose distribution in the patient, especially in bone where even alpha particles have a non-negligible contribution (Chibani and Ma 2003). These particles can be taken into account in MCNP and GEANT. The latter codes were not developed specifically for low-energy (radiotherapy) dosimetry, but large efforts have recently been made to provide reliable low-energy extensions of these systems.

In the next paragraphs, the four systems are described in more detail, focusing on the mutual differences. In general, it can be said that modelling of photon transport is quite similar in all four systems in the energy range of radiotherapy applications, although different cross section data are used. The main differences occur in the electron transport, which can be dealt with in several ways, having a large impact on the speed and accuracy of the systems. In the paragraphs below only a short introduction is given. For more details, the reader is referred to the corresponding references. An interesting overview has been given by Verhaegen and Seuntjens (2003).

### 5.1 EGS

In the past decade, much attention has been paid to the electron transport in EGS (Electron-Gamma Shower). In 1990, PRESTA (Parameter Reduced Electron Stepping Algorithm) was introduced in EGS4 (Bielajew and Rogers 1987), and in

2000 the EGSnrc code was released by Kawrakow and Rogers as the successor to EGS4. In EGS4 (Nelson et al 1985), the Molière (1948) multiple scattering theory is used, which is only valid for small scattering angles. In EGSnrc (Kawrakow and Rogers 2000, Kawrakow 2000a), an improved multiple scattering theory based on screened Rutherford elastic scattering is used instead. Furthermore, this code uses PRESTAIL (Bielajew and Kawrakow 1997). The main improvement of PRESTAIL compared to PRESTA is the introduction of a single scattering model of electron transport, making it possible to reduce the electron step length to very small values near material boundaries. These improvements are expected to improve the calculation accuracy of angular deflections for electrons, eliminate restriction on the maximum and minimum electron path length in EGS4/PRESTA-I imposed by the Molière theory, and provide an exact boundary-crossing algorithm by using single elastic collisions of electrons.

From the benchmarks applied to EGSnrc (Kawrakow 2000b, Verhaegen 2002), it can be concluded that this code is very accurate even in the vicinity of interfaces between materials with high and low atomic numbers ( $Z$ ). However, for MCTP applications EGS4 (PRESTA) seems good enough and is faster than EGSnrc. A disadvantage of EGS4 and EGSnrc is that users need to program their code in a macro Fortran code called Mortran. Obviously, only the geometry, source input, and tallying need to be programmed. In a pre-compilation step, the user code is connected to the EGS core.

Two user codes, designated BEAM and DOSXYZ (Rogers et al. 1995, Rogers et al 2002), are available for applications in MCTP. BEAM is an EGS user code specifically developed for the modelling of a linear accelerator. All components of the accelerator (target, primary collimator, flattening filter, monitor, jaws, MLC, etc.) are pre-programmed in so-called component modules. The user can build an accelerator by simply summing the required components. An input file must be generated in which the dimensions, materials and transport parameters of the individual components must be defined. No programming efforts are required. With BEAM it is possible to determine so-called phase-space files in a plane at the exit of the linear accelerator. These files contain all necessary parameters (direction, location, energy, charge, etc.) of particles passing through the plane. Such files can then be used as

input for dose calculations in phantoms or patients using the other pre-programmed user code, designated DOSXYZ. In this code CT data can be imported and translated to voxels with a certain material and density. Systems as MCDOSE, Peregrine, XVMC and DPM (section 13) are totally or partially based on BEAM and DOSXYZ.

## 5.2 MCNP

MCNP is a general-purpose, continuous-energy, generalised-geometry, time-dependent, coupled neutron/photon/electron Monte Carlo transport code. Two versions of the MCNP (Monte Carlo N-Particle) code, developed by different groups, currently exist. MCNP4C (Briesmeister 2000), is able to simulate the (coupled) transport of neutrons, photons and electrons, whereas MCNPX (Waters 2002) can simulate a variety of other particles as well. The photon and electron physics in the present version of MCNPX (version 2.5) are identical to those in MCNP4C. Hence, in the following we will denote both codes as MCNP. It is noted that the successor of MCNP4C, MCNP5 (Brown 2003), has been released, but is not yet available outside the USA.

The electron transport algorithms in MCNP are claimed to be equal to those in the ITS 3.0 system (Halbleib et al 1988), which in turn were derived from ETRAN (Seltzer 1988). The Goudsmit-Saunderson multiple scattering theory is used, while the sampling of energy loss is based on the Landau straggling theory. Several investigators have shown though that care should be taken with the electron transport (Jeraj et al 1999, Schaart et al 2002, Reynaert et al 2002). A systematic error is present in the default MCNP electron energy indexing algorithm. However, the user can choose to use the ITS electron energy indexing algorithm instead, which leads to correct results. An additional problem exists with MCNP4C when the geometry contains many boundaries, e.g. in the case of a voxelised phantom. MCNP4C requires the voxels in such a phantom to be modelled as separate material regions, even if they exist of the same material. It has been shown that in such cases the cumulative effect of many small boundary crossing artefacts may lead to significant errors in the calculated dose distribution (Schaart et al 2002, Reynaert et al 2002).

In contrast to EGS and GEANT4, MCNP does not require any programming by the user. Instead, the user only needs to provide an ASCII input file specifying the problem geometry (using a variety of available surface types and/or macrobodies such as spheres, boxes and cylinders), the source(s) (energy and angular spectra, etc.), the tallies (e.g. energy deposition or track length), and (optionally) the use of one or more of the many available variance reduction techniques. The simulation results are provided in ASCII output files. Graphical user interfaces, such as VISED (2004) are available to generate input files and to visualise the output data.

### 5.3 *PENELOPE*

PENELOPE (PENetration and Energy LOSS of Positrons and Electrons) has been introduced recently (Sempau et al 1997, Salvat et al 2003). The code simulates the coupled transport of electrons, positrons and photons with energies between a few hundred eV and 1 GeV. It is capable of handling complex geometries and static electromagnetic fields. Large efforts were made to make the simulation of electron transport as accurate as possible. Ideas introduced in PENELOPE have been implemented in EGSnrc and vice versa. So it can be expected that these codes will provide rather similar results. In PENELOPE a mixed scheme of single and multiple scattering is used, comparable to EGSnrc. The multiple scattering algorithms are based on the Goudsmit-Saunderson theory. In the PENELOPE implementation of multiple scattering, the angular deflection and the lateral displacement for each electron step are accounted for using the so-called random hinge method, which is a simple and fast method for obtaining an accurate geometric representation of the electron track. The user has to program the application in Fortran, although several user codes are available in the system. Benchmarks of PENELOPE against other codes and experiments have recently been published by Sempau et al (2001), Sempau et al (2003) and Ye et al (2004). These studies generally show good agreement with EGS and experiments. The applicability for linac modelling has been illustrated in Sempau et al (2003).

## 5.4 GEANT

GEANT (GEometry ANd Tracking) was originally developed for high-energy physics. It can be used for the simulation of many types of particle over a wide energy range. The current version, GEANT4, includes a low-energy electromagnetic physics package, which makes it useful for radiotherapy applications (Agostinelli et al 2003). Recently, an implementation of the PENELOPE electromagnetic physics has also been added to the code. The code can handle complex geometries, electromagnetic fields, (electronic) detector response, and allows for time-dependent (4D) modelling of e.g. decaying particles and/or moving objects. A variety of visualization tools is provided, as well as connectivity to data-analysis software and computer-aided design (CAD) programs (for geometry input). The user must provide a set of C++ objects that are built upon the Monte Carlo core of the program in an object-oriented approach.

Recently, GEANT4 has found use in a variety of medical physics applications (Barca et al 2003, Archambault et al 2004). Some benchmarks of GEANT4 electron and photon transport against other Monte Carlo codes and measurements have been published by Carrier et al (2004) and Rodriques et al (2004). These studies showed good agreement for photons. Carrier et al reported fair agreement for electrons, although some non-negligible differences with e.g. EGSnrc (4% for a 10 MeV parallel beam) were found (see also Torres et al 2004). Recently Poon and Verhaegen (2005) extensively benchmarked GEANT4 against EGSnrc for radiotherapy applications. In this paper, a very nice overview of the photon and electron transport physics modelled in the GEANT code is presented for the 3 different electromagnetic physics models (standard, low-energy, Penelope). For photon beams depth dose curves are in good agreement except in the buildup zone. For electron beams differences are more important. It is also illustrated that results depend highly on transport parameters as e.g. the electron step size. This is even more clearly demonstrated in the paper of Poon et al (2005), where a more fundamental study of the electron transport in GEANT4 is performed. Accurate results can be obtained after careful selection of transport parameters. In that case the code is an order of magnitude slower than e.g. EGSnrc. As new releases of GEANT4 are continuously

improved with respect to the code, it can be expected that the role of GEANT4 in medical physics may become more important in the near future.

In this context it is interesting to note that the OpenGATE collaboration has recently released the first version of GATE, a modular, scripted, GEANT4-based Monte Carlo code which, in contrast with GEANT4 itself, does not require the user to be familiar with C++ (Jan et al 2004). Although this code was primarily developed for nuclear medicine applications (modelling of PET and SPECT scanners), extensions into other domains such as radiotherapy are currently being developed.

## 6 Rationale for Monte Carlo treatment planning

### 6.1 Requirements on uncertainty in Treatment Planning

An interesting discussion on uncertainty in treatment planning is provided in AAPM report No 85 of the AAPM Task Group 65 (Papanikolaou et al 2004). As stated in this report, due to the steep slope of the TCP-and NTCP-dose relationships, a dose error of 5 % might lead to a TCP change of 10% to 20%, and to even larger NTCP changes (see also Fraass et al 2003). Clinical effects are already noticeable for dose errors of 7 % (Papanikolaou et al 2004). Therefore accurate dose information is required.

Between the dose prescription to a tumour and the actual dose delivery a large number of steps are involved. During each step, uncertainties are introduced, accumulating to an overall uncertainty for the full process of dose delivery. An overview of the various components of uncertainty is given in Table 1 of AAPM Report 85. An overall uncertainty of 4.3 % ( $1\sigma$ ) is obtained, which is in correspondence with the more familiar 5 % ( $1\sigma$ ) obtained in previous work (Mijnheer *et al.* 1987, ICRU 1976).

Improving the quality of the dose engine, i.e. reducing the uncertainty in the dose calculation, will reduce the overall uncertainty in the delivered dose. It should be noted that the use of an extremely accurate dose engine will not automatically lead to very low uncertainties in clinical dose delivery as several other factors contribute significantly to the overall uncertainty. However, in AAPM report 85 it is claimed that the overall uncertainty in the delivered dose will decrease to 2.5 % ( $1\sigma$ ), leading to a situation where the accuracy of the dose engine plays an important role. At present, it is generally believed that the dose calculation should be accurate to within 2% - 3% ( $1\sigma$ ) (Fraass et al 2003).

## 6.2 *Why Monte Carlo Treatment Planning*

Monte Carlo dose calculation engines have the potential to meet, or even perform better than, the 3 % ( $1\sigma$ ) uncertainty requirement, regardless of beam geometry and patient composition. As for any type of dose engine, however, the uncertainty for a Monte Carlo dose engine will never be zero due to, for example:

- imperfect matching of the Monte Carlo beam to the actual accelerator beam,
- uncertainties in the cross section libraries,
- the standard deviation due to the limited number of histories simulated,
- uncertainties in the conversion of CT data to material composition and density.

The quality of beam matching is very difficult to estimate, but in general it should be possible to achieve this within 1 % ( $1\sigma$ ) or better (Verhaegen and Seuntjens 2003 and Ma, Jiang 1999). Most authors assume that the uncertainty in cross section libraries is small enough to be negligible (Fraass et al 2003). The statistical uncertainty depends on the number of histories. The uncertainty associated with tissue characterization is difficult to quantify. Instead of using water with different densities for all tissue types, the real tissue composition must be estimated for the calculation of cross sections.

Taking all of the above-mentioned uncertainties into account, Monte Carlo treatment planning is expected to be able to offer an uncertainty in dose calculation well within 3 % ( $1\sigma$ ) required for accurate radiotherapy. Other advantages are given by Fraass et al (2003). One advantage over conventional dose engines is that the uncertainties are independent of the treatment setup. Furthermore, the Monte Carlo method could lead to an increase in confidence in the obtained dose distributions (see also Cygler et al 2005). This could lead to the delivery of a higher tumour dose to avoid recurrence, while having faith in the reported dose to critical organs.

An interesting discussion is provided in a point/counterpoint discussion between Mohan and Antolak (2001). Arguments against MCTP raised by Antolak include: the influence of (statistical) noise, the influence of approximations and variance reduction techniques introduced to limit the calculation time and the limited spatial resolution (voxel size) often used, again to speed up the calculations. These arguments are considered of minor importance by Mohan: approximations and variance reduction



techniques are illustrated to introduce no bias, the effect of statistical noise is very limited and resolutions up to 2 or 3 mm can be reached within a few minutes of calculation time. It is clear, however, that the added value of MCTP compared to superposition/convolution algorithms should be illustrated by examples. In the following two paragraphs a literature study of phantom studies and comparisons for clinical cases is provided.

### 6.3 *Phantom experiments*

In the vicinity of low density volumes (lung) and air cavities, Monte Carlo dose calculations have been reported to be more accurate than conventional techniques (Mohan et al 1997, Solberg et al 1998, Ma et al 1999, Keall et al 2000, Martens et al 2002, Heath et al 2004, Paelinck et al 2005). Mohan et al (1997) stated that conventional methods (including superposition/convolution techniques) will give rise to deviations ranging from 5 % to 10 % in the presence of tissue heterogeneities. The results of Ma et al (1999) illustrate that MCTP is certainly interesting for electron beams, as e.g. the FOCUS conventional dose calculation algorithm (pencil beam algorithm) leads to large deviations (up to 15 %) and isodose line shifts of more than 1 cm (see figure 6.1).

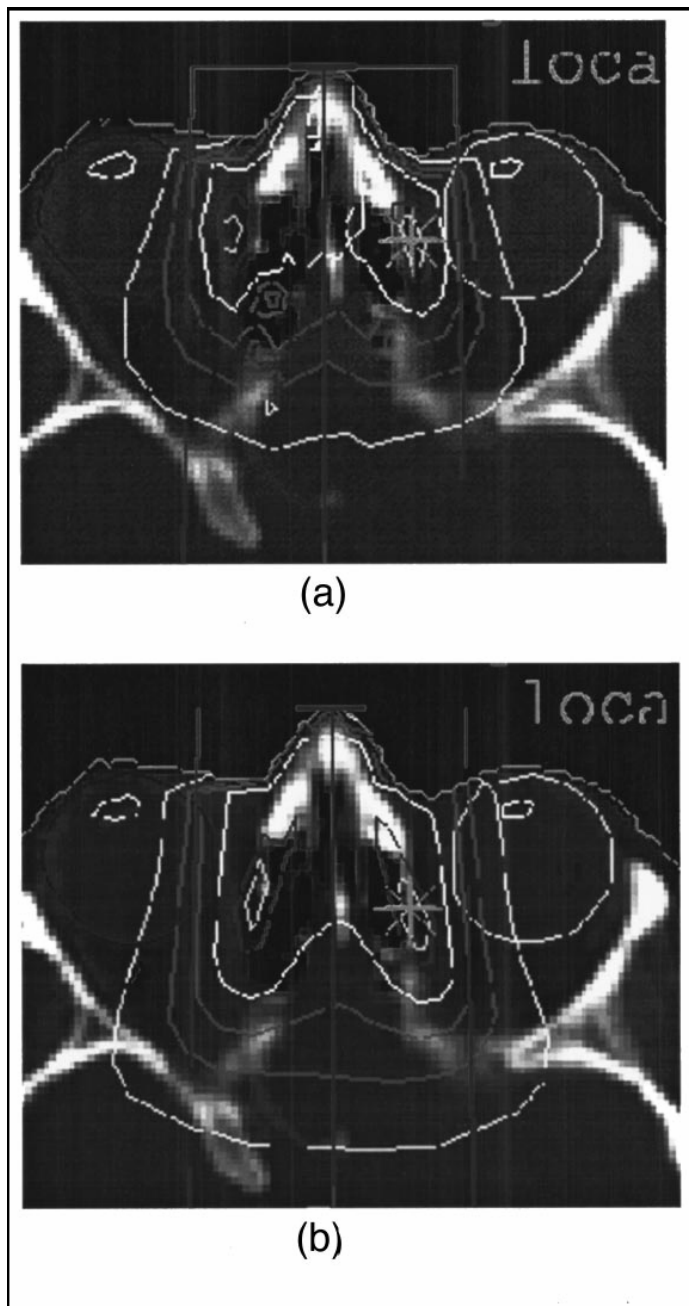


Figure 6.1: Isodose line shift between results obtained with the FOCUS pencil beam algorithm (a) and Monte Carlo calculations (b) (reproduced with kind permission of AAPM from Ma et al (1999)).

For photon IMRT applications, an added value of the MC method can be found in head-and-neck treatment and treatment of lung cancer, because of the presence of tissue inhomogeneities resulting in loss of electronic equilibrium. For IMRT the best available non-Monte Carlo dose calculation engines are based on the

superposition/convolution method (Boyer and Mok 1984, Mackie et al 1985, Ahnesjö 1989, Keall and Hoban 1996, Yu et al 1995). Ma et al (1999) obtained large differences between the FOCUS planning system and a Monte Carlo dose engine for a phantom containing lung or bone layers, even when the superposition convolution method of FOCUS was used. An interesting comparison of two superposition/convolution algorithms and the Monte Carlo method for a lung cavity is provided by Paelinck et al (2005) (see figure 6.2).

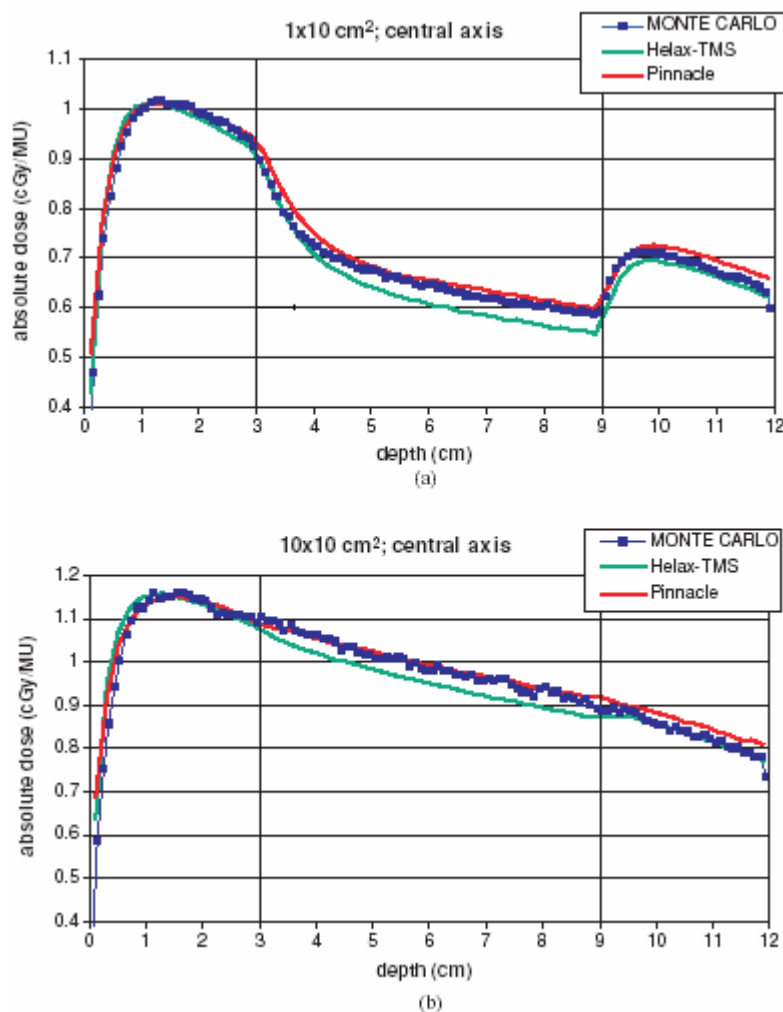


Figure 6.2: Comparison of two superposition/convolution algorithms and Monte Carlo calculations for a phantom with a lung insert in a 6 MV beam (reproduced with kind permission from Paelinck et al (2005)).

The Helax TMS system (Nucletron, Veenendaal, The Netherlands) systematically underestimates the dose in the lung-equivalent cavity by 6 %, while

the Pinnacle algorithm (Philips Medical Systems, Best, the Netherlands) overestimates the dose behind the cavity by 4 %. Also in the work of Crammer-Sargison et al (2004), significant deviations in lung equivalent material were obtained for the CadPlan pencil beam convolution algorithm (Varian Oncology Systems Inc., Palo Alto, CA). Arnfield et al (2000) obtained substantial deviations between measurements and superposition/convolution (Pinnacle) in and around lung-equivalent material, while the Monte Carlo results are in excellent agreement with the measurements. These deviations become more important when simulating a small (4x4 cm) high energy photon beam (18MV). Krieger and Sauer (2005) performed a comparison between the pencil beam (Helax TMS), superposition/convolution (Helax TMS) and Monte Carlo methods for a multi-layer phantom consisting of styrofoam (to simulate the low density of lung) and polystyrene layers for regular beams. In polystyrene, superposition/convolution and MC were in agreement with the measurements while the pencil beam algorithm deviated by 12 %. In styrofoam, however, even the superposition/convolution algorithm deviated by more than 8 % from measurements and MC results.

#### *6.4 Comparisons for clinical cases*

In the examples described above, extreme situations were investigated consisting of one single beam crossing a large lung/air cavity. It is not straightforward to extrapolate these findings to clinical practice. Therefore in this paragraph we will focus on examples of realistic clinical calculations. The results are discussed chronologically and the focus is on the most recent results as these are obtained with the most recent (and thus most accurate) versions of the available conventional dose calculation engines.

Wang et al (1998) developed a patient specific Monte Carlo dose engine that was evaluated for conformal lung treatment. The method was approximate as only one medium (water) was defined, although density variations were taken into account. The dose distributions obtained were compared against a conventional dose engine based on the equivalent path length (EPL) method. The Monte Carlo results illustrated that 20 % of the planning target volume (PTV) was underdosed, while the

maximum doses in cord and heart (two parameters used in the objective function of the treatment planning system) were underestimated by the conventional system by more than 25 %. Deviations were attributed to the approximate modelling of lateral particle transport in low density regions by the conventional dose calculation engine. In a follow-up study (Wang et al 2002), the same PB algorithm and MC code were compared for IMRT treatment of five lung patients and four head-and-neck patients. For one lung patient, a decrease of 10% in  $D_{95}$  and 6 % in  $D_{\text{mean}}$  was obtained, while for the other patients the PTV coverage decreased with 2-5%. For one of the head-and-neck patients (a patient with recurrence)  $D_{95}$  differed by 9 %. In lung, differences in  $D_{05}$  and  $D_{\text{max}}$  of up to 10 % were found. Also in the spinal cord, differences larger than 5 % were noticed. For all head-and-neck patients, dose differences in the optical chiasm were below 2 %. An interesting conclusion is that larger effects are observed for individual fields than for the composite plan.

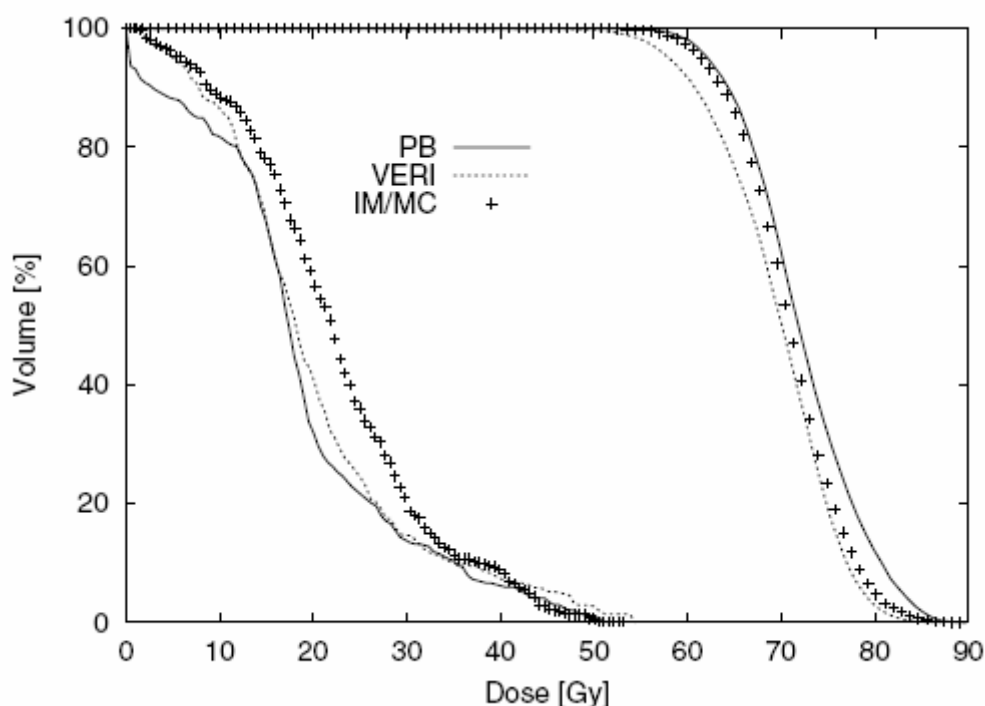


Figure 6.3: Comparison between Konrad Pencil beam calculations and EGSnrc for head and neck treatments (reproduced with kind permission from Laub et al (2000)). DVHs are for the PTV and optical chiasm. Abbreviations used: PB (Pencil Beam), Veri (EGS4 Verification calculation), IM/MC (intensity modulated/Monte Carlo). IM/MC is the dose distribution obtained from the Monte Carlo inverse planning system.

Laub et al (2000) obtained large differences between the KonRad Pencil Beam algorithm with 1D inhomogeneity correction (and accounting for lateral electron transport) on one hand and EGS4 (Nelson et al 1985) on the other hand for head-and-neck treatments (see figure 6.3).

The Monte Carlo result in the PTV was systematically lower than the PB result, although it is not clear whether the MC dose was expressed as “dose to water” (presence of large air cavity with corresponding low stopping powers in the PTV can lead to differences in DVH of PTV, see par 10.4 for a more detailed explanation). Differences were attributed to the rebuild-up behind the air cavity. According to the MC results the dose constraint in the chiasm was violated.

Francescon et al (2000) compared the superposition/convolution algorithm of Pinnacle with the Monte Carlo code BEAM (Rogers et al 1995) for mediastinal and breast treatments. Deviations were below 2.5 % and thus within 2 standard deviations of the Monte Carlo calculation. Also for single fields and large inhomogeneities the differences were negligible. The study was restricted to large beams. As stated by Ahnesjö (1989) larger deviations are expected for smaller fields.

Jeraj et al (2002) illustrated that two types of error are introduced when using an approximate dose calculation algorithm for inverse treatment planning, namely a systematic error due to errors in the dose calculations and a convergence error resulting from the fact that the optimised beam settings obtained by the approximate dose engine will differ from those obtained with an accurate dose calculation algorithm. In this study, results obtained by Monte Carlo, superposition/convolution and pencil beam methods were compared. Systematic errors were below 1% of  $D_{\max}$  in the tumour and slightly larger outside the PTV for the superposition/convolution method and around 5% for the pencil beam algorithm. The authors concluded that pencil beam algorithms should be replaced by superposition/convolution or Monte Carlo algorithms.

Leal et al (2003) compared the Plato PB algorithm (Nucletron, Veenendaal, The Netherlands) with the Monte Carlo program BEAM for different clinical cases. As illustrated in figure 6.4, significant differences were obtained when comparing the DVHs in the bladder and the rectum.

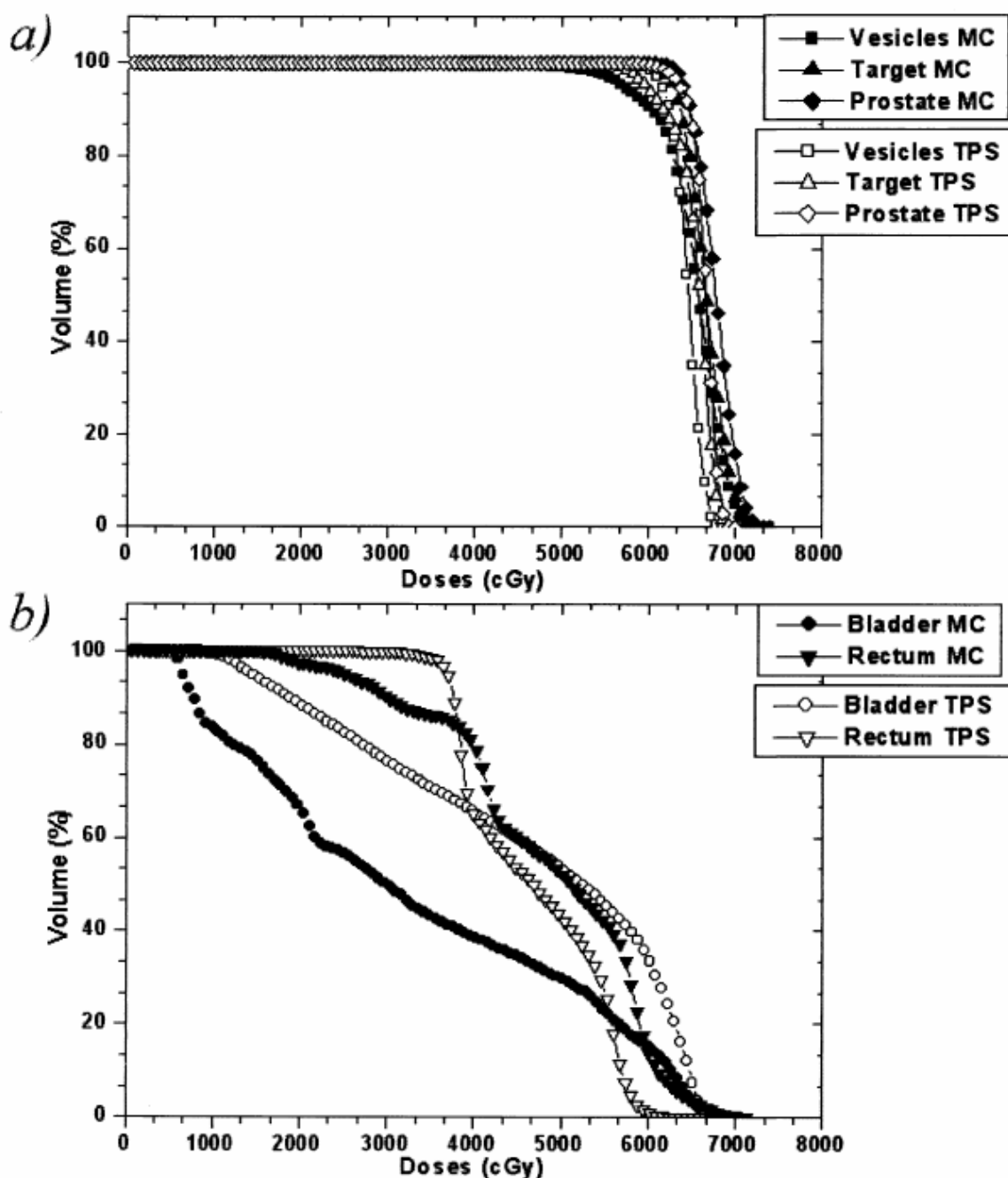


Figure 6.4: Plato PB algorithm (TPS) versus Monte Carlo (MC) for a prostate treatment (reproduced with kind permission from Leal et al (2003)).

As recently stated by Chetty et al (2005): when comparing Monte Carlo results with conventional dose calculation engines, it would be interesting to distinguish between effects related to differences in the beam model and effects related to the particle transport within the patient geometry. Therefore Chetty et al used two

versions of an equivalent path length algorithm, namely a version with an approximate beam model, and one with an accurate beam model that provides excellent agreement when comparing calculational results with measurements in a homogeneous phantom.

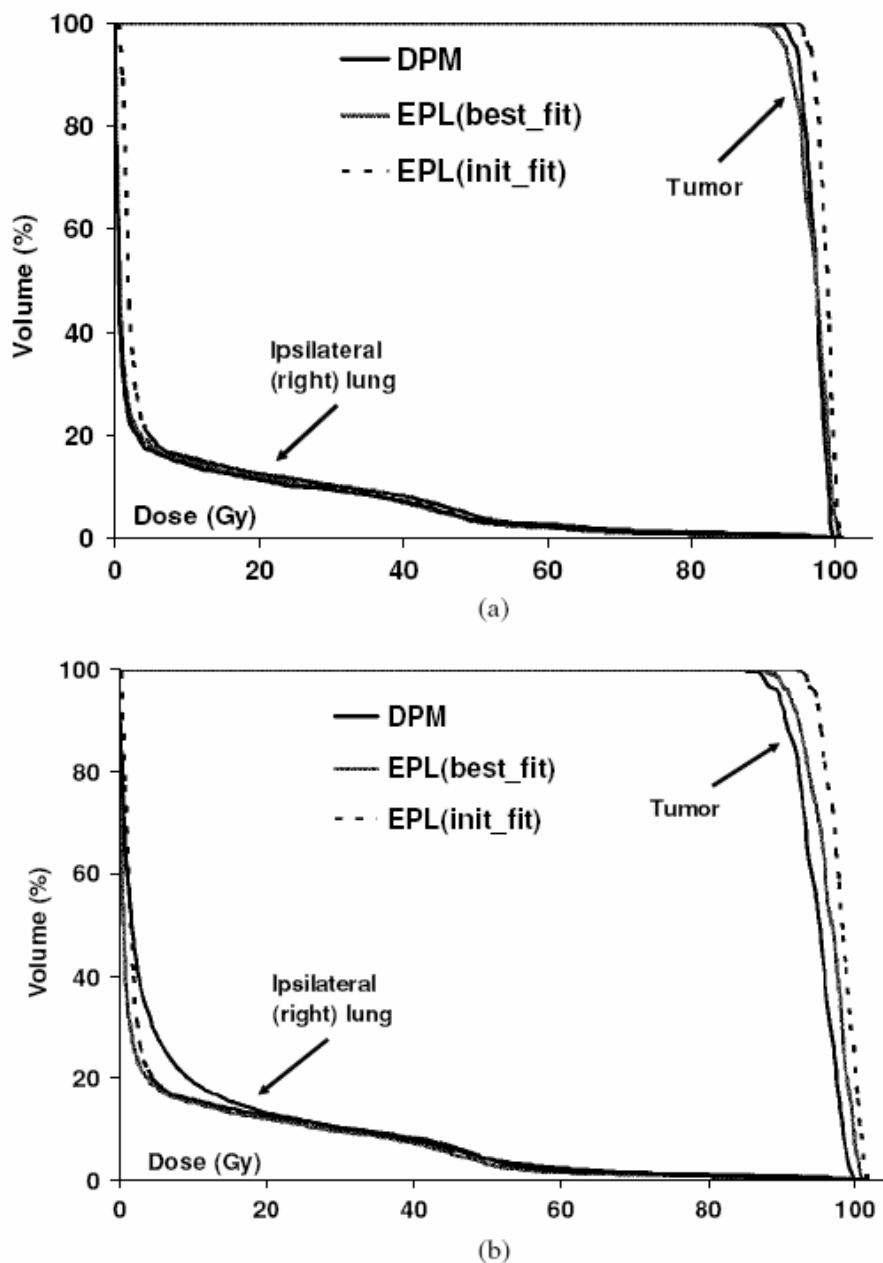


Figure 6.5: Comparison of equivalent path length (EPL) algorithm with Monte Carlo calculations (DPM) illustrating the importance of accurate tuning for a homogeneous phantom (above) and a heterogeneous phantom (below). The results depicted with “best fit” are obtained with the accurate beam model. (reproduced with kind permission from Chetty et al (2005)).



These two models were compared with the DPM (see section 14.2 for a description of DPM) Monte Carlo dose engine for a homogeneous phantom, a heterogeneous thorax phantom and a lung patient plan (see figure 6.5).

The importance of an accurate beam model was illustrated by the fact that the EPL algorithm using the accurate beam model (“best-fit results”) gave rise to a much better agreement with the Monte Carlo results for 6 MV in a homogeneous phantom. For the lung phantom though, the disagreement between the mean lung dose of the best-fit results and the MC method was 30 % for 15 MV. This illustrates (as stated by the authors) that especially at high energy (15 MV) the inhomogeneity effects (transport of secondary electrons in low density regions) may be more significant than beam model approximations.

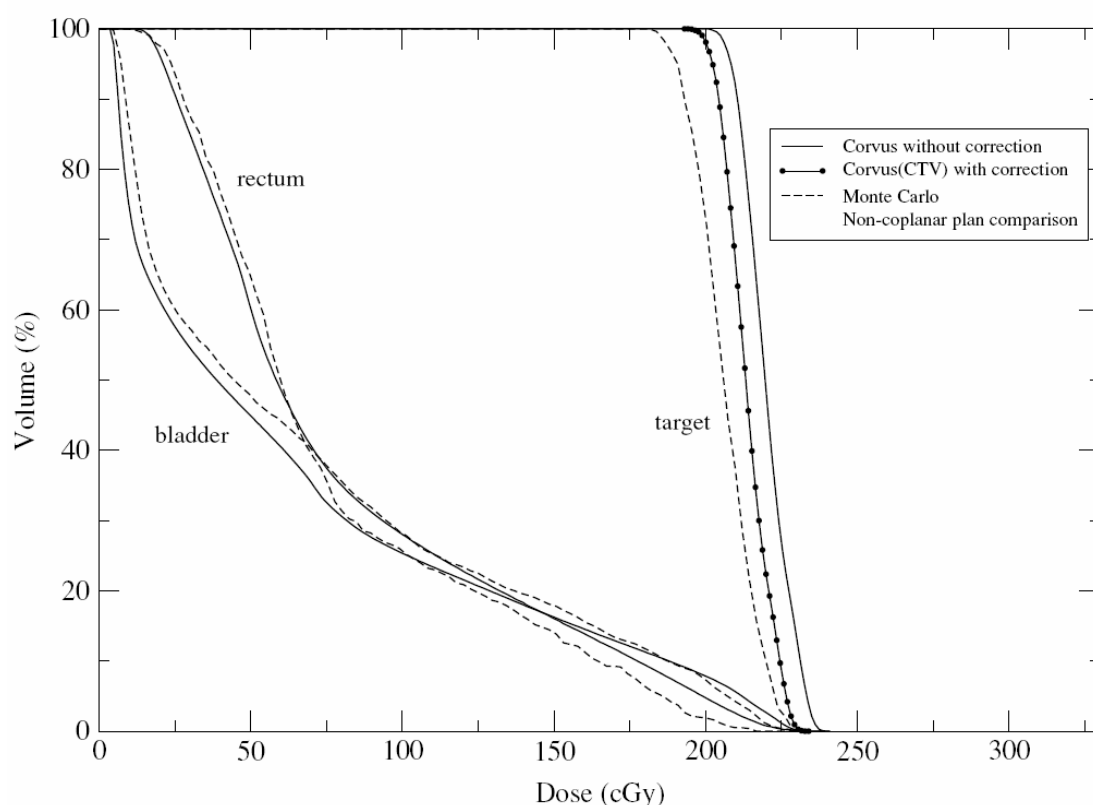


Figure 6.6: Comparison of Corvus pencil beam algorithm with MCSIM Monte Carlo calculations for the prostate (reproduced with kind permission from Yang et al (2005)).

Yang et al (2005) compared the Corvus finite-size PB algorithm (with and without inhomogeneity corrections) with Monte Carlo calculations (MCSIM, see

section 14.3) for 25 coplanar and 5 non-coplanar IMRT plans for the prostate (see figure 6.6).

For the coplanar plans the agreement between MCSIM and Corvus was within 3 %. For the non-coplanar plans, differences up to 7 % in  $D_{\text{mean}}$  and above 8 % in  $D_{98}$  were obtained in the PTV. Another conclusion was that it was necessary to apply the EPL heterogeneity corrections in Corvus.

Boudreau et al (2005) compared Corvus (with and without EPL correction) with the Peregrine Monte Carlo method (see section 14.5) for IMRT head and neck treatment planning (see figure 6.7 and table 6.1).

Table 6.1: Summary of ratios between Corvus and Peregrine results obtained by Boudreau et al (2005) (reproduced with kind permission of Boudreau et al (2005)).

	$D_{50}$	$D_{\text{mean}}$	$D_{\text{max}}$	$V_{25}$
Spinal cord (11)	N/A	$0.999 \pm 0.003$	$1.00 \pm 0.01$	N/A
Parotid glands (22)	$0.96 \pm 0.01$	$0.96 \pm 0.01$	$0.993 \pm 0.005$	$0.94 \pm 0.01$
Brainstem (8)	N/A	$0.94 \pm 0.02$	$0.99 \pm 0.02$	N/A
Mandible (8)	N/A	$1.02 \pm 0.01$	$1.00 \pm 0.01$	N/A

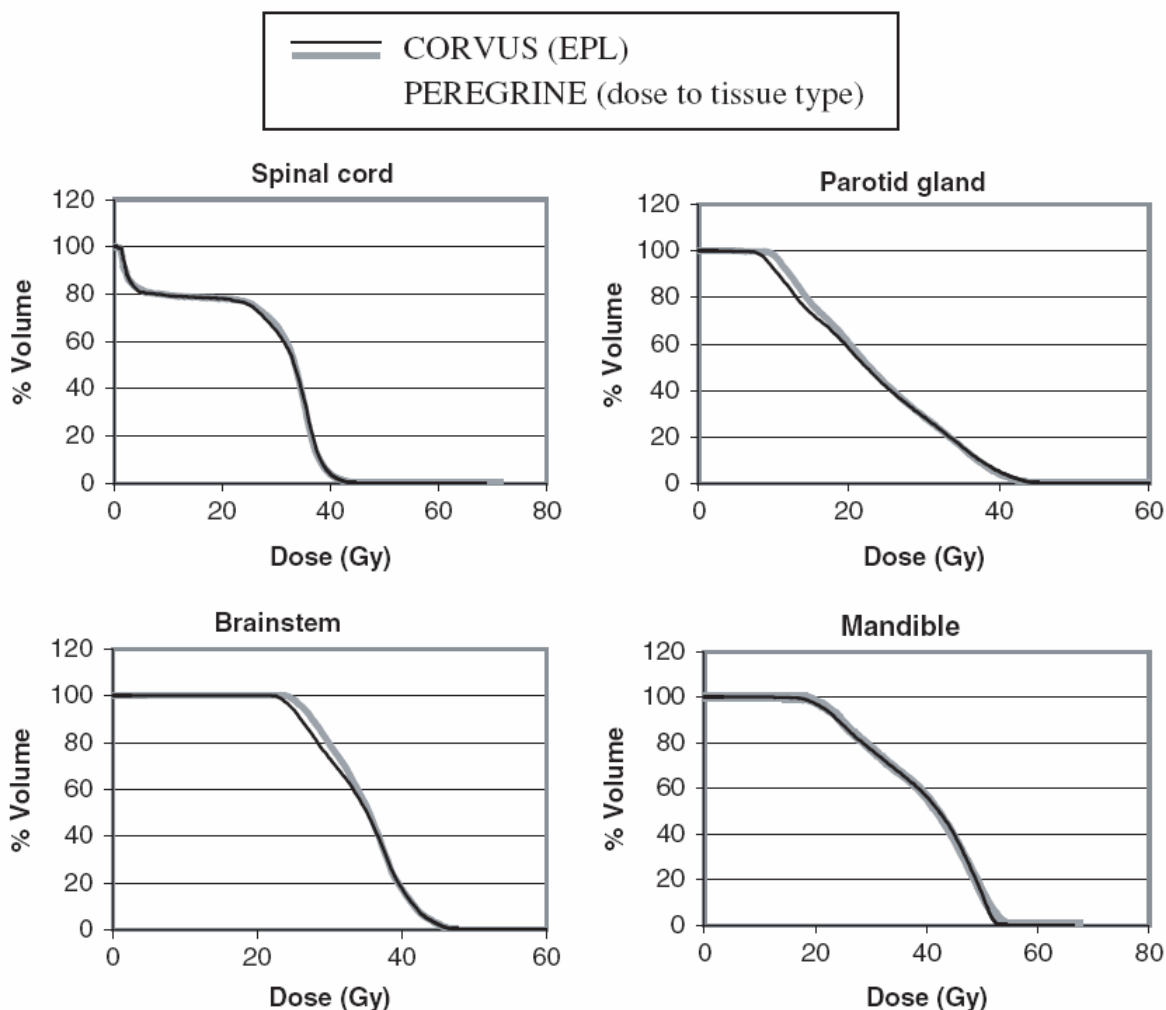


Figure 6.7: Comparison of Corvus system with Peregrine Monte Carlo calculations (reproduced with kind permission from Boudreau et al (2005)).

For the brainstem, Peregrine delivered on average a 6% higher  $D_{\text{mean}}$ , so for individual patients even larger differences were obtained. The Peregrine system was extensively benchmarked against measurements (Heath et al 2004).

Reynaert et al (2005) presented a comparison between two Monte Carlo dose calculation engines (Peregrine and MCDE) and the Helax TMS superposition/convolution algorithm for a head-and-neck patient (see figure 6.8).

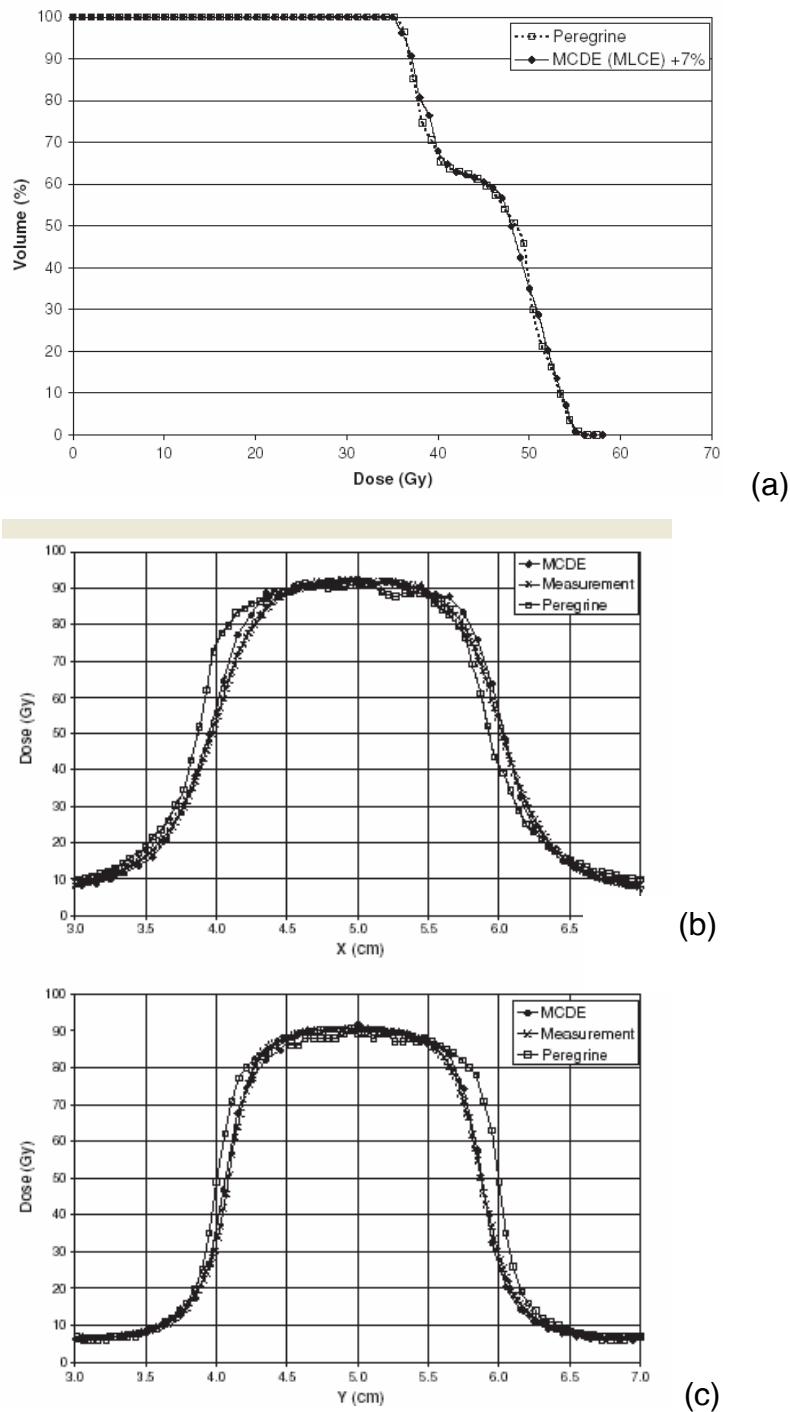


Figure 6.8: Comparison between the Monte Carlo dose calculation engines Peregrine and MCDE. In part (a) the MCDE doses (obtained with the MLCE model for the Elekta MLC) were systematically multiplied by 1.07, illustrating a dose difference of 7 % in the optical chiasm. In part (b) (lateral profiles of 2x40 and 40x2 beam segments) the cause of the discrepancies is demonstrated (problem with MLC model). (reproduced with kind permission from Reynaert et al 2005).

In this work it was demonstrated that Peregrine provided systematic errors in the DVHs in the optical chiasma, due to a systematic error in the leaf projection. The superposition/convolution results are in acceptable agreement with MCDE. Only one patient was studied.

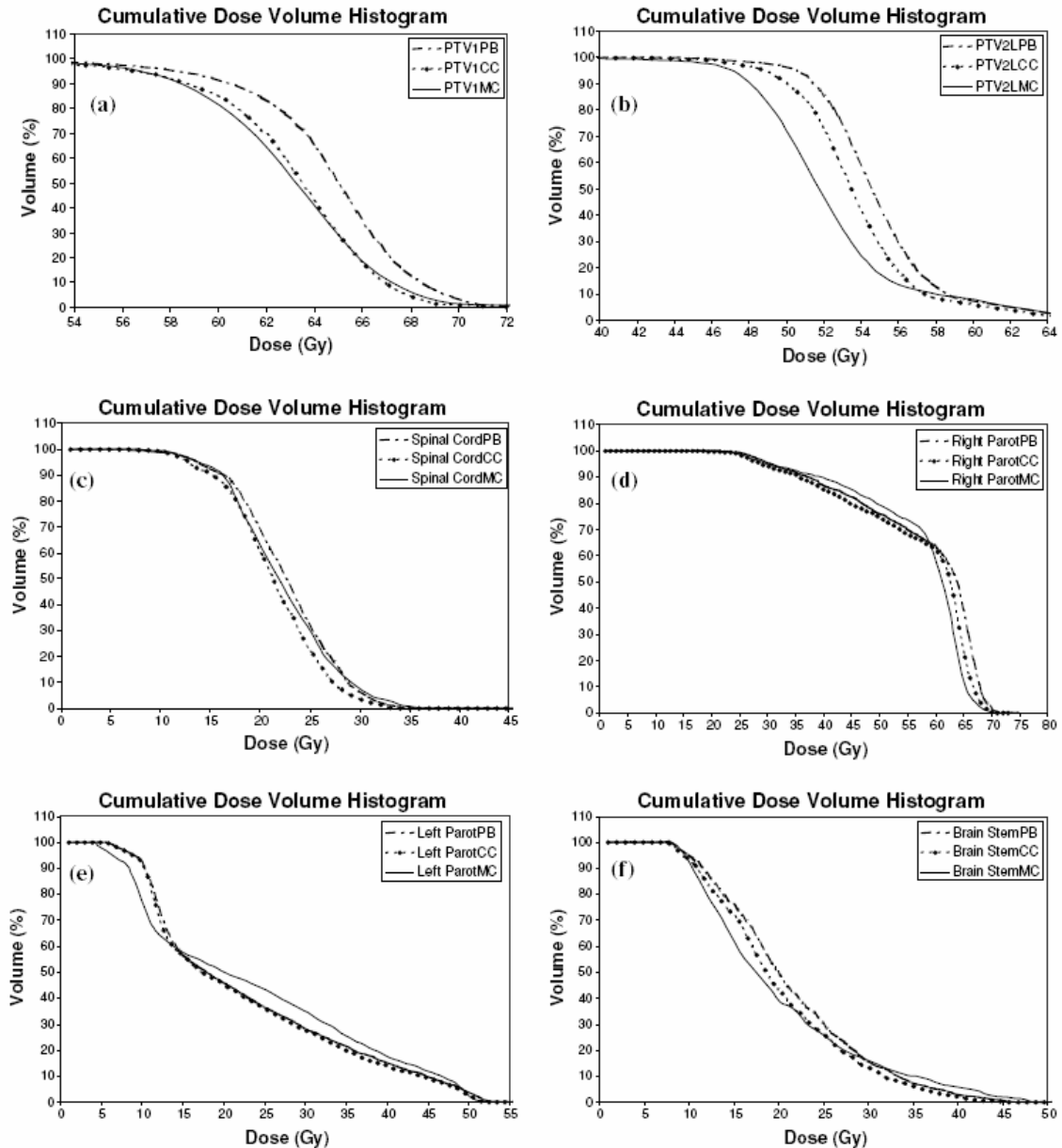


Figure 6.9: Comparison of PB algorithm, superposition/convolution (Helax TMS) and BEAMnrc/DOSXYZnrc Monte Carlo calculations for a head and neck patient. (reproduced with kind permission from Seco et al (2005))

Seco et al (2005) performed a comparison between a PB, a superposition/convolution (Helax TMS) and a MC system for a head and neck patient (see figure 6.9).

Large differences were obtained in the PTV but, as stated by the author, this was largely caused by the fact that the MC dose in the air cavities was expressed as “dose to medium” (see section 10.4). In the critical structures the Monte Carlo DVHs differed significantly from the PB and superposition/convolution results.

The most direct way to determine the added value of MCTP is to try to link observed differences in dose maps to clinical outcome. This can be done by e.g. comparing post-treatment CT scans with (1) possible recurrence within the PTV with regions of underdosage (as predicted by the MC results) and (2) possible side effects in critical tissues in regions of overdosage. Data on this topic is still missing. An interesting paper on this topic was published by De Jaeger et al (2003). Lung cancer patients, originally planned with an EPL algorithm, were retrospectively recalculated with a superposition/convolution algorithm, illustrating large differences in the mean lung dose (up to 20 %). The Lyman model was used to illustrate that these dose differences can lead to complications in lung tissue.

## 6.5 Conclusions

Based on single beam phantom experiments it can be concluded that well-benchmarked MC dose engines clearly outperform both PB and superposition/convolution algorithms regarding dosimetric precision. Also for realistic clinical plans the MC codes are superior to PB calculations. More studies are needed to investigate to what extent the replacement of superposition/convolution algorithms by MC may result in a benefit for clinical plans.

Most published MC results for photon beams were obtained by MC experts with well benchmarked research systems. The influence of the approximations and

variance reduction methods introduced in commercial MCTP systems on the uncertainty are not yet clear. Moreover, even an MCTP system without approximations or variance reduction methods can contain systematic errors. Consequently, every individual MCTP system must be benchmarked before clinical use.

An important conclusion is that Monte Carlo dose calculation engines, when carefully validated against measurements, provide an additional benchmarking tool for treatment planning, in situations where measurements are difficult or even impossible (Mohan 1988).

## ***Part II: Fundamentals of Monte Carlo***



## 7 Modelling of particle transport

The following discussion will be restricted to coupled photon-electron transport as this is the focus of the present report. In a recent paper, Chibani and Ma (2003) investigated the influence of photonuclear reactions in the linac head for high-energy photon beams (18 MV and higher). The effects of neutrons, protons and alphas on dose (taking into account the RBE of the particles) are below 0.7 %. Therefore it is unlikely that these particles will ever be taken into account in a MCTP system for photon and electron beams.

### 7.1 *Photon transport*

In general, the types of photon interaction taken into account in a Monte Carlo treatment planning code are the photoelectric effect, Compton scattering, Raleigh scattering and pair production.

In the case of photoelectric absorption, the photon interacts with a (tightly bound) atomic electron. In this process, which is dominant at low photon energies, the photon disappears and all of its energy is transferred to the electron, which is ejected from the atom with a kinetic energy equal to the difference between the initial photon energy and the electron's binding energy. As a result of this process, one of the atomic shells is left with a vacancy which is promptly filled by a less tightly bound electron, resulting in the emission of a fluorescence X-ray or one or more Auger electrons. In a detailed Monte Carlo simulation, all of the secondary particles (photo-electrons, X-rays and Auger electrons) may be transported. However, in cases where this does not significantly influence the end result, computing time may be saved by switching off the transport of one or more of these types of secondary particles.

In case of Compton scattering, a photon interacts with a free (i.e. unbound) electron. If the photon energy is high with respect to the binding energy of an electron in its atom, this electron can be considered free for this purpose. Part of the photon energy is transferred to the electron. The scattered photon and the electron emerge from the interaction at angles relative to the direction of the initial photon that are related to the particle energies because of the conservation of energy and

momentum. Compton scattering is an important process for the energies of interest in radiotherapy, especially in low-Z materials.

In Raleigh scattering, essentially no energy is exchanged; only the direction of the photon is changed, usually by a small angle. Raleigh scattering is also called coherent scattering since the photon scatters elastically off an entire atom, where all electrons behave coherently. The importance of Raleigh scattering is relatively small, but not always negligible.

In the case of pair production, the photon disappears and an electron-positron pair is created. This process is only possible if the photon energy is higher than twice the electron rest mass ( $2 \times 511$  keV), and dominates at high energies in dense materials. The positron created in the interaction will annihilate with an electron when it comes to rest, resulting in the emission of two 511 keV annihilation photons.

In Section 1, an example is given on how the transport of photons is simulated. It is explained that, for each photon emitted by the source, the distance to the first interaction is sampled, based on the probability  $\exp(-\mu l)$  that the photon will not interact over a distance  $l$ .

The photon is then transported to the location of the first interaction. Subsequently, the type of interaction to be simulated is sampled, based on the partial cross sections for the different interactions contained in the interaction data tables (see section 7.3). The selected type of interaction is then simulated. Here, use is made of the well-known theories describing the kinematics of the various types of photon interaction, see e.g. Attix (1986). In case of, for example, a Compton interaction, the energy and direction for the scattered photon are sampled. If electron transport is taken into account, the energy and direction of the electron participating in the interaction are also calculated. This particle is put on the stack for later transport. Then, the distance to the next interaction is sampled for the Compton scattered photon, and the process is repeated until the photon is absorbed and all secondary particles have been transported.

If a photon is transported through a phantom consisting of multiple materials, it is possible that the sampled distance to the next interaction exceeds the distance to the nearest material boundary. In such cases, the photon is first transported to the boundary. Then, the distance to the next interaction is sampled using the cross

sections of the material into which the photon is entering. The photon track is then continued into the new material region (without changing the direction of flight).

In some calculations, the transport of the fast electrons created by photons can be ignored since they transport energy over negligibly small distances and/or charged-particle equilibrium exists. Since electron transport tends to consume a lot of computation time in Monte Carlo simulations, it may be attractive to switch off electron transport in such cases. However, the fast electrons may in turn produce (bremsstrahlung or X-ray) photons, which may have a significant effect on the end result. Therefore, some Monte Carlo codes offer the possibility to generate such secondary photons even if electron transport is turned off. The algorithms used for this purpose rely on certain assumptions (e.g., in the *tick-target approximation* it is assumed that each secondary electron is completely absorbed in the same material in which the corresponding photon interaction has taken place) and therefore need to be used with some caution.

The physics of photon transport is implemented very similarly in most modern Monte Carlo codes. Small details can nevertheless be different, e.g. the handling of the Compton effect regarding the binding of the atomic electron. A condensed overview of these differences can be found in Verhaegen and Seuntjens (2003).

## 7.2 *Electron transport*

The physical processes to be modelled when simulating the transport of electrons through matter are elastic scattering by (screened) atomic nuclei, inelastic collisions with atomic electrons causing either excitation or ionisation, Bremsstrahlung production, and the emission of X-rays and Auger electrons following electron-impact ionisation. Nuclear processes (which only occur at high electron energies) are often neglected. Positrons are sometimes simply modelled as electrons with the addition that annihilation photons are created when the particle comes to rest. More elaborate models use separate positron cross-section tables and include rare positron decay processes such as in-flight annihilation and three-photon annihilation.

An important difference between modelling of electrons and photons lies in the fact that photons undergo a relatively small number of discrete interactions per

particle track, whereas electrons undergo a very large number of Coulomb interactions with the electrons and atomic nuclei in the material. It is computationally very expensive to simulate each of these individual Coulomb interactions, and therefore this is not normally done in general-purpose codes or dose engines for treatment planning.

Instead, a so-called condensed-history approach is usually applied (Berger 1963). In such a model, each electron track is subdivided into a series of short track segments, usually called 'steps'. Instead of modelling the individual elastic and inelastic collisions along each step, the resulting (cumulative) energy loss and angular deflection are sampled once per step only.

The sampling of angular deflection may be based on a so-called multiple-scattering formalism. One example is the implementation, in EGS4, of the theory by Molière (1948). The Molière distribution is a universal function of a scaled angular variable, which makes it relatively easy to sample the angular deflection for arbitrary step lengths during a run. A disadvantage of this theory is that it is based on a small-angle approximation, so large-angle deflections are modelled less accurately. Another multiple-scattering theory, the Goudsmit-Saunderson (1940) formalism, is valid for all scattering angles. However, sampling the angular deflection for arbitrary step lengths during a run is less straightforward, so codes based on this theory (such as ETRAN, ITS and MCNP) usually sample the deflection angle from stored multiple-scattering distributions that have been calculated for a pre-selected set of path lengths during the initiation phase of the run (Berger and Wang 1988).

The sampling of electron energy loss may be done in different ways. A distinction is commonly made between so-called class I and class II algorithms (Berger 1963, Rogers and Bielajew 1988), see Figure 7.1.

In a class I code the primary electron is not directly influenced by the generation of a secondary electron. Instead, energy straggling (i.e., the fluctuation in electron energy due to differences in the energy lost by different electrons of equal initial energy traversing the same path length) due to the creation of secondary electrons is taken into account explicitly in the algorithm used to sample the energy loss for each electron step. Examples of such codes are ETRAN and MCNP, in which the energy loss is sampled from the Landau (1944) straggling distribution. An advantage of this

approach is that energy straggling is always modelled accurately, even if a high energy threshold for knock-on production is applied. This may greatly speed up a simulation if the transport of low-energy secondary electrons is not important. A disadvantage of the class I approach is the possibility for negative energy loss events in small voxels. Such events may occur if the energy carried out of a voxel by a secondary electron created within it is larger than the amount of energy deposited in the voxel by the primary (and secondary) electron.

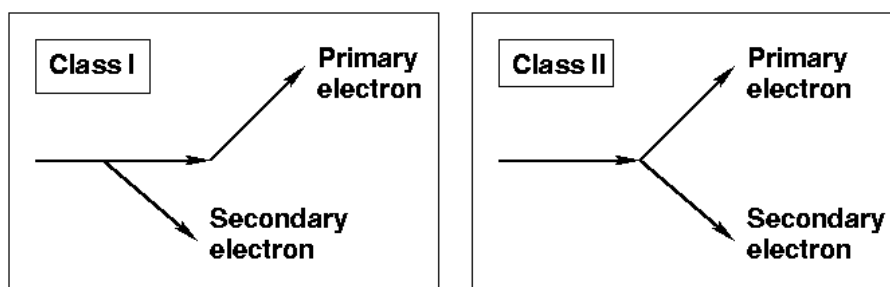


Figure 7.1 Different ways to perform a sampling of electron energy loss, class I and II algorithms. When a secondary particle is generated, the primary particle step is stopped in a class II algorithm, and a new energy and angle are selected for the primary particle in correlation with the parameters of the secondary particle (preservation of energy and momentum on a microscopic scale). In a class I code this is not the case: the primary particle step does not depend directly on the parameters of the secondary particle, although a linkage through the cross sections is obviously present (preservation of energy and momentum on a macroscopic scale).

In a class II code such as EGS the energy loss and angular deflection of the primary electron are directly affected by the generation of the secondary electron. The main advantage of this approach is that the creation of knock-on electrons is simulated in a way that is analogous to reality. This may be important in some cases. For example, when simulating the passage of electrons through a thin foil, the energy of the small fraction of electrons that have been scattered to large angles by a knock-on collision will be much lower than their initial energy, as the remainder has been transferred to the secondary electron. A disadvantage of the class II approach is that the accuracy of the simulation of energy straggling depends on the cut-off energy for

knock-on (secondary electron) production. Since the number of knock-ons to be simulated increases quickly when this cut-off energy is decreased, long computation times may be required in cases where energy straggling due to low-energy secondary electron creation is important.

It is noted that the same distinction between class I and class II algorithms can be applied to the creation of Bremsstrahlung photons. However, most codes, including EGS, ETRAN and MCNP, use a class II algorithm for sampling radiative energy losses.

Some codes allow the user to switch off the sampling of energy loss and to use the expectation value of the energy loss per unit path length instead (i.e., the stopping power) for calculating the energy loss per electron step. This is called the continuous-slowing-down-approximation (CSDA). In cases where the effect of energy straggling is not important, for example when it is small compared to the influence of path length straggling (i.e., the fluctuation in electron energy due to differences in the total path length travelled by different electrons of equal initial energy traversing the same thickness of material), simulations may be speeded up greatly by using the CSDA.

An important parameter in any condensed-history model is the electron step size. On one hand, the step size must be large enough so that a sufficiently large number of Coulomb interactions occur within each step for the applied multiple-scattering- and energy-loss-models to remain valid. On the other hand, the step size must be small enough so that any errors due to the approximation of the curved electron track by a series of straight line segments remain negligible. In addition, the fractional energy loss per step must remain small since multiple-scattering algorithms are usually based on the assumption that the electron energy remains constant during a step.

Some Monte Carlo codes apply a path length correction to each simulated (straight) electron step to correct for the difference with the corresponding (curved) segment of the “true” electron track. Similarly, one may apply a correction for the lateral displacement that occurs during each electron step. EGS4 and EGSnrc, for example, offer such corrections through the PRESTA (Parameter Reduced Electron Stepping Algorithm, Bielajew and Rogers 1987) and PRESTAIL (Bielajew and

Kawrakow 1997) algorithms, respectively. Such algorithms may allow the use of fewer, larger electron steps, increasing the speed of the simulation without compromising the accuracy of a simulation.

With any condensed-history approach, one may encounter problems in very small material regions. When the electron step size becomes comparable to or larger than (one or more of) the dimensions of the region of interest (e.g. a small, gas-filled ionisation chamber), the electron tracks within the region of interest are no longer accurately modelled and so-called step-size artefacts may occur. In such cases, one may try to solve the problem by reducing the electron step size, as is indeed possible with some codes. Since reducing the step size will slow down the calculation, it is preferable to reduce the step size only in the region(s) where artefacts are to be expected. In any case, however, one must be cautious not to reduce the electron step size below the point where the underlying multiple-scattering theory ceases to be valid. As an example, in MCNP the electron tracks are subdivided into so-called (major) steps with pre-selected path lengths corresponding to an average energy loss of  $\sim 8.3\%$  (Briesmeister 2000). These steps are further subdivided into an integer number of sub-steps. The energy loss is sampled at the level of the major steps, the length of which cannot be changed by the user. Angular deflections are sampled for each sub-step to increase the geometric accuracy of the simulated electron track. The user can adjust the number of sub-steps per major step, to increase the accuracy of the simulation in thin material regions. An average of at least 10 sub-steps per electron track crossing a material region is recommended (Briesmeister 2000).

Yet another problem lies in the crossing of material boundaries, as the applicability of the multiple-scattering theories commonly used in Monte Carlo codes is limited to electron steps that occur within a single material. In some codes, an electron step crossing a material boundary is simply terminated at the boundary and a new step is begun at the same point. To improve the accuracy of the simulation in geometries involving many boundaries, some of the codes that use pre-selected step lengths apply a correction to the sampled energy loss and angular deflection for the interrupted step, to account for the fact that the length of this step is less than the length anticipated at the beginning of the step (Seltzer 1988).

If the code uses arbitrary step lengths, one may gradually reduce the step length when an electron approaches a boundary. (Of course, for the electron to be able to eventually cross the boundary, the reduction of the step length must be stopped at some finite minimum value, which may e.g. be based on the minimum path length constraints of the multiple scattering algorithm being used.) After the boundary has been crossed, the step size is gradually increased again while the electron moves away from the boundary. In this way, the number of interrupted steps as a fraction of the total number of steps may be minimised, improving the accuracy of the simulation at the expense of an increase in computing time. It is noted that this approach may also be used to avoid step size artefacts in geometries involving very small material regions. This type of boundary-crossing algorithm has, for example, been implemented in the PRESTA algorithm. It has been shown, however, that PRESTA may still not be adequate when simulating the dose deposited in a small air cavity or in the neighbourhood of high-Z interfaces. This led to the introduction of PRESTA-II (Bielajew and Kawrakow 1997) which allows the user to revert to a single scattering model in the close neighbourhood of boundaries, thereby reducing the minimum path length to very small values. This appears to resolve the problems observed in the above-described circumstances. Another interesting solution to the boundary crossing problem is provided by the random-hinge method implemented in PENELOPE. It is claimed that this algorithm, although it handles interface crossing in a relatively simple (and therefore fast) way, gives rather accurate results (Salvat 2003).

### *7.3 Interaction data tables*

#### *7.3.1 Photon interaction data*

In the example in chapter 1 it was explained that the total linear attenuation coefficient  $\mu$  is needed to sample the distance to the next collision for a given type of particle with a given energy in a given material. For simplicity, let us assume that the material consists of a single element. Then, the total linear attenuation coefficient is related to the total atomic cross section  $\sigma_{\text{tot}}$  of that element as follows:



$$\mu = \frac{\rho}{m_u A} \sigma_{\text{tot}} . \quad (7.1)$$

Here,  $\rho$  is the mass density of the material,  $m_u$  is the atomic mass constant ( $m_u = 1$  u, where u is the unified atomic mass unit defined as 1/12 of the mass of one atom of the nuclide  $^{12}\text{C}$ :  $1 \text{ u} = 1.66053886 \cdot 10^{-27} \text{ kg}$ ), and  $A$  is the relative atomic mass of the target element. Note that the quantity  $\rho/m_u A$  (which may also be written as  $\rho N_A/M$  where  $N_A = 6.0221415 \cdot 10^{23} \text{ mol}^{-1}$  is the Avogadro constant and  $M$  is the molar mass of the target element) equals the number of atoms per unit volume.

The total atomic cross section can be expressed as the sum over the cross sections for the different processes by which photons may interact with the atoms of the target element:

$$\sigma_{\text{tot}} = \tau + \sigma_{\text{incoh}} + \sigma_{\text{coh}} + \kappa_n + \kappa_e + \sigma_{\text{ph.n.}} , \quad (7.2)$$

where  $\tau$  is the atomic cross section for the photo-effect,  $\sigma_{\text{incoh}}$  and  $\sigma_{\text{coh}}$  are the cross sections for incoherent (Compton) and coherent (Raleigh) scattering, respectively,  $\kappa_n$  and  $\kappa_e$  are the cross sections for pair productions in the field of the nucleus and in the field of the atomic electrons (triplet production), respectively, and  $\sigma_{\text{ph.n.}}$  is the photonuclear cross section. It is noted that atomic cross sections are often expressed in units of b (barn) per atom, where  $1 \text{ b} = 10^{-28} \text{ m}^2$ .

In a Monte Carlo simulation, not only the total cross section, but also the cross sections for the individual processes are needed to sample, for each collision, the type of interaction to be simulated. Data libraries containing these cross sections as a function of photon energy for (most of) the elements (as well as a list of relative atomic masses or molar masses of the elements) are normally provided with a Monte Carlo code. Some codes allow the user to choose between different data libraries and/or to use his own cross sections. It is to be noted that cross sections for relatively rare interactions, such as triplet production or photonuclear reactions, may not be included in the data tables provided with a given code, or they may be included for a limited number of elements only.

The densities of the materials used in a simulation are normally to be specified by the user, since these depend on the state of aggregation (gas, fluid, solid or plasma) and physical condition of the material (e.g. liquid water vs. water vapour,

graphite vs. diamond, high-density vs. low-density polyethylene). During the initiation phase of a run, these densities are used to calculate the linear attenuation coefficients for all materials used in the simulation. This may be done according to equation (6.1) if a material consists of a single element.

For chemical compounds and mixtures, the user additionally needs to specify either the atom fractions  $f_i$  or the weight fractions  $w_i$  of the different elements present in the material. The linear attenuation coefficients may then be calculated using the *mixture rule*, which sums (7.1) for the different elements. If the atomic fractions  $f_i$  are given,

$$\mu = \frac{\rho}{\sum_i f_i m_u A_i} \sum_i f_i \sigma_i, \quad (7.3)$$

where  $A_i$  is the relative atomic mass of the  $i$ -th element present in the material. This equation may be understood by realising that the first term on the right-hand side equals the total number of atoms per unit volume in the material. If the weight fractions  $w_i = f_i A_i / \sum f_i A_i$  are given, equation (7.3) can be written as:

$$\mu = \sum_i \frac{w_i \rho}{m_u A_i} \sigma_i. \quad (7.4)$$

Here, the term  $w_i \rho / m_u A_i$  equals the number of atoms of element  $i$  per unit volume.<sup>1</sup>

It has been pointed out that the mixture rule ignores changes in the atomic wave function resulting from changes in the molecular, chemical, or crystalline environment of an atom (ICRU 1989). With the exception of the fine-structure regions above absorption edges, errors arising from this approximation are expected to be less than a few percent for photon energies above 10 keV. At very low energies (10-100 eV), errors of as much as a factor of two can occur.

A variety of photon cross section compilations have been published during the past decades. A few examples are the works by Biggs and Lighthill (1988), Cullen et

---

<sup>1</sup> For Monte Carlo treatment planning purposes, a method has been proposed to derive the linear attenuation coefficients of the various tissues present within the patient directly from CT data, rather than calculating them from their density and chemical composition. This is discussed in more detail at the end of section 8.3.

al (1989, 1997), Hubbell (1969, 1982), Hubbell and Seltzer (1995), Johns and Cunningham (1983), McMaster et al (1969), and Storm and Israel (1970). Such compilations are usually based both on theoretical calculations and experimental data and may contain cross sections for (almost) all elements over a wide range of photon energies. An extensive overview of the current status of photon cross section data in the medical and biological context has recently been published by Hubbell (1999). Nowadays, computer programs such as XCOM (Berger and Hubbell 1987, Berger et al 1999) and EPICSHOW (Cullen et al 1997, Cullen 2002) are available to extract photon interaction data for elements, compounds and mixtures from large databases. The reader may be interested to know that some databases are available online, for example the XCOM database (<http://physics.nist.gov/xcom>) and the EPDL97 database (<http://www-nds.iaea.org/epdl97/>, see also <http://www.llnl.gov/cullen1/>)

The uncertainties in recent compilations of cross sections vary depending on the energy range and element. For low-Z materials, one currently assumes an uncertainty in the total attenuation coefficient of about 5% between 1 keV and 5 keV, about 2% between 5 keV and ~20 keV, about 1% for ~20 keV to ~10 MeV, above which it falls to about 0.5% at ~30 MeV (Hubbell 1999, ICRU 2001). Although there are no clear statements on how these uncertainties are to be interpreted, it seems reasonable to assume that they correspond to a confidence limit of 95% (approximately two standard deviations) and are of type B (ICRU 2001). If photonuclear reactions are ignored, this may lead to errors in the total attenuation coefficient in excess of 5% (but never more than 10%) at the peak energy of the photonuclear giant dipole resonance, which occurs around 12 MeV for heavy elements and around 24 MeV for light elements.

Needless to say, the accuracy of any radiation transport calculation depends critically on the accuracy of the input data, of which the cross sections form an important part. Differences between simulation results obtained for the same problem with different codes are sometimes due to differences in the radiation transport algorithms (in other words, differences in the way in which the physics are modelled by the codes), but they may also be due to differences in the input data. Such differences may exist in the input data provided by the user (e.g. differences in the

specifications of the materials and/or the problem geometry), or in the interaction data libraries provided with the code. As an example of the latter situation, DeMarco et al (2002) reported differences of up to 10% in the photoelectric cross section for water at 30 keV between the standard (DLC-200) data set used by MCNP, which is based on photoelectric cross sections from the compilation by Storm and Israel (1970), and the most recent XCOM dataset (Berger et al 1999). It is noted that the calculation of the total photoelectric cross section for materials in for example EGSnrc, performed by the PEGS utility, is also based on the Storm and Israel (1970) data (Kawrakow and Rogers 2003).

### 7.3.2 *Electron interaction data*

The Coulomb-force interactions between fast electrons (or positrons) and a material can be categorised into three types according to the relative magnitude of the classical impact parameter  $b$  compared to the atomic radius  $a$  (Attix 1986).

In so-called soft collisions, the electron passes the atom at considerable distance ( $a \gg b$ ) and therefore interacts with the atom as a whole, leading to excitation, or ionization by the ejection of a valence-shell electron. Thus, the amount of energy transferred per interaction is of the order of a few eV only. However, since large values of  $b$  are clearly most probable, an electron undergoes many soft collisions and these are therefore responsible for a significant fraction of the total energy transferred to the medium. Under certain conditions a very small part of the energy spent in soft collisions can be emitted in the form of Cherenkov radiation. However, the corresponding energy loss is negligible ( $<0.1\%$ ) compared to that due to ionization and excitation and therefore this effect is normally neglected in dose calculations.

When  $b \sim a$  (hard or knock-on collisions) it becomes more likely that the incident electron will interact primarily with a single atomic electron, which is then ejected from the atom with considerable energy and is called a delta ray or knock-on electron. Although hard collisions occur much less frequently than soft collisions, a considerable fraction of the energy of the primary electron may be transferred to the secondary electron in a single interaction.

When  $b \ll a$ , the Coulomb-force interactions takes place mainly with the nucleus. In the majority of these interactions, the electron is scattered elastically, only losing the negligible amount of kinetic energy necessary to conserve momentum. Elastic scattering is therefore not a mechanism for energy transfer, but it is an important means of deflecting the electron. In condensed-history Monte Carlo simulations, elastic scattering is often treated separately from the energy-loss interactions. In a few percent of the cases in which the electron passes near the nucleus, an inelastic radiative interaction occurs resulting in the emission of a bremsstrahlung photon.

It is customary to subdivide the electron stopping power (i.e., the expectation value of the energy loss per unit path length,  $dE/dx$ ) into the collision stopping power, which accounts for the energy loss due to soft and hard collisions, and the radiative stopping power, which accounts for the energy loss due to bremsstrahlung production:

$$\frac{dE}{dx} = \left( \frac{dE}{dx} \right)_{\text{col}} + \left( \frac{dE}{dx} \right)_{\text{rad}} \quad (7.5)$$

We first discuss the collision stopping power. If the material consists of a single element with atomic number  $Z$ , the energy loss per unit path length due to collisions in which less than a fraction  $\eta$  of the electron kinetic energy  $E$  is transferred can be written as (ICRU 1984):

$$\left( \frac{dE}{ds} \right)_{\eta} = \frac{2\pi\rho m_e c^2 r_e^2 Z}{\beta^2 m_u A} \left[ \ln\left(\frac{E}{I}\right) + \ln\left(1 + \frac{\tau}{2}\right) + F^{\pm}(\tau, \eta) - \delta \right] \quad (7.6)$$

where, for electrons:

$$F^{-}(\tau, \eta) = -1 - \beta^2 + \ln[4\eta(1-\eta)] + \frac{1}{1-\eta} + (1-\beta^2) \left[ \frac{\tau^2 \eta^2}{2} + (2\tau+1) \ln(1-\eta) \right] \quad (7.7)$$

or, for positrons:

$$F^{+}(\tau, \eta) = \ln(4\eta) - \beta^2 \left[ 1 + (2 - \xi^2)\eta - (3 + \xi^2) \frac{\xi \tau \eta^2}{2} + (1 + \xi \tau) \frac{\xi^2 \tau^2 \eta^3}{3} - \frac{\xi^3 \tau^3 \eta^4}{4} \right] \quad (7.8)$$

In these equations,  $\rho$ ,  $m_u$  and  $A$  have the same meaning as in equation (7.1),  $Z$  is the atomic number,  $\tau$  is the electron kinetic energy in units of the electron rest energy  $m_e c^2$ , and  $r_e$  is the classic electron radius. Furthermore,  $\beta$  equals the electron

speed as a fraction of the speed of light  $c$  and  $\xi = (\tau + 2)^{-1}$ . Finally,  $I$  is the mean excitation energy in the same units as  $E$ , and  $\delta$  is the density effect correction. The latter two quantities will be discussed further below.

The quantity given in Equation (7.6) is the restricted stopping power, which accounts for the energy loss due to soft collisions plus those hard collisions in which the fraction of primary electron energy transferred to the secondary electron is less than  $\eta$ . This may be the quantity of interest in Class II codes (see section 7.2), in which the energy loss (and angular deflection) of the primary electron is calculated for each individual collision in which a knock-on with an energy larger than a certain minimum is created. In such codes, the condensed history approach is only used to account for those collisions in which an amount of energy smaller than this minimum is transferred.

In Class I codes, the energy loss due to all collisions is accounted for by the multiple scattering formalism. In this case one may be interested in the (unrestricted) collision stopping power, which follows from Equation (7.6) by substituting  $\eta = 1/2$  for electrons, or  $\eta = 1$  for positrons.<sup>2</sup> This only affects the quantity  $F^\pm(\tau, \eta)$ , as follows:

$$F^-(\tau, \eta) = 1 - \beta^2 + \frac{\tau^2/8 - (2\tau + 1)\ln(2)}{(\tau + 1)^2} \quad (7.9)$$

$$F^+(\tau, \eta) = 2\ln(2) - \frac{\beta^2}{12} \left[ 23 + \frac{14}{(\tau + 2)} + \frac{10}{(\tau + 2)^2} + \frac{4}{(\tau + 2)^3} \right] \quad (7.10)$$

It is to be noted that Equation (7.6) is valid under the condition that the velocity of the incident electron is large compared to that of the atomic electrons. This condition may no longer be satisfied if the incident electron energy becomes comparable to or smaller than the kinetic energies of the most tightly bound (K-shell) atomic electrons, which may exceed 100 keV for high-Z elements. In principle, a so-called shell correction may be added to Equation (7.6) to extend the validity of this equation to lower energies. While this is commonly done in the calculation of cross-sections for heavy charged particles, such a correction is less straightforward for

---

<sup>2</sup> If the primary particle is an electron, the two electrons emerging from the collision are indistinguishable according to the Dirac theory. By convention, the electron with the largest energy is therefore referred to as the primary, so the maximum value of  $\eta$  is 1/2.

electrons and positrons, as is for example discussed in Report 37 of the ICRU (1984). Therefore, no shell correction has been included in the well-known cross-section compilation given in that report, and the same is true for the electron and positron cross sections used in many current Monte Carlo codes; see, for example, Briesmeister (2000) and Kawrakow and Rogers (2003). It has been estimated that the possible error resulting from this approximation may be about ~3% at 5 keV, ~7% at 2 keV and 10-15% at 1 keV in low-Z materials such as water. In high-Z materials, however, the error could be considerably larger (ICRU 1984).

The only non-trivial quantities in Equation (7.6) are the mean ionization energy  $I$  and the density effect correction  $\delta$ . These parameters are discussed in the following.

The mean excitation energy, a geometric average of all the excitation and ionization energies of a medium weighted by the corresponding oscillator strengths, is a parameter that needs attention in the calculation of stopping powers. Except for some simple atomic gases, this parameter cannot be derived by calculation alone. For most materials,  $I$  is therefore determined with the help of experimental data (ICRU 1984, Berger 1988). A complication is that, due to molecular binding effects, the value of  $I$  depends on the chemical composition and the physical state of the medium. A well-known collection of  $I$ -values for the elements and various materials of dosimetric interest has been compiled by the ICRU (1984). Estimated uncertainties in the ICRU compilation range from a few to more than 10% percent. However, it is pointed out that the sensitivity of the collision stopping power to changes in  $I$  (i.e., the relative variation in magnitude of the collision stopping power divided by the relative variation in  $I$ ) is only moderate. For e.g. liquid water the sensitivity is  $> 0.1$  for energies below ~500 keV (~0.2 at 1 keV) and falls off to a few percent around 10 MeV.

When an electron or positron passes through a material, this results in the polarization of the atoms in the material. This dipole distortion of the atoms in turn decreases the electromagnetic field acting upon the particle. The density effect correction  $\delta$  accounts for the resulting reduction of the collision stopping power which is particularly noticeable in condensed media. Different methods to derive the density effect correction have been discussed in Report 37 of the ICRU (1984) and by Berger (1988). The method used most often today is the one proposed by Sternheimer (see,

for example, Sternheimer et al. 1982), which in principle is approximate but has the important advantage that it can be used to calculate  $\delta$  for any material in a way that is consistent with the experimentally determined mean excitation energy and appears to show very good agreement (within a few tenths of a percent) with values obtained by more elaborate methods.

For an accurate calculation of the mean excitation energy and the density effect correction, some codes require the user to specify whether the material is in the gaseous or condensed (solid or liquid) state and whether the material is a conductor or an insulator. (Report 37 of the ICRU (1984), for example, may provide the interested reader with an impression of how such information can be used in the derivation of these parameters.) For accurate results, it is important that the user pays attention to such details. A Monte Carlo code may also provide the user with options to print out the stopping powers, mean excitation energies, density effect corrections, etc., that have actually been used in a calculation. This may provide an important means to check the validity of a calculation or to explain differences between results obtained with different codes.

The equations given above for calculating the mass collision stopping power are valid for materials consisting of a single element. The mass collision stopping power for a compound or mixture can be calculated using the mixture rule, i.e., as the weighted sum of the mass collision stopping powers of the constituent elements. However, if the same mean excitation energies are used for the constituents as for the corresponding elemental substances, some error is introduced because of the neglecting of molecular binding effects. In Report 37 of the ICRU (1984) it is discussed how the accuracy of the mixture rule can be improved by assigning values for  $I$  that depend on the type of compound and the physical state of the medium.

It is noted that for accurate modelling of knock-on collisions, knowledge of just the collision stopping power is not yet sufficient. More detailed information regarding the electron impact ionisation cross section may be required, such as, for example, shell-by-shell total cross sections in order to calculate the probability of emitting X-rays and Auger electrons subsequent to inner-shell ionisations. This subject has for example been discussed by Seltzer (1988).



The expectation value of the energy loss per unit path length due to radiative collisions, or the radiative stopping power, is given by (ICRU 1984, Seltzer 1988):

$$\left(\frac{dE}{dx}\right)_{rad} = \frac{\rho}{m_u A} \left( \int_0^E k \frac{d\sigma_n}{dk} dk + Z \int_0^{E'} k \frac{d\sigma_e}{dk} dk \right) \quad (6.11)$$

where  $d\sigma_n/dk$  is the differential cross section for the emission of a photon of energy  $k$  due to the interaction of the electron with the screened Coulomb field of the nucleus and  $d\sigma_e/dk$  is the corresponding cross section due to the Coulomb interaction with one of the atomic electrons, while the upper limit of the energy of the photons emitted in electron-electron interactions is:

$$E' = \frac{m_e c^2 E}{E + 2m_e c^2 - \beta(E + m_e c^2)} \quad (6.12)$$

Expressions for  $d\sigma_n/dk$  and  $d\sigma_e/dk$  cannot be given in a general form covering all energies. Instead, separate evaluations are usually made for low energies (typically  $< 2$  MeV), intermediate energies (typically 2-50 MeV) and high energies (typically  $> 50$  MeV). The radiative stopping power tends to increase nearly linearly with  $E$  in the MeV region. Furthermore, it is approximately proportional to  $Z^2$ . Electrons are attracted by atomic nuclei and repelled by the atomic electrons. The opposite is true for positrons, and therefore the bremsstrahlung cross sections for electrons and positrons are not the same. The differences are small at high energies, but at low energies the bremsstrahlung cross sections for positrons are considerably smaller than those for electrons.

The estimated uncertainty stated in Report 37 of the ICRU (1984) for collision stopping powers is 1% to 2% for electrons with energies above 100 keV. Between 10 keV and 100 keV, they are estimated to be 2% to 3% for low-Z materials and 5% to 10% for high-Z materials. The uncertainty of radiative stopping powers are estimated to be 5% below 2 MeV, 2% to 5% between 2 MeV and 50 MeV and 2% above 50 MeV. These uncertainties are considered to be approximately at the level of two standard deviations and of type B (ICRU 2001).

Although the uncertainties in the cross sections give rise to uncertainties in the end result of any dose calculation, it is to be noted that the relationship between these uncertainties is not simple. It is, for example, possible for errors to (partly) cancel out against each other in a simulation involving many electrons of different

energies moving along different paths. In this context, it is worthwhile to note that, for example, measured dose distributions from electron beams in water are very well reproduced by Monte Carlo results obtained with recent codes and cross section libraries.

## 8 Geometry and material specification

### 8.1 Volumes

Geometric volumes are defined by their boundary surfaces. Examples of surfaces are planes, cylinders, spheres, cones and more complicated structures. Codes such as GEANT4 and MCNP provide powerful geometric capabilities using so-called “combinatorial geometry” where complicated volumes are defined by defining logical operations on intersecting surfaces or volumes. In Penelope, surfaces are defined by matrix equations, which is a valuable tool for complicated geometries. For the modelling of a linear accelerator, however, a combination of relatively simple surfaces generally suffices.

### 8.2 Voxelised phantoms

For the modelling of the patient, a voxelised geometry is usually defined based on CT data. The voxels are rectangular and the resolution is based on the CT resolution. In general the dose is scored in CT-based voxels. The material composition and density of each voxel are determined from the CT number in that voxel as explained in the following.

### 8.3 Conversion of CT numbers into tissue parameters

#### 8.3.1 Conversion of CT numbers into electron density

Each pixel in a CT image is coded with a CT number  $H$ , which is given in Hounsfield units as:

$$H = 1000 \cdot \left( \frac{\bar{\mu}}{\bar{\mu}_{\text{H}_2\text{O}}} - 1 \right) \quad (8.1)$$

where  $\bar{\mu}$  and  $\bar{\mu}_{\text{H}_2\text{O}}$  are the mean values of the linear attenuation coefficients for the material in the voxel and for water, respectively.

Already in 1978 the first approaches to use CT numbers for determining tissue parameters were published (Kijewski et al 1978). A year later Parker et al (1979) derived a relationship between CT number and electron density for tissues at energies where the Compton interaction is dominant (so that photon absorption due to the photoelectric effect is negligible). Compton scattering is proportional to electron density. This is not the case for photoelectric absorption, which may contribute for approximately 10% to the attenuation at typical CT photon energies (Brooks et al 1981). Therefore it is recommended that the highest available energy on the CT scanner be used. In the work of Brooks, the Compton component of the Hounsfield unit  $H_C$  was determined by using dual-energy scanning or with a theoretical correction based on the chemical composition. The relative electron density  $\rho_e$  can then be determined from the relationship:

$$\frac{\rho_e}{\rho_{ew}} = 1 + \frac{H_C}{1000} \quad (8.2)$$

where  $\rho_{ew}$  is the electron density of water. The electron density can then be converted to mass density  $\rho$  via:

$$\rho = \rho_w \left( \frac{n}{n_w} \right) \left( \frac{\rho_e}{\rho_{ew}} \right) \quad (8.3)$$

where  $n$  and  $n_w = 1.802$  are the number of atomic units per electron for the specific material and for water, respectively, and  $\rho_w$  is the density of water. These two relations demonstrate that a CT scanner can be calibrated in terms of both electron density and mass density.

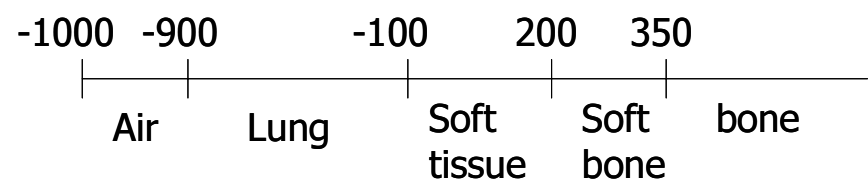
When using conventional treatment planning systems, CT calibration is mainly needed to determine inhomogeneity corrections for dose calculations. As the correlation between the heterogeneity correction factors and the electron density is well known, scanners are therefore calibrated in terms of electron density (Constantinou et al 1992). For Monte Carlo applications, however, it is primarily the mass density that is of interest (as this is an input parameter in most Monte Carlo engines). Nevertheless electron density is often used in Monte Carlo systems

because most scanners are already calibrated for conventional planning systems, so that this calibration curve can be used directly (Ma et al 1999).

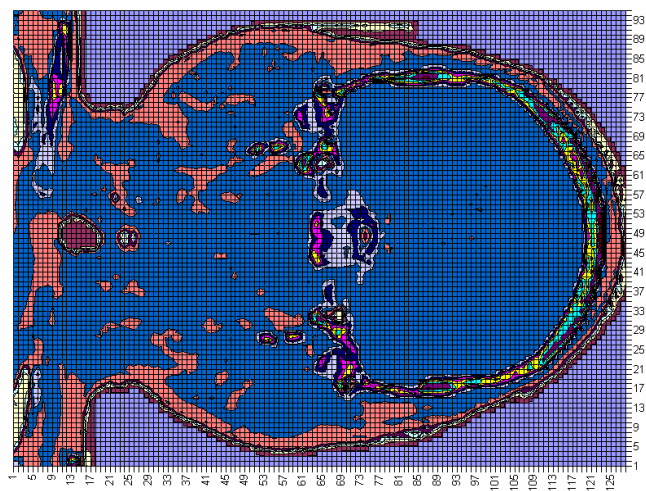
In the work of Henson and Fox (1984) a direct linear relationship between the CT number and the linear attenuation coefficient is demonstrated for cortical bone, without a need for determining the Compton component of the Hounsfield unit. Parker et al (1979) already did the same for calcium chloride solutions. McCullough and Holmes (1985) obtained a calibration curve consisting of two linear parts corresponding to the high- and low-Z regions. The curves show an overlap around  $H \approx 100$ . In that region care should be taken. An alternative is the use of discrete electron density - CT number pairs and a linear interpolation between those pairs (Ma et al, 1999). Constantinou *et al* (1992) demonstrated significant differences between calibration curves of different scanners, which illustrate the importance of individual scanner calibration.

### 8.3.2 *Conversion of CT numbers into tissue composition*

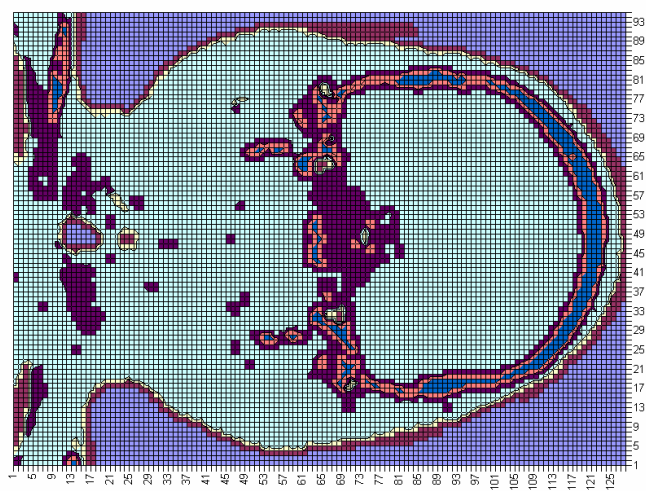
In a Monte Carlo dose engine not only the density needs to be determined but also the material (chemical composition) of each voxel. For Monte Carlo treatment planning the conversion from CT numbers to material properties is one of the steps that determine the accuracy of a calculation (du Plessis et al 1998). To correlate the CT number with the elemental compositions of the tissues, the CT number scale is often divided into discrete intervals corresponding with different tissues (De Marco et al 1998, Hartman Siantar et al 1997, Ma et al 1999, Wang et al 1998, McCullough and Holmes 1985). Normally up to six media are defined: air, lung, adipose, water, muscle, bone (in the example in figure 8.1, 5 materials are defined).



(a)



(b)



(c)

Figure 8.1: (a) Example of a conversion scheme from CT HUs to material compositions using 5 pre-defined materials (the given numbers are arbitrarily selected and should not be used in practice). Figure (c) illustrates the medium numbers obtained by converting the Hounsfield number data shown in figure (b).

In some of the previously mentioned papers, the CT scanner was calibrated with tissue equivalent materials to relate HUs with electron density. However, the chemical compositions of the tissue substitutes differ from those of real tissues. This appears to lead to large dose deviations (Verhaegen and Devic 2005). An interesting solution to this problem is introduced by Schneider et al (1996). Their method, the stoichiometric calibration method, is summarised below because of its importance:

- A set of materials (these materials do not really need to be tissue equivalent) with known chemical compositions are scanned in the appropriate CT scanner in order to obtain the corresponding Hounsfield units.
- This information is fitted to an equation linking the Hounsfield unit and the electron density. Via linear regression the three parameters of this equation can be determined.
- With these fitted parameters the Hounsfield units of real tissues are calculated using the tabulated chemical composition of these tissues.
- These data are then fitted to obtain the calibration curve for conversion of Hounsfield units into tissue /chemical composition.

This method is not free from criticism: as stated by De Kock and Schreuder (1996) the procedure is not valid for high-Z elements such as calcium. The influence of this inaccuracy is not known, however.

Du Plessis et al (1998) investigated the influence of different tissues on the dose distribution. Using Monte Carlo calculations, 16 body tissues were investigated and combined in subsets that can be assumed dosimetrically equivalent. The tissues in each subset are then given the same chemical composition. They found that the use of seven subsets is enough to obtain an accuracy of 1 %. In the cases of bone and lung a further subdivision corresponding with the mass density appeared to be necessary. In this subdivision all subsets have the same chemical composition – this assumption is a drawback for skeletal tissues (Schneider et al 2000) - but a different mass density. This means that not only the chemical composition but also the density must be discretised.

An alternative method is described by Ma et al (2002): in the EGS4 code used in MCDOSE the density is determined from the linear relationship between Hounsfield unit and mass density in a continuous way (as opposed to using a fixed density per interval). This has the disadvantage that the density correction on the stopping powers, which is applied to all materials before the actual Monte Carlo calculation, is generally calculated for a different density (the average of the corresponding CT subset). It appears that this effect can safely be neglected, however.

As stated by Schneider et al (2000) the method described by du Plessis et al (1998) has the disadvantage that it is applied for one specific beam quality only (i.e., an 8 MV photon beam). In principle it should be applied for all beam qualities used. Therefore Schneider et al (2000) describe an alternative way by focussing on the tissue parameters extracted from CT. Their method is based on the stoichiometric method introduced by Schneider et al (1996). Their scanner was calibrated by scanning 16 materials with known chemical composition to determine the parameters in the equation that link mass densities to Hounsfield units, using a least square fit. With the resulting equation they calculated the Hounsfield units for 71 human tissues, illustrating that it is difficult to identify tissues with different density and chemical composition by their Hounsfield unit, especially in the Hounsfield unit range between 0 and 100 (the soft tissues). The dosimetric effect of this limitation was not investigated, however. For Monte Carlo calculations, a database of 24 subsets with different chemical compositions was proposed. This number was not based on dosimetric results as in the work of du Plessis (1998), but on the estimated accuracy of the calculated Hounsfield units of the tissues. For the determination of the mass density, a bi-linear relationship was obtained with a discontinuity around  $H \approx 100$ .

### *8.3.3 Conversion of CT numbers into interaction probabilities*

Instead of converting Hounsfield units to material properties such as density and chemical composition, it is also possible to extract interaction probabilities directly from the Hounsfield unit. This technique was applied by Kawrakow et al (1996) in the electron Monte Carlo code VMC where the collision and radiation stopping powers are correlated with the Hounsfield unit. The photon extensions XVMC (Fippel 1999)



and VMC++ (Kawrakow 2000) of VMC also extract the attenuation coefficients for Compton scattering and pair production directly from the CT data. This method seems interesting as all material properties vary continuously with the Hounsfield unit and thus there is no influence of arbitrarily chosen boundaries separating discrete material subsets. In addition, this method does not require a calibration of the CT scanner.

On the other hand, it is not straightforward to implement this method in existing Monte Carlo software. Furthermore it is very difficult to model all possible interactions of electrons and photons with materials. Therefore in VMC and XVMC some types of interaction were neglected.

## 9 Accelerator modelling

### 9.1 General aspects

In Monte Carlo simulations, modelling of any radiation source consists of sampling required information about initial particles, namely the type of particle, its starting coordinates, direction cosines, energy, charge and particle weight. The particle weight is a statistical parameter necessary for the application of variance reduction techniques, see section 11. In the case of MCTP the primary source is the initial electron beam that enters the linac head (see figure 9.1).

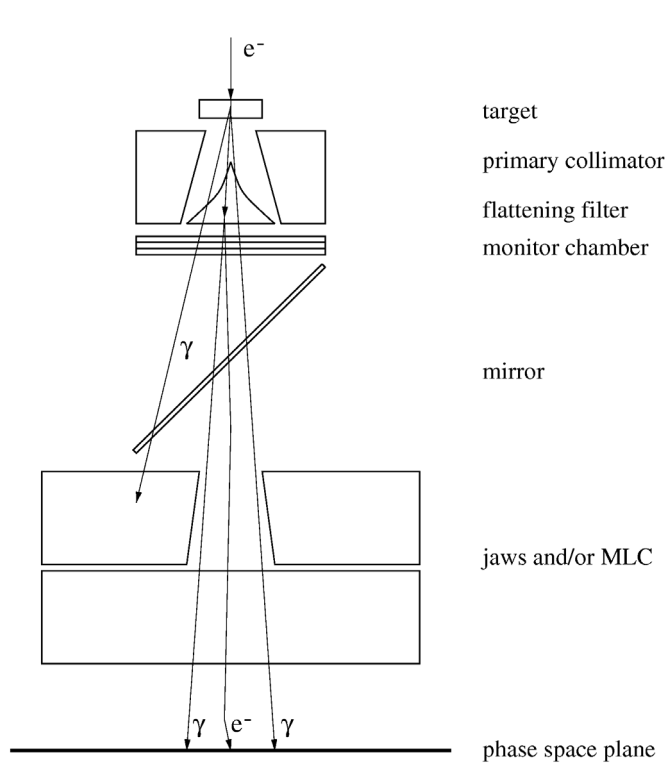


Figure 9.1: A model of a linac head (reproduced with kind permission of M. Fippel). The upper part consists of an electron source hitting the target and all components from target to mirror. The lower part contains the beam modifiers (MLC and jaws). For MCTP applications the phase space plane is usually situated just below the mirror, in contrast with this figure.

The linac can be divided into an “upper” part consisting of components that remain fixed for all possible beam settings (patient independent part) and a “lower” part consisting of the beam modifiers (patient dependent part). The upper part is modelled only once and a so-called phase-space file is generated at the entrance of the lower part. This phase-space file contains all required parameters (particle type, coordinates, direction cosines, energy) of a large number of particles entering the lower part of the linac. This file (possibly in parameterised form, see section 9.3) is then used as input for the actual MCTP calculation in which the lower part of the linac (beam modifiers) and the patient are handled in one process.

Since the first papers of Petti *et al* (1983a, 1983b), numerous works about the application of Monte Carlo techniques for modelling of linear accelerators have been published. Among the most prominent is the paper of Udale-Smith (1992), illustrating modelling of a complete linac for electron beams using EGS4. However, at that time Monte Carlo results were either very noisy or required very long calculation times (sometimes up to weeks). Another important event was the introduction of BEAM in 1995 (Rogers *et al* 1995), a system based on EGS4 but fully prepared for radiotherapy physics. Although other Monte Carlo code systems are also used for radiotherapy, EGS4 has had a significant lead in the field since the introduction of BEAM. Therefore, the following paragraphs are written from the BEAM-point of view. Still, for other code systems the methodology will be similar, apart from some additional work to develop the module for describing and modelling the linac.

## 9.2 *Modelling of the linac head*

As modelling of the linac head is the subject of an excellent topical review recently provided by Verhaegen and Seuntjens (2003) this subject will only be handled briefly here. Accurate dose calculations for radiotherapy treatment planning are only possible when the radiation beams are accurately modelled. In order to perform an accurate simulation of a linac beam, the following information is required:

- An accurate description of the characteristics of the initial electron beam as it emerges from the bending system. The minimum data set consists of peak energy and approximate spot size (Sheikh-Bagheri and Rogers 2002).

- An accurate description of all parts in the linac head and their mutual position. This description not only contains the geometry of the parts, but also the material composition and density (Antolak et al 2002, Van Battum et al 2003, Van der Zee and Welleweerd 1999). It should be noted that the density of sintered parts, such as X-ray targets, depends on the degree of sintering. Furthermore, metallic parts may consist of more than one metallic element, e.g. a tungsten target may be alloyed with rhenium. It is therefore important to obtain accurate information from the linac manufacturer in this respect.
- The objective of the simulation, as this can greatly influence the settings for cut-off energies and whether the use of variance reduction techniques is permitted (see section 11). The required standard deviation determines the number of source particles to be simulated.

### 9.3 *Virtual source model*

A phase-space file describing the output of the upper part of the linac head can be used as input for the particle transport through the beam modifiers (jaws, MLC, etc.) and the patient. As this file can be as large as several gigabytes, a virtual source model may be used as an alternative .

A virtual source model (see figure 9.2) is a parameterisation of a phase space file consisting of several sub-sources and serves as a particle generator for a Monte Carlo simulation. In figure 9.2, which represents a schematic overview of the virtual source model used in XVMC (Fippel et al 2003), two virtual photon sources are modelled (representing the contribution from target and flattening filter) and one electron source. It should generate particle distributions that are similar to the distributions from the original phase space file (within the accuracy required).

The validity of the virtual source model has been proven for fixed field size electron and photon beams (Deng et al 2000, Fix et al 2001, Fippel et al 2003, Francescon et al 2004, Schach von Wittenau et al 1999). The main advantage of the source model is the fact that it can be rapidly optimised for different linacs, starting from a set of measurements. Detailed information of the upper part of the linac head is less crucial. This is advantageous as it is not always straightforward to obtain correct information from the vendors. Another advantage (especially of a

measurement based source model) is that it does not contain noise as a phase-space file does. So noise in the phantom/patient then originates solely from the dose deposition itself and the so-called latent variance (Sempau et al 2001) is negligible.

A virtual source model should successfully pass a number of tests to verify that it mimics the original phase space file with great accuracy:

- Particle distributions generated by the virtual source model are similar to the original distributions from the phase space file (e.g. energy and angular distributions).
- Combined distributions generated by the virtual source model, such as the combination of angular and energy distributions, are similar to the original distributions from the phase space file.
- The virtual source model is capable of generating correct dose distributions for irregular and offset fields compared to measurements.

It is important not to incorporate too much detail about the construction of different linacs, as this greatly reduces the general applicability of the source model.

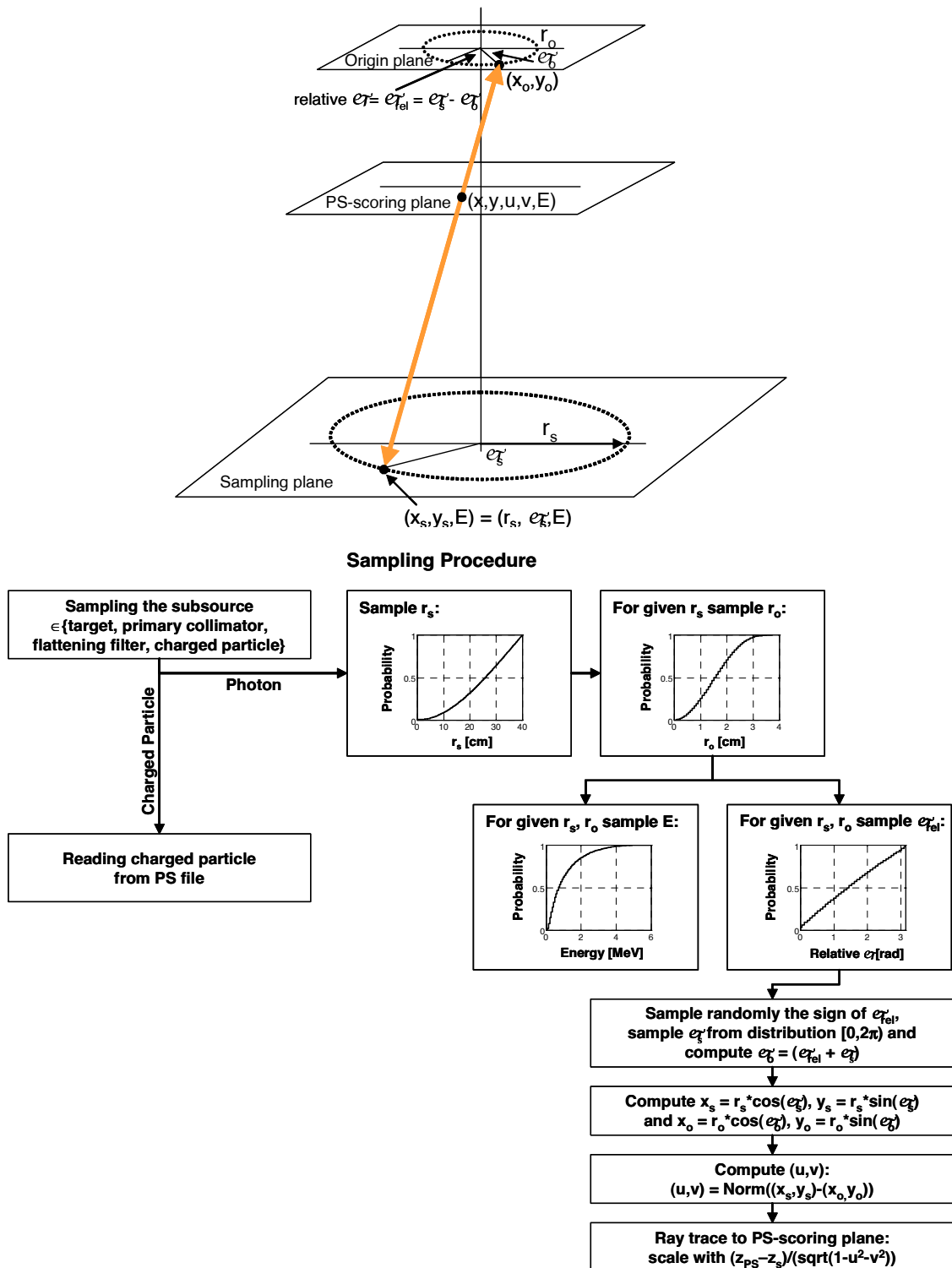


Figure 9.2: The concept of a virtual source model (reproduced with kind permission of AAPM from Fix et al (2004)).

## 9.4 Beam modifiers

Most of the calculation time of a full MCTP system is spent in the jaws and MLC. When tracking photons or electrons through thick, high-Z materials, many particles are lost, so it requires a lot of CPU time to obtain sufficient particles that manage to cross these parts. Much attention has been paid to modelling of these components, especially the MLC. Effects of tongue and groove geometry, inter-leaf leakage and intra-leaf transmission have been investigated thoroughly (Kim et al 2001, Deng et al 2001, Van de Walle et al 2003, Heath et al 2004).

To avoid the waste of CPU time on tracking of photons and electrons through the MLC and other collimating devices, approximations are often introduced. Boyer and Li (1997), focusing on the differences between the light field edge and the radiation field edge for an MLC with curved leaf ends, investigated an analytical solution for transmission through the leaf ends. This paper affected the ideas of other groups. For example the Stanford group, who had introduced the Monte Carlo dose engine MCDOSE, worked out a ray-tracing based method for calculating transmission through the MLC geometry (Chen *et al* 2000). This method only works with virtual source models, so a phase-space file cannot be used as input. To enable a full understanding of the order of the approximation introduced by this method, it is described in some detail below.

- Assuming a sub-source of a virtual source model, a line can be drawn with a certain angle from the source through the MLC to the isocentre plane. In the MLC this line is split up into many short intervals and for each end point of an interval it is determined whether the point falls inside or outside tungsten. By summing all the points inside the MLC material, the total distance travelled through tungsten is estimated. Based on this distance, a weight correction factor  $e^{-\mu(x,y)}$  can be determined, with  $\mu$  the attenuation coefficient (averaged over the energy spectrum determined from a measurement of the transmission through a leaf) and  $x, y$  the coordinates of the projection point in the isocentre plane.

- Electrons in the tungsten are immediately discarded.
- Every particle hitting one of the jaws is immediately discarded.
- For extended virtual sources the distance travelled through tungsten in the MLC is approximated as if the source is a point source. The initial particle weight is taken into account (convolution method).

The advantage of this method is that the weight correction map (sometimes called an ‘attenuation map’, or a ‘fluence matrix’, or even an ‘intensity matrix’) can be calculated before the actual particle transport is started, i.e. before performing the particle transport through the beam modifiers (this is even possible for dynamic MLC movements). During particle transport, a straight line is drawn from the source to the phantom, applying the already known attenuation correction, so that no CPU time is wasted in the collimating devices.

Deng *et al* (2001), also from the Stanford group, introduced MLC2MAP to investigate the influence of tongue and groove, which was originally not taken into account in MCDOSE. They illustrated that for a single IMRT treatment field the maximum tongue and groove effect could be up to 10 %. But for a treatment using more than 5 gantry angles the effect can be ignored for the cases they studied, especially taking into account patient set-up errors.

The group of Richmond, Virginia (the authors of the dose engine MCV), criticised the method described above as no beam hardening effect was taken into account (Keall *et al* 2001, Siebers *et al* 2002). Therefore they introduced a ray-tracing technique comparable to that of the Stanford group but with several extensions.

- First order Compton effect is included, to take into account leaf scatter.
- The attenuation coefficient is energy dependent.
- Tongue and groove is taken into account.
- Phase-space files can be used as input.

Their method can be described as compressing the MLC into a thin layer (Keall *et al* 2001). Siebers *et al* (2002) enhanced the accuracy further by dividing the leaf geometry in different so-called non-re-entrant regions (see reference for details).



Within these regions no cross leaf transport is taken into account. Siebers *et al* (2002) give a few examples of transport errors that can occur in this model, although they state that these errors can be minimised by increasing the number of non-re-entrant regions. They also state that the beam-hardening effect of the MLC is very well reproduced by including first-order Compton scattering, while ignoring electron transport (bremsstrahlung, electron scatter) and pair production. Several benchmarks provide good results. This method is 200 times faster than full Monte Carlo transport (using MCNP) when applying the model to a fully blocked field (all leaves closed). So, even though this is a ray-tracing technique that needs to be applied for every single particle (it is not possible to determine an intensity matrix in advance due to the generality of the phase-space file), a large increase in speed is obtained. An illustrative explanation of ray-tracing which is generally applicable (also for phase-space files) is given in figure 9.3.

For electron beams, instead of fully simulating the electron applicator, a parameterization can be used which takes into account the general construction of the applicator (Ebert and Hoban 1995, Cygler *et al* 2004). However, electron beams are quite sensitive for small details such as material composition (Rogers *et al* 1995, Antolak *et al* 2002, Van Battum *et al* 2003), which may differ between manufacturers.

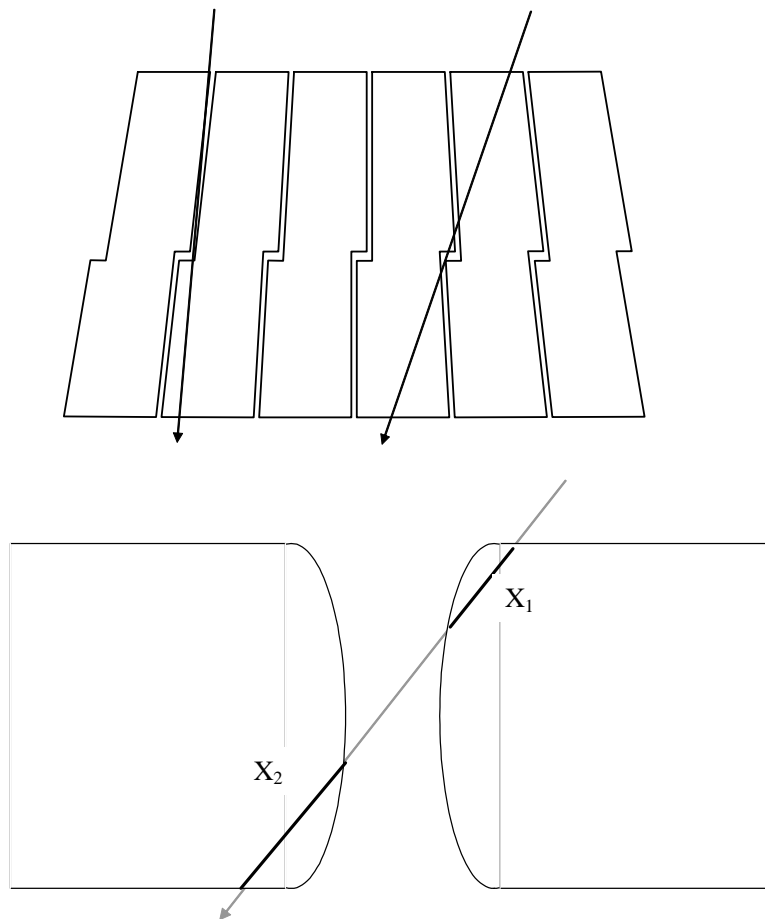


Figure 9.3: Ray-tracing technique. As illustrated in the figure, one simply sums the geometric path lengths  $X_1$  and  $X_2$  in the leaf material to apply an attenuation correction.

## 10 Dose scoring

### 10.1 Dose determination

To calculate the dose in a given volume, essentially two approaches are in use by current Monte Carlo programs: the kerma approximation and summing of the energy deposited. These methods are described in the following.

#### 10.1.1 Kerma approximation

When charged particle equilibrium is assumed, one can use a simplified algorithm for calculating the dose. Charged particle equilibrium implies that in any volume, the amount of energy carried out of that volume by electrons, is equal to the amount of energy carried into it by electrons. Therefore, under this assumption, one can neglect electron transport. It is well known that this approximation is often not accurate enough, but in some cases it may be applied to parts of the dose calculation (see Chapter 11).

The main advantage of the kerma approximation is that the dose can be calculated as the photon fluence  $\Phi(E)$  times an energy dependent fluence-to-dose function  $H(E)$ , where  $E$  is the energy of the (incoming) photon. (Sometimes  $H(E)$  is written as  $E(\mu/\rho)$ .) The function  $H(E)$  can be determined for each material at the beginning of the simulation. During the simulation of the particle tracks, one can calculate the fluence efficiently by a so-called track length estimator. Such an estimator uses the fact that the average length of a track through a volume is an unbiased estimator of the fluence in that volume. So if a photon with energy  $E$  travels a distance  $d$  through a cell, the program will add  $H(E)d/m$  to the dose estimate, where  $m$  is the mass in the volume.

#### 10.1.2 Energy deposition

The dose can also be calculated by summing the energy deposited in voxels. In this case, for each source particle, we need to know how much energy entered the

voxel, and how much left it: the difference being the energy left behind in the voxel. No approximations are needed for this method.

A possible concept for implementing this method is illustrated by the so-called \*F8-tally of MCNP. For each particle that crosses one of the boundaries of a voxel, its energy is added to, or subtracted from the dose estimate, depending on whether the particle enters or leaves the voxel.

An alternative approach (as applied in EGSnrc) is that for each particle step the energy deposition is scored in the corresponding voxel. As this scoring procedure is very fast (the voxel number is always in memory and must not be searched for as in MCNP) this does not significantly slow down the code.

## 10.2 Scoring grids

In most dose engines for Monte Carlo treatment planning, dose is scored in geometric voxels that are based on CT data. Unless the CT resolution is decreased to limit the number of voxels, this may lead to unacceptably high memory usage (> 2 GB for a phantom consisting of 150 slices of 512x512 voxels per slice). An alternative to decreasing the CT resolution, is the usage of a scoring grid that is superimposed on the geometric grid, decoupling scoring from geometry (see figure 10.1).

This is e.g. the case in Peregrine (Hartmann Siantar et al 1997) where the maximum number of scoring voxels is limited to  $150^3$ , and in MCDE (Reynaert et al 2004). The scoring grid can be defined in such a way that particle transport is minimally slowed down by the scoring voxels (De Smedt et al 2004). The same technique is used in the ORANGE code, which is an efficient extension of MCNP for scoring dose in a large number of voxels (Van der Marck and Hogenbirk 2004, Van der Zee et al 2005).

Due to decoupling of scoring and CT grids, it becomes possible to choose smaller grid spacings in certain regions (e.g. in interesting anatomical structures), and larger ones elsewhere.

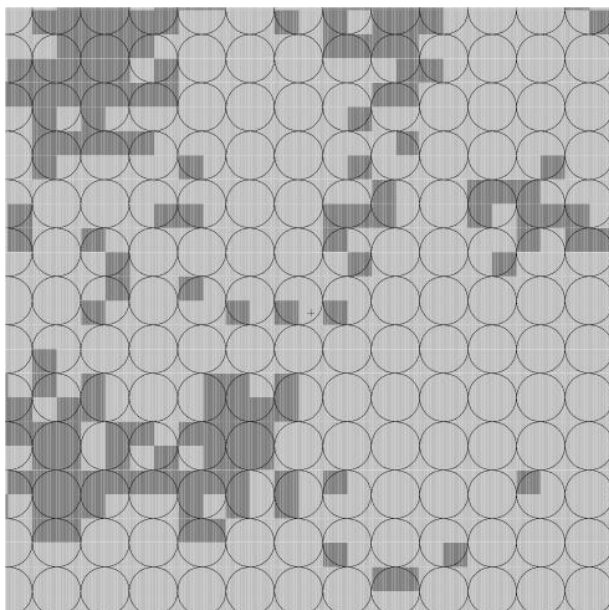


Figure 10.1: The principle of using a scoring grid (spherical voxels), which is independent from the CT-based material grid.

### 10.3 Spatial resolution

The scoring resolution (volume of the scoring voxels) is an important parameter that has a large effect on calculation time. The statistical uncertainty in the dose depends on the number of events occurring in, or in the direct neighbourhood of, a specific voxel. Therefore, increasing the volume of a voxel with a factor 2 has the same effect on the uncertainty in that voxel as doubling the number of histories. So to gain efficiency, large scoring voxels can be used. On the other hand, the use of excessively large voxels may lead to volume-averaging artefacts, especially in the neighbourhood of large dose gradients.

For dose engines that have the dose scored directly into the CT voxels, modifying the resolution of the CT grid has two effects: the first effect is the definition of the CT materials which influences the particle transport; the second effect is the volume-averaging of the energy deposited in each voxel. When a separate scoring grid is used (as discussed in the previous paragraph) both resolutions can be chosen independently, which may offer advantages (De Smedt et al 2005). So it is always

best to optimise this parameter for a set of patients before using the dose engine in clinical practice.

This issue becomes even more important in low density regions such as lung tissue. On one hand, it seems necessary to model the geometry with a high resolution because of highly inhomogeneous tissue. On the other hand, statistical uncertainty is an important concern in lung tissue due to its low density. Hence the possibility to choose the geometric and scoring resolutions independently is of much advantage in lung tissue.

#### *10.4 Conversion of Monte Carlo results to dose to water*

Monte Carlo dose calculation systems normally determine the dose to the medium in which the transport is simulated. Conventional dose calculations for photon beam treatment planning report dose to water. When comparing Monte Carlo results with results obtained in conventional systems the Monte Carlo results must therefore be converted to dose to water.

Additional arguments why dose to medium should be converted to dose to water are that dosimetry calibration protocols are based on absorbed dose-to-water standards and that TCP and NTCP data are given in terms of dose to water. The first of these additional arguments can be countered by stating that it is possible to convert measurements and conventional dose results to dose to medium. The last argument may seem somewhat stronger since biological data in terms of dose to media are not available. When using a treatment planning system with a TCP/NTCP based objective function it therefore seems best to determine dose-to-water. On the other hand one might argue that dose to medium is closer to reality. An interesting point/counterpoint discussion on this topic is provided by Liu and Keall (2002).

A conversion method based on the Bragg-Gray cavity theory is proposed in the work of Siebers et al (2000b, 2000c). The conversion factors are the unrestricted water-to-medium mass collision stopping power ratios averaged over the energy spectrum of the electrons (excluding delta rays). With MCNP calculations these authors determined the conversion factors as a function of depth in a phantom for 6 MV and 18 MV photon beams of a Varian linear accelerator. A depth dependence

was only found for air. Upon conversion, the dose conversion is about 1% for soft tissues and lung, and up to 12 % for bone depending on the beam quality. For a clinical case a shift of the dose volume histograms (DVHs) in target and critical organs is clearly visible.

This paper raised an interesting discussion concerning the uncertainty in the Monte Carlo dose information due to the CT data to medium conversion. Because of the large medium to water conversion factors, the choice of the material boundaries on the Hounsfield scale becomes critical (Fippel and Nüsslin 2000). This is an argument in favour of either the use of many material subsets in the CT conversion process or the use of a non-discrete conversion method such as that implemented in VMC (Kawrakow et al 1996), XVMC (Fippel 1999) and VMC++ (Kawrakow 2000). A possible improvement might be obtained by using imaging-based automated recognition of organs and bones to improve the accuracy of composition determination (Siebers et al 2000c).

## 11 Variance reduction techniques and approximations

### 11.1 Introduction

Obtaining sufficient accuracy in Monte Carlo calculations may require very long calculation times. To make Monte Carlo calculations more efficient, variance reduction techniques have been introduced. The efficiency  $\eta$  is defined as  $\eta=1/(\sigma^2 T)$ , where  $\sigma^2$  is the variance and  $T$  is the total calculation time for  $N$  histories (sample size). The variance,  $\sigma^2$ , is proportional to the inverse of the sample size  $N$ . Therefore the efficiency is a sample size independent quantity. If the calculation time per history decreases or the variance decreases for a fixed sample size, the efficiency of the Monte Carlo calculation increases, as a consequence of the definition of efficiency. For instance, the use of variance reduction techniques and approximations is required in electron transport codes to obtain sufficient accuracy within acceptable calculation times.

The success of variance reduction techniques depends on the situation, as the application of a variance reduction technique costs some additional calculation time per source particle. This loss (additional calculation time per source particle) has to be weighed against the gain (reduction in statistical uncertainty for a given number of simulated source particles). Because one is interested in knowing the dose with a prescribed (statistical) uncertainty, success depends on the reduction of the calculation time that is needed to obtain the required accuracy. However, it is not uncommon to find that a specific variance reduction technique in fact increases the calculation time.

An extensive description of variance reduction in general can be found in James (1980). Recent work on the application of variance reduction for dose calculations is described by e.g. Kawrakow and Fippel (2000).

In the next sections we discuss how the variance is determined and several commonly available variance reduction techniques in Monte Carlo dose calculations.



## *11.2 Variance of a Monte Carlo calculation*

As the Monte Carlo method is a stochastic process, the result obtained is an estimate of the mean and corresponding standard deviation. The most straightforward method is to split the calculation into e.g. 10 sub-calculations (starting with different random seeds) and to combine the obtained dose results to determine the mean and the standard deviation. A better estimate is provided by determining these values on a history by history basis (see Rogers et al 2002). When working with phase-space files (when modelling a linear accelerator head e.g.) the problem becomes more complicated as the mean and standard deviation should be determined as a function of the primary histories that enter the linac head, while the phase space file contains secondary particles as well. In BEAMnrc this problem is solved by tagging the primary histories.

## *11.3 Variance reduction techniques*

### *11.3.1 Particle splitting*

In a simulation of a linac and a patient, it is inefficient to track all particles in all directions, even if they do not go towards the patient. The simulation should be geared towards getting more particles to the patient, so as to deposit energy in the target volume. The technique called “particle splitting” is designed to do that: as soon as a particle gets closer to the target volume than a prescribed distance, the particle is “split into two”. This means, the program copies the current properties of the particle (position, energy, direction of flight) to a newly created one, which the program will “save” temporarily. Then the program goes on with the simulation of the first particle, almost as if nothing has happened. After the program has finished with this particle, it returns to the “copy” of the particle, and simulates the subsequent flight and interactions of that one. However, because different random numbers will be used for this one, this particle will follow a different path, and deposit energy at different places compared to the original particle.

In essence we have simulated one particle in the linac to get two particles in the patient. This is clearly more efficient, but also it is clear that we have affected the result itself, not only the statistical uncertainty: we have increased the probability that a certain particle will enter the patient. We have to balance this effect by assigning less importance to particles that have been split. In a Monte Carlo program, each particle is assigned a statistical “weight”. The calculated physical effect of each particle has to be proportional to its weight. In case of an energy deposition algorithm, a particle with weight  $w$ , that deposits energy  $E$  inside a certain voxel, contributes  $wE/m$  to the dose estimator inside that voxel (where  $m$  is the mass inside the voxel).

So when the Monte Carlo program splits a particle into two, it reduces the weight of both particles by half. In that way, the total energy that can be deposited by both particles is  $\frac{1}{2}wE + \frac{1}{2}wE = wE$ , which is the same as for the initial particle. Similarly, the program can split particles into e.g. five particles and reduce the weight of all five to  $w/5$ . The application to a particular situation will determine to what extent this is useful.

Particle splitting is e.g. often used for the bremsstrahlung photons in the target inside the linac head. Splitting factors of the order of 25 are not uncommon.

### *11.3.2 Russian roulette*

Russian roulette is the inverse of particle splitting. Particle splitting multiplies particles that get closer to the target volume and reduces their weight. Russian roulette, on the other hand, reduces the number of particles that move away from the target volume, while increasing the weight of the remaining ones.

Suppose a particle with energy  $E$  and weight  $w$  moves further away from the target volume than a prescribed distance. The program chooses whether to keep this particle (with, for example, 50% probability) or not. If it keeps it, the weight is multiplied by two. If it does not, the particle is “killed”, that is, the program simply forgets about it.

The Russian roulette technique can also be applied to situations where some particles have very low weights compared to others. Such situations can arise because of other variance reduction techniques.

### 11.3.3 Interaction forcing

It is very inefficient to track many particles through the target volume if they hardly ever deposit energy. For such cases, there is a technique called interaction forcing that ensures that whenever a particle enters certain designated volumes, it will undergo an interaction in that volume (and thereby deposit energy in that volume). The way in which this is implemented is the following. Suppose that for a particle with Monte Carlo weight  $w$ , the probability that an interaction in the designated volume will occur is 5%. The Monte Carlo program splits the particle into two: one particle (with weight  $0.05w$ ) that will interact in the volume, and an identical particle (with weight  $0.95w$ ) that will not.

The only difficulty is now the selection of the step size for the particle that will interact. Without interaction forcing, the probability that an interaction will occur is  $P(d)=1-\exp(-\mu d)$ , where  $d$  is the distance the particle would travel through the volume when not colliding anywhere in it (see also Chapter 2). To force an interaction, this has to be re-scaled to unity, making the probability to travel some distance  $l < d$  equal to  $P(l)/P(d)$ . The Monte Carlo program generates a random number  $r$ , and solves  $r=P(l)/P(d)$  for  $l$ :

$$r = (1 - e^{-\mu l}) / (1 - e^{-\mu d}) \quad \Rightarrow \quad l = -\frac{1}{\mu} \ln[1 - r(1 - e^{-\mu d})] \quad (11.1)$$

This expression is a modification of that in the example in Section 2.3.

### 11.3.4 Exponential transform

The exponential transform technique is designed for situations where the particle flux drops exponentially in a certain direction. This is typically the case in highly absorbing (shielding) materials. The exponential transform technique stretches the path length between interactions in a preferred direction. Also in this case, this distortion of the ‘true physics’ has to be compensated by a suitable redefinition of the particle weights. This variance reduction technique should be used sparingly and with great care.

### 11.3.5 Importance sampling

Importance sampling is a technique that samples preferentially in those areas where the largest contribution to the dose comes from, i.e. where “it is most important”. An example of this technique was already discussed in Section 2.3, where the step length of a photon was set to  $l = -(1/\mu)\ln(r')$ , to ensure that it is distributed as  $\mu \exp(-\mu l)$ . In this way, path lengths are generated according to the desired distribution, and one can set the weight of each step to one. The alternative, which is much less efficient, is to generate a flat distribution for the path length between 0 and a large maximum length, and set the weight of this step to  $\mu \exp(-\mu l)$ . The result would be many steps with very low weight, which would lead to very inefficient simulations.

Mathematically, importance sampling corresponds to a change of integration variable  $f(x)dx \rightarrow f(x)/g(x) dG(x)$ , where  $G(x)$  is the primitive function of  $g(x)$ . Points are chosen according to  $G(x)$  instead of uniformly, and  $f(x)$  is weighted inversely by  $g(x) = dG(x)/dx$ . Also in other numerical integration techniques (and even in analytical integration techniques) this is a well-known method often with very good results.

The same idea can also be used in a more approximate manner, which can be useful if it is not known a priori where the important contributions come from. In this case one can e.g. define a spatial grid, and for each sub-volume of the grid keep track of its importance for the dose at a certain location. The importances, calculated on a grid, can be used for the subsequent histories by incorporating them in the weights of the particles. One can then use particle splitting and Russian roulette to keep the weights of all histories between reasonable bounds, again to reduce variance. Some examples of importance sampling are:

- Source biasing: particles are preferentially started in the direction of interest, instead of isotropically.
- Simulating a disproportionate number of high-energy particles, because these contribute more to the dose.

- Biasing of secondary particle production, such as bremsstrahlung photons, most of which are very soft. In this case it usually helps to have a bias towards more energetic photons.

### *11.3.6 Stratified sampling*

We may feel intuitively that the reason why Monte Carlo simulation has such a large uncertainty is that the parameter values are sampled unevenly by the process of random generation, and that if the points were in this case more uniformly distributed the fluctuations would be smaller. Intuition is not always right, but there is some truth in it. The technique called stratified sampling addresses this point. Instead of sampling a random number 'as usual', the interval between 0 and 1 is divided into several sub-intervals ('strata'), and one generates random numbers within each of the sub-intervals. The technique enforces that if all intervals are of equal size, they will have the same number of random numbers. For instance, if there are 10 intervals ranging from 0 to 0.1, and from 0.1 to 0.2, etc., then each interval will get  $N/10$  random numbers. It is intuitively clear that by doing so the points will be more uniformly distributed. One can show that this type of uniform stratification will reduce variance, although the reduction may not be large. In general this technique is safe, and can be used with confidence.

### *11.3.7 Quasi-random numbers*

Another way of forcing the Monte Carlo parameter values to be uniformly distributed is to use so-called quasi-random numbers. The concept of quasi-random numbers arises from the realisation that the mathematical randomness of the usual pseudo-random numbers (see Appendix B) is neither attainable in theory nor necessary in practice. It is more meaningful to assure that the 'random' sequence has the properties, required to produce the desired result. In Monte Carlo calculations each random number is considered independent of the others, and the order in which they appear is immaterial. That is, correlations between successive points are usually of no importance, and this aspect of randomness can safely be abandoned for most

applications. An interesting comparison of integration by pseudo-random numbers with integration by quasi-random numbers for a specific example can be found at [www.fenews.com/fen24/levy.html](http://www.fenews.com/fen24/levy.html).

For the Monte Carlo application at hand, the dose calculation, use of quasi-random numbers is most probably an apt tool for variance reduction. Although it is a relatively safe technique, an option to switch it on and off is to be preferred in order to be able to check its impact. The Sobol' quasi-random number sequence has been implemented e.g. in XMVC (Fippel, 1999). An example of Sobol' points to sample the energy and angle of a particle is presented in table 11.1. The energy and angle are viewed as a two-dimensional phase-space that needs to be filled 'quasi-randomly'.

Table 11.1: Example of the use of quasi-random numbers.

Quasi-random number for generating energy $E$	Quasi-random number for generating angle $\vartheta$
0.5	0.5
0.75	0.25
0.25	0.75
0.375	0.375
0.875	0.875
0.625	0.125
0.125	0.625
0.1875	0.3125
0.6875	0.8125
0.9375	0.0625
0.4375	0.5625
0.3125	0.1875
0.8125	0.6875
0.5625	0.4375
0.0625	0.9375

This example shows that quasi-random numbers do not even appear to be random, but they do fill the integration volume more uniformly. The numbers above were generated with a program downloaded from [www.csit.fsu.edu/~burkardt/m\\_src/sobol/sobol.html](http://www.csit.fsu.edu/~burkardt/m_src/sobol/sobol.html).

#### *11.3.8 History repetition*

History repetition is a technique that re-uses pre-calculated histories in water. This is performed primarily for electron histories, because these are most CPU-intensive. The pre-calculated histories are 'applied' to the patient with different starting positions, and different directions of the 'recycled' particles. Corrections are made to the pre-calculated histories to make them applicable to the heterogeneous patient environment in which they are used. These corrections are based on the small angle approximation for multiple elastic scattering, whilst ignoring differences in the discrete interaction cross sections per unit energy loss between the different materials. The influence of these approximations on the dose results should be investigated. It was reported by Kawrakow and Fippel (Kawrakow and Fippel, 2000), that inclusion of history repetition and various other techniques did not cause XVMC to deviate from EGSnrc by more than 0.8% for two different phantoms.

The advantage of history repetition is that all interactions and tracks have to be sampled only once, and can be re-used several times.

#### *11.3.9 Woodcock tracing*

For Woodcock tracing, the maximum cross section for a large region, say the whole patient, is determined. The method then adds a fictitious cross section such that everywhere the cross section equals the maximum cross section. On the basis of this maximum, the next interaction site is calculated as explained in Section 2.3. This can be done irrespective of all the voxel boundaries in the patient. Next, it is determined whether this will be a 'real' interaction, or a 'fake' one (which is due to the fictitious cross section we have added). This depends on the local value of the 'real' cross section: if it is substantially smaller than the maximum, the probability is large that this will be a fake interaction. If so, the particle direction is unchanged, and the

tracking mechanism is started anew, from this new location. If, however, the interaction is determined to be 'real', then an interaction type is chosen, and the outgoing particles, and particle energies and angles are generated in the usual way.

The advantage of this tracing technique is that it does not need to account for many voxel border crossings, which slow down the particle transport. This technique has been reported to yield an efficiency gain of roughly 20% (Kawrakow and Fippel, 2000).

#### *11.3.10 Simultaneous transport of particle sets*

The dose engine VMC++ (Fippel, 1999) includes a particular technique dubbed 'simultaneous transport of particle sets'. It uses the continuous slowing down approximation (section 7.2) in combination with the transport equation in terms of energy (instead of path length). The claim is that in this formulation all materials are almost equal, which allows the program to simulate several particles simultaneously. The program is able to sample several quantities, such as scattering angles and distances to the next interaction, just once for all particles in a 'set'. Clearly this will result in a speed-up of the calculation. The effect on dose results is not clearly demonstrated in the paper in which this technique was introduced (Kawrakow, 2000).

#### *11.3.11 Kerma approximation*

In general the kerma approximation assumes that there is charged particle equilibrium (see also section 10.1.1). In this approximation no electron movement is considered, i.e. all electrons are immediately absorbed locally once they are created. In general, this approximation is not accurate enough for radiotherapy applications. However, when applied carefully, one can speed up the calculation while compromising the dose distribution only marginally. For instance, one could apply the kerma approximation only to secondary and higher order photons below a certain cut-off energy (Fippel, 1999). Alternatively one can apply it far away from the patient, because electrons in that area will probably not reach the patient (Ma *et al*, 2002).



### *11.3.12 Energy cut-off*

A simulation can be made much faster, by stopping a particle once its energy drops below a certain threshold. Based on insight in its physics, one can estimate the path length for a particle, given its energy and given the material it is travelling through. If this path length is below the required spatial resolution, we can stop the particle and assume its energy is absorbed locally. This can be done for both photons and electrons, but the typical cut-off energies will differ for both particle types.

### *11.3.13 Step size*

In case of electron transport, the step size in the program is important (section 7.2 for details). In some programs the user can vary the step size to achieve either greater accuracy (by choosing smaller steps) or faster simulations (by choosing larger steps). This choice should be carefully made.

## *11.4 Risks of variance reduction*

### *11.4.1 Two types of risk*

Basically, there are two ways to increase the efficiency of Monte Carlo dose calculations. One is to lower the variance  $\sigma^2$  of the problem by means of 'statistical methods'. The other is to reduce the amount of time spent per history, which can e.g. be done by tampering slightly with the physics of the problem, without influencing the end result, the dose distribution, too much. Both techniques have inherent pitfalls.

Reduction of the variance is often achieved by probing selected parts of the geometry more than other parts or by generating selected energies, or selected angles, etc., more than others. For example, if we are able to force many photons towards the patient, the variance of the dose calculation in the patient will be reduced. However, the danger is that other parts of the geometry, say parts of the shielding of the accelerator head, may not have been probed at all. In reality photons can scatter off the shielding and then hit the patient. If our Monte Carlo calculation did not generate such photons, relevant dose contributions will be missed. If this under-sampling is severe, it is possible that also the statistical error estimate does not

include this effect. Then, we are led to believe that the error is small, whereas in fact we have not accounted for entire parts of our geometry. Therefore care should be taken when applying statistical techniques to reduce variance. Still, these techniques are powerful tools to improve the efficiency of a Monte Carlo calculation.

Reducing the calculation time per history by simplifying the physics involved may also be dangerous. For instance, selecting a photon energy cut-off (photons below this energy are not transported any more), one assumes that these low-energy photons will deposit their energy at their current location. In reality, they will travel a short distance before being absorbed somewhere. The value for the cut-off should be chosen carefully, in accordance with the required spatial resolution. For each simplification, which is applied to achieve a higher efficiency, one should estimate the effect on the dose distribution to justify the simplification. If this is difficult, one can always perform a single run without the simplification, or with a less severe one, just to check.

#### *11.4.2 Example of variance reduction*

In this subsection the example of a beam collimator will be considered (see Figure 11.1). Photons entering the collimator material are far less likely to eventually reach the phantom below, compared to photons that pass through the opening in the middle. Therefore the efficiency can be increased by not always following a photon, and the electrons it creates, once the photon has entered the collimator. This can be achieved by applying Russian Roulette (10.2.2). For instance, if only one photon in a hundred should be tracked through the collimator, Russian Roulette with a 1:100 survival rate can be applied.

To estimate the effect of this variance reduction technique on the dose calculation, the dose profile across the beam just after entering the phantom is plotted. The dotted curve gives the results without using Russian Roulette, the dashed curve when applying Russian Roulette 1:100, while the solid line holds for RR 1:10000. In all three simulations the calculation time was the same.

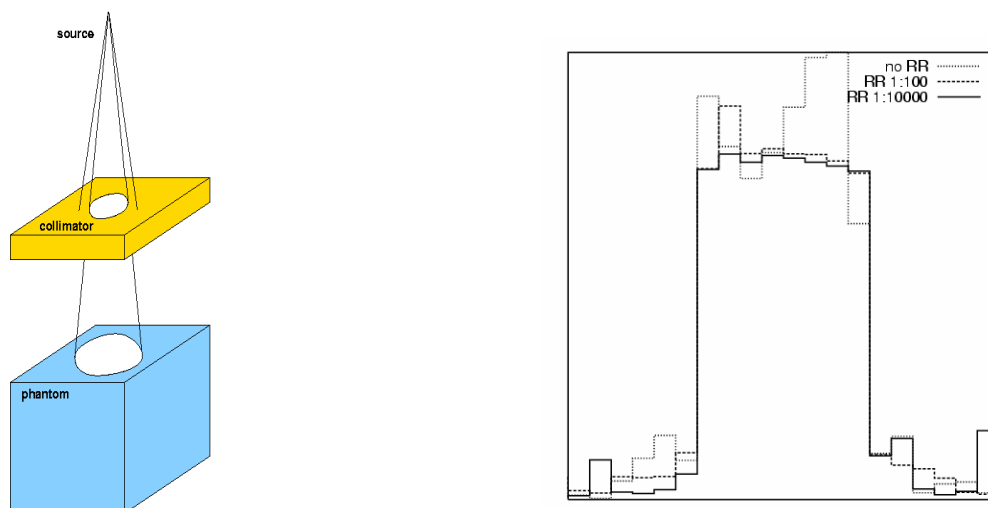


Figure 11.1: Example of variance reduction a: simulated geometry; b: fluence profiles for three different RR-values.

The plot illustrates that the dose profile calculation inside the primary beam benefits from the Russian Roulette technique. On the other hand, just outside the beam, the solid curve underestimates the dose. This was caused by “killing” most photons that entered the collimator. What is not shown in the picture is that this underestimation is larger than the estimated standard deviation. Therefore, if we would only look at the solid line and its standard deviation, we could not possibly know that there is a problem. Another interesting example is provided by Ma et al (2005).

## 11.5 Denoising

### 11.5.1 Introduction

The Monte Carlo dose calculation technique is a stochastic method, providing a mean dose and a statistical variance on the mean dose. Sufficient histories must be sampled to achieve “smooth” dose distributions. Noise introduces several negative effects in Monte Carlo treatment planning:

- Due to the noise the visualisation of dose distributions can be degraded (Miao et al 2003).
- Noisy dose distributions can cause problems in the optimisation process (Fippel and Nüsslin 2003) when using gradient methods. Problems can be expected when the objective function contains a factor that maximises the dose homogeneity in the PTV. In that case noise may appear as dose inhomogeneities to the optimisation process.
- Buffa and Nahum (2000) illustrated that DVHs can be broadened by noise when the statistical variance is too large. This is especially important in the PTV because of the sharp gradient at the high dose region of the DVH (Jiang et al 2000).
- TCP estimates can be underestimated due to noisy dose distributions (Buffa and Nahum 2000). This is a result of low dose values (due to noise) in some voxels, which influences the TCP as all tumour cells must be killed to be able to control the tumour. Any “cost function” shows a systematic difference when it is calculated using a noisy distribution. This is shown in a mathematically rigorous way in Kawrakow 2004. In the same work it is also illustrated that this effect can be corrected for.
- Dose prescription cannot be based on one point as in conventional planning, due to the noise in that voxel (Ma et al 2005). A possible solution is to use a relative isodose surface for prescription, as stated by Ma et al (2005).

So, apart from leading to uncomfortable visualisation, noise can also have an effect on the actual treatment planning. One possible solution is the simulation of a large number of histories to minimise statistical fluctuations. This is generally not practical without the application of variance reduction techniques, approximations and/or denoising. Recent overviews of effects of statistical noise on treatment planning are provided by Kawrakow (2004) and Ma et al (2005).

### *11.5.2 Denoising of DVHs*

Two groups introduced techniques for smoothing the DVHs (Jiang et al 2000, Sempau and Bielajew 2000). In the method of Jiang et al (2000) the Monte Carlo

DVH is treated as blurred from the noiseless DVH. A technique similar to image restoration is then used to obtain the noiseless DVH. To this end an estimate of the noiseless DVH is blurred and the difference with the MC image is minimised with a least-squares minimisation method. An iterative method is used to solve this problem. This procedure was applied to a hypothetical case and to some clinical applications where the differential DVH contained only one peak. For more general cases the algorithm has not been tested. In the paper of Sempau and Bielajew (2000) a deconvolution method was used. They regarded the DVH obtained with a limited number of histories as the “true” DVH (obtained by using an infinite number of histories) convolved by the noise.

### *11.5.3 Denoising of 3D dose distributions*

The methods described in the previous section have as limitation that only DVHs are smoothed while other dose distribution based output is not (TCP, visual inspection isodoses). Therefore Kawrakow (2002) introduced a method to denoise the dose distribution. A three-dimensional generalisation of a Savitzky-Golay digital filter was used with an adaptive smoothing window size (i.e. the number of surrounding voxels that is used). The size of the smoothing window is based on the statistical uncertainty in the voxel that is smoothed. A rejection method is used to ensure that no systematic bias is introduced. Five evaluation tests were introduced to validate the denoising method and to ensure that no bias is introduced. For these tests two dose distributions are compared, namely the “smoothed result” which is the dose distribution obtained with a limited number of histories and de-noising; and the “benchmark result” obtained by simulating a large number of histories (without de-noising). The five tests are summarised below:

- By visual inspection of isodose-lines the differences between the benchmark and smoothed results should be minimal (this was used in the work of Deasy (2000)).
- Difference area: to quantify the difference between the two DVHs corresponding to the smoothed and the benchmark result, the difference area of the DVHs is determined. This difference should be small.

- Maximum dose difference:  $D_{\max}$  in the PTV will be over-predicted by the MC-calculation due to noise. The difference between  $D_{\max}$  and the average dose must be small. For this technique a homogeneous dose in the PTV is assumed.
- Mean-square difference: a measure of the agreement between the benchmark and the smoothed dose distribution.
- x%/ y mm test: the fraction of voxels with a smoothed dose value that differs more than x% from a benchmark dose value at this point and there is no point in the benchmark dose distribution which is closer than y mm to this point that has the same dose (see Van Dyke et al 1993).

These evaluation tests have become a standard for smoothing algorithms used in Monte Carlo treatment planning. In comparison with simply running sufficient histories to reduce the noise below a certain level, a speed increase of 2 to 20 was obtained, depending on the accuracy test used.

Deasy et al (2002) introduced a method based on wavelet threshold denoising. The dose distribution  $d$  is separated into the smooth function  $s$  and noise  $n$ , i.e.  $d = s + n$ .  $d$  is an array of dose values that is linearly transformed into its discrete wavelet coefficients  $W(d) = W(s) + W(n)$ . All  $W(d)$  values below a positive threshold are set equal to zero. When  $d$  is then reconstructed from  $W(d)$ , the dose array  $d$  will be smoother. Again the calculation speed can be increased by a factor 2 or more.

Fippel and Nüsslin (2003) introduced the so-called IRON (iterative reduction of noise) method, which is based on the minimisation of the second partial derivative of the dose with respect to the three coordinates of a voxel. As the first derivative is not altered, dose gradients should be maintained. Only local dose differences are smoothed in this way. A restoration function is used to limit the correction applied to the dose. The statistical uncertainty is used, but the method also works without this information. This method was tested for phantoms and an IMRT treatment plan, obtaining reliable results whilst increasing calculation speed by a factor of 2 to 10.

Miao et al (2003) used adaptive anisotropic diffusion filtering. In this technique, smoothing is formulated as a diffusive process, which is suppressed or stopped at boundaries by selecting locally adaptive diffusion strengths. During each iteration, the

dose in a voxel will be augmented or decremented with a value that is determined by taking into account the partial differentiation in each direction of the three dimensions multiplied by their importance, based on the statistical uncertainty in this voxel. The number of iterations must be specified by the user. Using an excessive number of iterations alters the resulting dose information. In a recent paper by El Naqa et al (2005) the techniques described above were compared with the Content adaptive median hybrid filters introduced by El Naqa et al (2003). Three criteria were used for this comparison, namely improvement of the mean square error with respect to a reference dose map (obtained by applying a large number of histories), by the maximum dose difference relative to the reference dose map, and by a 2%/2mm pass/fail. It is postulated that pre-denoising uncertainties larger than 5 % are too large. None of the smoothing techniques were found to make the agreement to the benchmark worse in all cases studied (including real clinical cases).

## 12 Monte Carlo treatment planning

At present, Monte Carlo dose calculation engines are mostly used as a benchmarking tool for conventional TP systems, both retrospectively or prior to treatment. The ultimate goal is to obtain a treatment planning system entirely based on a Monte Carlo dose engine, i.e. where the dose engine is integrated into the optimisation loop (forward optimisation or inverse planning). As stated by Jeraj et al (2002), using an inaccurate dose algorithm will not only introduce dose errors, but will also lead to a wrongly optimised beam set used for treatment, the so called “convergence error”.

There are, however, several problems. The effect of statistical uncertainties on the calculated dose distribution (noise) might complicate the optimisation process if dose inhomogeneities in the PTV are penalised (Jeraj and Keall 2000). The main problem is that it seems practically impossible to restart the Monte Carlo calculation several times within the optimisation loop, as one calculation is quite time consuming already.

There are two major possibilities to tackle this problem, which can roughly be described as forward versus inverse planning. In a forward planning process, which is easiest to implement, the Monte Carlo method is used in combination with a conventional dose engine (e.g. pencil beam), providing an initial guess of the fluence distribution (or of the beam configuration concerning beam weights and leaf settings). The conventional dose engine is also used for intermediate steps. An interesting method described by Laub et al (2000) can be summarised as follows:

1. Use a pencil beam algorithm and optimise the beam settings (MLC settings and segment weights) in the conventional way
2. Perform a Monte Carlo calculation with the beam settings obtained in step 1
3. Use this Monte Carlo dose map to obtain new beam settings with the pencil beam optimisation routines and determine the “difference beams”, which are obtained by comparing the new beam settings with those obtained in the previous step



4. Determine the Monte Carlo dose distribution for the difference fields and add this contribution to the Monte Carlo dose map (obviously this contribution can be negative)
5. If the algorithm has converged, stop here; otherwise go back to step 3

The number of histories used in step 2 is only 80 % of the number required to obtain acceptable statistics. The number of extra histories in step 4 is limited because of the small cross section of these fields. The authors claim that the total number of histories needed for the entire optimisation is only 20 % higher than that of a single calculation. The problem of mixing different dose calculation methods is that the optimisation might fail to converge. Laub et al (2000) introduced a theorem concerning the maximum difference in accuracy that can still lead to convergence for a gradient based optimisation process. They conclude that the conventional dose engine should at least be a finite-size pencil beam algorithm. An equivalent method is applied in the Hyperion software (with the XVMC dose engine) of the Tübingen group (private communications M Fippel). This method is illustrated in figure 12.1.

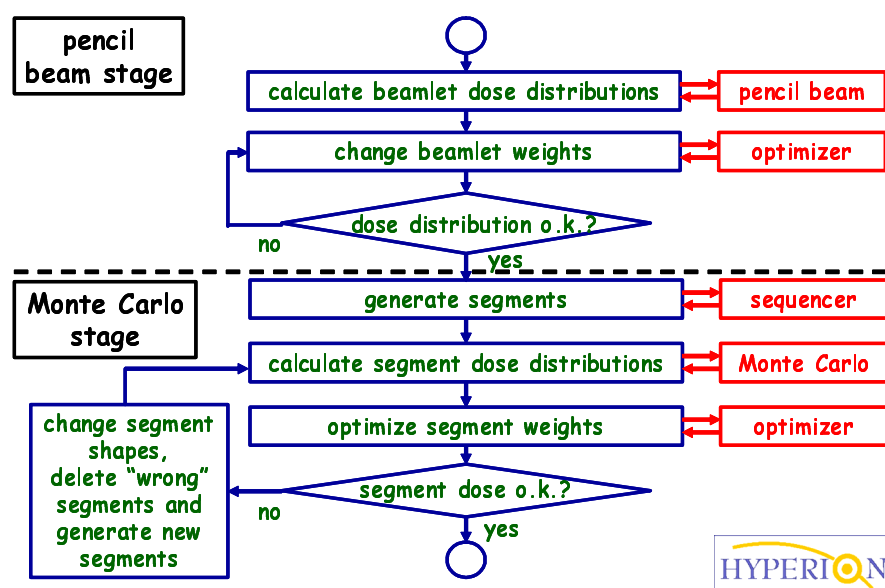


Figure 12.1: The optimisation process used in Hyperion (reproduced with kind permission of Fippel and Alber).

Monte Carlo calculations are performed for beam segments generated with the pencil beam algorithm. The Monte Carlo dose maps of the individual segments are then used for a monitor unit (MU) optimisation. From this, the value of the objective function (cost function) is determined. If the results are not satisfactory, then a number of beam segments, that have a negative effect on the cost function are removed and new segments are generated.

In the methods described above, the Monte Carlo dose engine is fitted into an existing optimisation process. In a full inverse process the optimisation algorithm is specifically devised for the Monte Carlo dose engine (internal optimisation). It is not necessary to combine this method with conventional calculations although it is always possible to use the pencil beam algorithm to obtain an initial guess of the beam settings.

In the paper of Jeraj and Keall (1999) the initial guess is obtained by adjoint MCNP calculations, starting from a photon source homogeneously spread over the PTV (see figure 12.2).

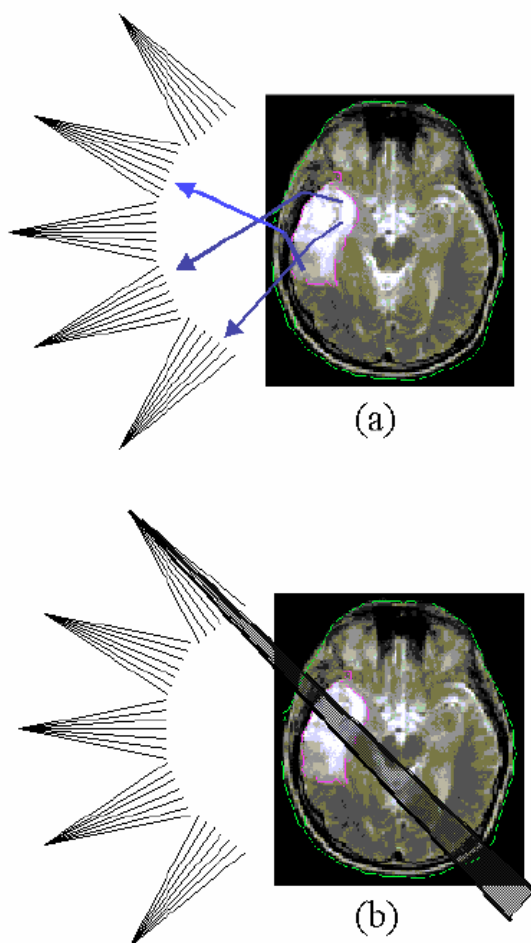


Figure 12.2: Principle of inverse optimisation for Monte Carlo treatment planning (reproduced with kind permission from Jeraj and Keall (1999) ).

This initial guess is then the starting point of the iterative optimisation process. All beams are divided into so called bixels (or beamlets) with small dimensions and for each individual bixel a dose distribution is obtained before the actual optimisation algorithm determines the weights of the individual bixels. In the paper of Jeraj and Keall a simulated annealing optimisation algorithm is used. The method only works in 2D (because of the high memory requirements).

Approximately the same method was used by Bogner et al (1999) and by He (2003). In this last work (which is a PhD thesis), the method was applied in 3D and the memory problem was solved by only keeping in memory dose information for all voxels within the beam surface of an individual bixel. The Monte Carlo dose engine used was based on MCNP but speed was increased by a factor of 11000 by

implementing a faster particle transport algorithm. With this method no convergence problems occur, as it is purely based on Monte Carlo. It is not straightforward, however, to take the contribution of scatter into account in the bixel dose maps (dose maps of individual bixels), so accuracy might be compromised.

Finally MCDOSE (Ma et al 1999) also provides the possibility of determining dose distributions for individual beamlets for inverse planning.

## 13 4D Monte Carlo dose calculations

Time dependent geometries are a challenge in radiotherapy dose calculations. One source of variation is the linear accelerator (virtual wedge, dynamic MLC). In the past these sources of motion have successfully been introduced in Monte Carlo models in the past. For instance, to tackle the dynamic MLC movement, the leaf positions can be randomised during the simulation taking into account the time dependent position distributions (Keall et al 2001, Liu et al 2001, Verhaegen and Liu 2001).

Another aspect of a varying geometry is patient motion. This again can be divided into three sources of uncertainty (Ding et al 2003): positioning errors (different position during treatment compared to CT scan), interfraction organ motion (e.g. digestive system), and intrafraction organ movement (e.g. respiration-induced motion). Here we will focus on the intrafraction organ movement as this can actually be taken into account into the treatment plan.

The effect of (residual) organ motion on radiation treatment has been investigated for over 20 years. Several techniques for reduction of respiration-induced motion have been introduced, ranging from active breathing control, deep inspiration breath-hold, gated radiotherapy, and real-time target tracking. As this is not MCTP specific, readers are referred to the paper by Ding et al (2003) and the references therein.

In general, organ motion is taken into account by defining the planning target volume (PTV) as the clinical target volume (CTV) with a margin large enough to ensure that the whole target is irradiated homogeneously. But in regions where organs at risk are close to the tumour some of this critical tissue may get included in the PTV (e.g. lung tissue, parotid glands, optical nerves, rectum, bladder, etc) and receive a high dose.

Here we will focus on the incorporation of respiratory organ motion in the dose calculation. Monte Carlo is an interesting candidate for this approach as the calculation time of a Monte Carlo simulation does not scale with the number of CT data sets used for 4D planning, as is the case for conventional dose calculation techniques.

In the paper by Ding et al (2003) two CT scans are used (total inhalation and total exhalation) and scans for intermediate respiration phases are interpolated (see figure 13.1).

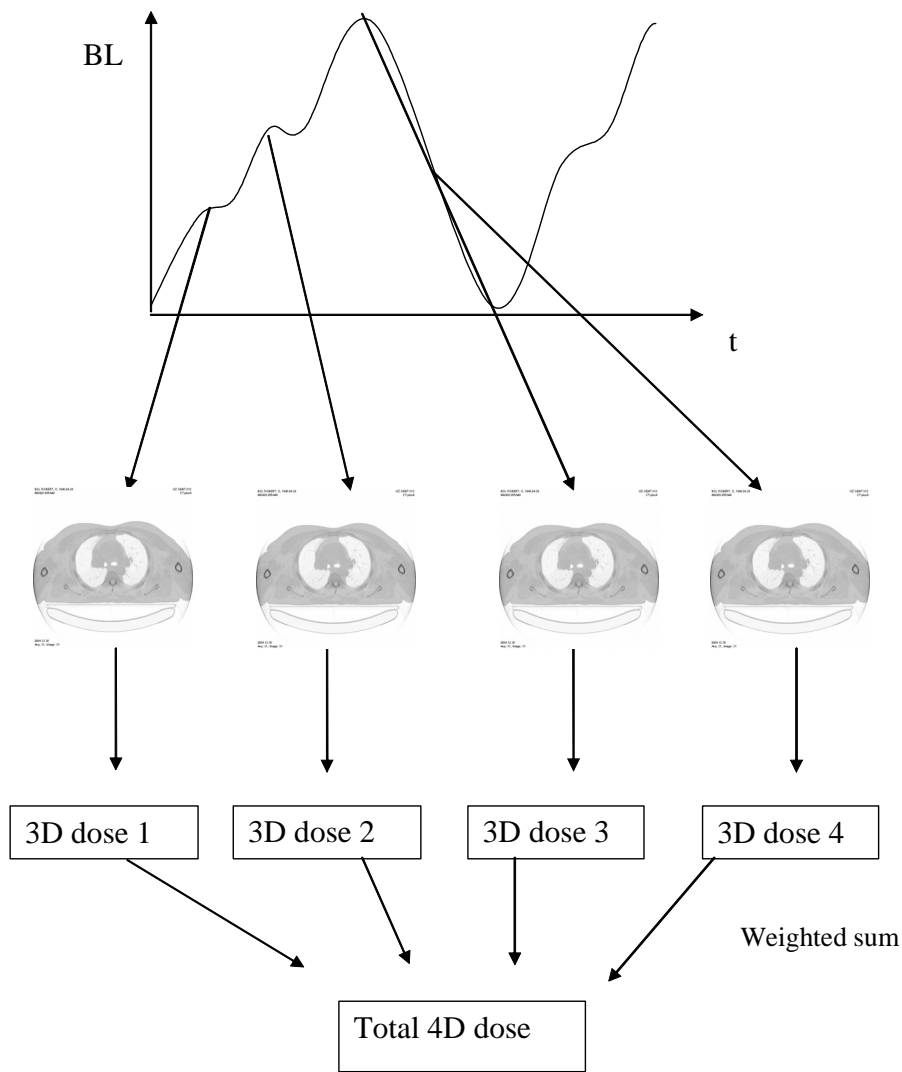


Figure 13.1: 4D MCTP method as e.g. used by Ding et al (2003) and Keall et al (2004). In this example four breathing levels (BL) are selected. For each BL a CT data set is obtained and the corresponding dose distributions are then summed to obtain the total 3D dose information.

The correlation of the geometric points in the two CT maps is not trivial. Dose calculations are performed on different reconstructed CT phantoms corresponding to different intervals of the respiratory cycle (see figure 13.2).

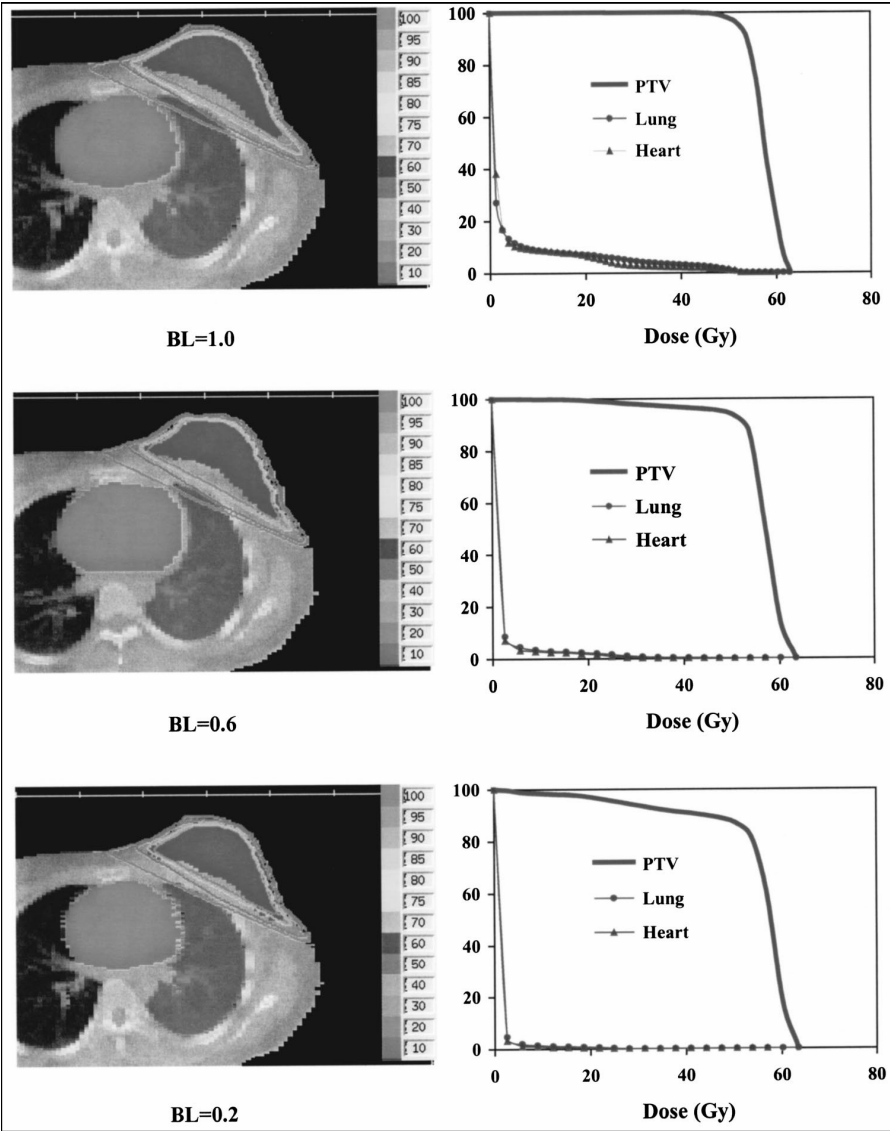


Figure 13.2: Dose distributions corresponding to different intervals of the respiratory cycle (BL= breathing level) (reproduced with kind permission of AAPM from Ding et al (2003)).

The obtained dose maps are summed taking into account the weights of the different maps. These weights are obtained by measuring the respiratory cycle with an external optical tracking system, detecting the movement of the chest-wall.

The method above described determines the actual dose distributions, taking into account organ movement, but the treatment itself is unaffected. This problem is tackled in the paper by Keall et al (2004). For each patient several CT datasets corresponding with different intervals in the breathing cycle are obtained. For each CT dataset the same beam directions are used, but the MLC settings are confined to the PTV of the dataset and thus differ from one set to another, simulating tumour tracking. The dose maps obtained are then combined into the so-called 4D treatment plan (see figure 13.3).

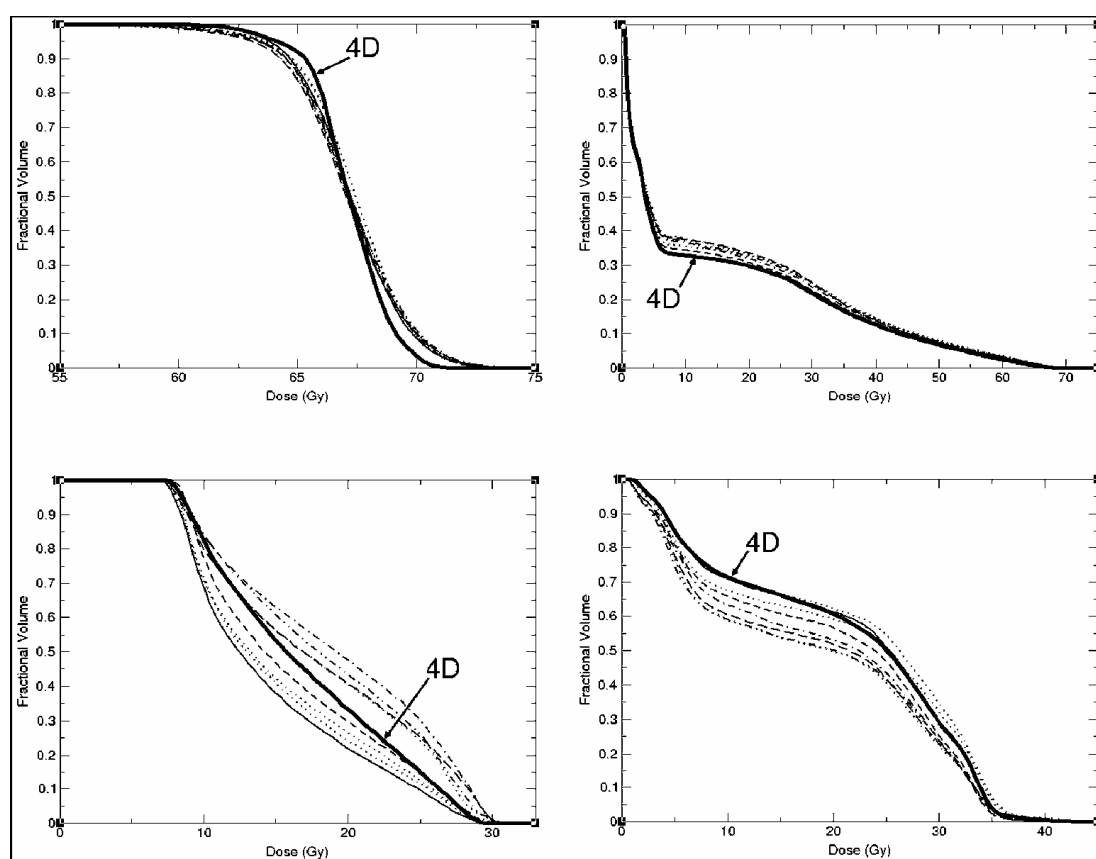


Figure 13.3: Comparison of 4D Monte Carlo results for tumour tracking with the MLC with 3D results at different instants of the breathing cycle (reproduced with kind permission from Keall et al (2004)). The DVHs are for PTV, lungs, spinal cord and heart, respectively.

Only a limited number of histories is required for each individual dose map as it is the sum of all maps that should provide enough statistics. Therefore the 4D Monte



Carlo calculation does not take more time than a 3D calculation. For a conventional TP system the calculation time is proportional to the number of breathing intervals.

A different approach was introduced by Paganetti et al (2005). To take into account interplay effects between patient and linac movement the time information is included into the Monte Carlo calculation geometry by transforming voxels. Voxel displacement maps (VDMs) based on 4D CT information were obtained, describing the positional changes of voxels within a volume of interest. This work focussed on proton beam Monte Carlo, but the underlying principle is general. This method is claimed to be less cumbersome compared to the method of Keall et al and Ding et al, described above (Paganetti et al 2005). Recently Heath and Seuntjens (2005) introduced a so-called direct voxel tracking algorithm to take into account internal and external contour deformation by reshaping the voxels as a function of time.

### ***Part III: Monte Carlo Treatment planning in practice***

## **14 Monte Carlo dose calculation engines for treatment planning**

### *14.1 Pioneering work*

Excellent reviews of the application of the Monte Carlo technique in medical physics have been published by Raeside (1976), Mackie (1990), Rogers and Bielajew (1990) and Andreo (1991). In the first reference a didactic explanation of the principles of the Monte Carlo technique, random number generators and variance reduction is presented, clearly illustrating that the method was not widely used at that time due to the unavailability of computers and/or unacceptable long calculation times. The review of Mackie (1990) focussed on Monte Carlo in radiotherapy, while that of Rogers and Bielajew reviewed Monte Carlo applications in dosimetry in general. The topical review of Andreo (1991) illustrated that the Monte Carlo technique gained importance in radiology and nuclear medicine, but also in radiotherapy. More specifically, an overview of the first efforts of using Monte Carlo for treatment planning is presented. Nahum (1988), Mackie (1989) and Ahnesjö and Aspradakis (1999) pointed out that the Monte Carlo technique was not going to be used for routine treatment planning due to the long calculation times. So the method was mainly used for verification of results obtained with conventional methods. As will be illustrated in the next sections, introduction into the clinic is presently ongoing. Webb (1979) performed calculations, ignoring the time demanding electron transport, leading to erroneous results close to interfaces and inhomogeneities. The problem of the long calculation times led to the introduction of hybrid systems as e.g. the superposition/convolution algorithms (Boyer and Mok 1984, Mackie et al 1985, Chui 1985, Ahnesjö 1987). For these systems the Monte Carlo method is used to generate so-called kernels, which represent the dose distribution of secondary particles generated in a photon interaction. During the actual treatment planning calculation the pre-computed kernels are convolved in the patient geometry. Although the input of these systems is based on Monte Carlo calculations, these are not regarded as actual MCTP systems. Yu et al (1995) extended this method by including explicit electron transport, leading to longer calculation times. The macro Monte Carlo

method (MMC, see section 14.6) was introduced in 1992 (Neuenschwander and Born 1992) and further enhanced in 1995 (Neuenschwander et al 1995) as a fast code for the transport of electron beams. The method uses pre-determined electron histories obtained in spherical volume elements (“kugels”) of different materials using EGS4. The actual MMC code then transports particles using the pre-determined kugel histories. Another variant of this method is the Super Monte Carlo (SMC) code, introduced by Keall and Hoban for electron beams (1996) and x-ray beams (1995). For further details the reader is referred to the excellent review paper on this and other dose calculation methods for treatment planning, provided by Ahnesjö and Aspradakis (1999). Currently, the superposition/convolution algorithms offer the best available “conventional” alternative for MCTP.

Direct Monte Carlo calculations on a CT phantom were performed by Manfredotti et al (1990), using the UNION algorithm to limit the number of CT voxels by combining neighbouring voxels of the same material in one large voxel.

The OMEGA project led to the introduction of the BEAM/DOSXYZ software (a set of EGS4 macros and subroutines specific for modelling of linear accelerators); an important step towards the practical implementation of Monte Carlo treatment planning (Rogers et al 1995). The code allows for detailed modelling of a linear accelerator head and in DOSXYZ, CT data, representing the patient geometry, can be inserted, by only generating a couple of input files. Most MCTP dose engines currently used in the clinic are partly based on this software package. Although applicable for actual MCTP calculations, large calculation times were the remaining drawback.

Therefore, the Voxel Monte Carlo (VMC) code was introduced by Kawrakow et al (1996) as a fast (direct) Monte Carlo dose engine for electron beams with a set of sophisticated variance reduction techniques (see section 14.4). For photon beams, Peregrine (Hartmann Siantar et al 1997) was introduced as a Monte Carlo dose engine using multiple variance reduction techniques (see section 14.5).

Wang et al. (1998) described a photon beam Monte Carlo dose calculation method for clinical cases, based on EGS4. Several variance reduction techniques were implemented into this dose engine. First, the number of first collisions in each image voxel is determined based on attenuation or through ray tracing. This

minimises the statistical uncertainty due to the otherwise random sampling. The derived improvement in calculation speed is about 5 to 10 fold. Second, by treating contiguous voxels having a similar atomic number  $Z$  as a single medium with varying density, they eliminate the need to resample interaction parameters at each voxel boundary. Only three different materials were defined, based on the density or Hounsfield units, namely water, bone and metal.

Francescon et al. (2000) applied the BEAM code to realistic mediastinal and breast treatments and compared the Monte Carlo results with those of the Pinnacle treatment planning system using the collapsed cone convolution algorithm (CCC). The agreement was reasonable (within 2.5%) for large fields. For narrow beams, one can expect disagreement between the Monte Carlo calculation and the treatment planning system (Francescon et al 2000). This latter situation was not explicitly investigated.

In the following sections, clinically applied MCTP dose engines are described.

## 14.2 DPM

DPM (Dose Planning Method, Sempau et al 2000) was introduced for simulating the transport of electrons and photons in radiotherapy. DPM achieves its performance by employing transport mechanics and electron multiple scattering distribution functions, which have been derived to permit long transport steps (of the order of 5 mm), that can cross heterogeneity boundaries. This is also made possible because of the stability of the random hinge algorithm employed in PENELOPE (Salvat et al 2003) across heterogeneities.

The underlying algorithm is a class II consensed-history scheme, with differential cross sections for hard inelastic collisions and bremsstrahlung events described in an approximate manner to simplify sampling. The continuous energy loss approximation is employed for energy losses below some predefined thresholds, and photon transport (including Compton, photoelectric absorption and pair production) is simulated in an analogue manner. Woodcock ray tracing is adopted to minimise the computational costs of transporting photons across voxels (dimension typically 1mm).

### 14.3 MCDOSE/ MCSIM

MCDOSE (Ma et al 1999) was developed as a routine dose calculation tool for radiotherapy treatment planning (RTP) based on EGS4 (Nelson et al 1985). Important features of MCDOSE are:

- Advanced virtual source models are used as source input for both photons and electrons
- Beam modifiers such as jaws, wedges, blocks, static and dynamic MLC fields are included in the patient simulation.
- Several variance reduction techniques such as photon interaction forcing, Russian roulette, electron range/region rejection and electron history repetition have been implemented (speed increase typically a factor of 10-30).
- Beamlet dose calculation for Monte Carlo inverse planning for both photon and electron beams.
- Dose volume histogram (DVH) construction using patient contour information
- Ray tracing through the beam collimating devices

The most recent version of this code is called MCSIM and includes, in addition to MCDOSE, a collection of interfacing software.

### 14.4 VMC, XVMC, VMC++

VMC (Voxel Monte Carlo system) was developed by Kawrakow et al (1996) as a fast calculation engine for electron beams. The stopping and scattering powers for the multiple-scattering simulation of electrons are determined directly from the Hounsfield number distribution in a continuous way and need no material specification (see section 7.3.3).

Later VMC was extended for photon beams in the fast X-Ray Voxel Monte Carlo system (XVMC) (Fippel 1999). XVMC was further optimised by Kawrakow and Fippel (2000). This code was re-programmed in C++ independently by Kawrakow leading to

VMC++ (Kawrakow 2000a) and by Fippel who continued to call his code XVMC (private communication I. Kawrakow). For dose calculations, XVMC and VMC++ offer significant speed improvements due to an efficient boundary crossing algorithm, variance reduction techniques like particle splitting, Russian roulette and history repetition. The efficiency can be further improved by optimizing transport parameters such as the electron cut-off, maximum electron energy step size, photon energy cut-off and a cut-off for kerma approximation. As XVMC and VMC++ are currently being introduced in several commercial TP systems, both engines are discussed below.

#### 14.4.1 XVMC

In XVMC the beam collimating devices are handled by full Monte Carlo transport (although the electrons are modelled using the CSDA). This is, however, programmed more efficiently than in BEAM (Fippel 2004).

Originally, the energy of an electron at the end of its track was deposited locally when its energy drops below the cut-off energy. A new approach has been implemented in which track-end electrons instead are transported by their residual range in a single 'normal' condensed history step. This modification increases the CPU time per history but allows higher cut-off energies, so that on balance the speed of the calculations is increased. A kerma approximation (only applied to secondary or higher order photons with energy below the kerma cut-off energy  $K_{\text{cut}}$ ) is introduced.

XVMC (the Fortran version developed by Kawrakow and Fippel (2000)) is currently being implemented by scientific groups such as the McGill group of Montreal (Seuntjens et al 2004). They introduced an interface between a conventional TP system and a Monte Carlo PC cluster. The C++ version of XVMC is currently being introduced in commercial MCTP software, but is also used by scientific groups as illustrated by Krieger and Sauer (2005).

#### 14.4.2 VMC++

In VMC++ (Kawrakow 2000a), instead of introducing a virtual source model the speed of the simulation of the upper part of the linac head is increased by several

orders of magnitude by using the so-called directional radiative splitting (DRS). This technique is an advanced particle splitting method. Bremsstrahlung photons generated in the target are split into N sub-particles. Photons that are not pointed to a pre-defined region of interest are handled with Russian roulette. This technique ensures that less calculation time is spent on photons (and corresponding secondary electrons) that will not reach the patient (only 2-3 % of the photons generated in the target reach the patient). With the combination of the DRS method and other variance reduction techniques, the simulation of the upper part of the linac takes only about 10-20 % of the calculation time in the phantom/patient geometry. VMC++ has been implemented as a dose engine in the commercial planning system of Nucletron for the simulation of electron beams. A separate “fluence engine” or source model generates particles that are tracked through the patient geometry using VMC++.

#### *14.5 PEREGRINE*

PEREGRINE is a Monte Carlo dose calculation engine which is commercially available from North American Scientific NOMOS Radiation Oncology Division since early 2002. It is implemented in their Corvus inverse treatment planning system, but can also be integrated in other planning systems that allow import and export in an extended RTOG file format. The software is installed on a PC cluster which is also delivered by the vendor.

In PEREGRINE the beam-delivery system is divided into two parts: an accelerator-specific upper portion and a treatment specific lower part (Hartmann Siantar et al 2001).

The upper part, consisting of the electron target, primary collimator, flattening filter(s) and monitor chamber is pre-defined by NOMOS based on the linac vendor's model specific information. BEAMnrc generated phase space files, scored below the monitor chamber, are analysed and condensed into correlated histograms which describe the energy, radial and angular distributions for each sub-source of the source model (Schach von Wittenau 1999). These correlated histograms, along with information about the treatment specific lower part, consisting of beam modifiers such as MLC, collimators, apertures, blocks and wedges, are stored in a so called device



file for each accelerator model. To correct the output for particles that are backscattered in the monitor chamber, a monitor chamber correction function is included in the device file (Hartmann Siantar et al 2001). Finally, a dose per monitor unit calibration factor is included for the conversion of the number of delivered monitor units to the number of incident particles.

The patient transport mesh is a Cartesian map of material composition and density determined from the patient's CT scan. Dose deposition is scored in a scoring grid (dosels), which is independent of the material transport mesh. During the dose calculation, the standard deviation in the dosel receiving the highest dose is tracked and when this reaches a level specified by the user the simulation is terminated. The particle transport is based on EGS4. As a simplification, electrons and positrons are treated equally (Hartmann Siantar et al 2001). Variance reduction techniques such as Woodcock tracing, particle splitting, Russian Roulette, range rejection, and source particle reuse are applied to increase the efficiency of photon and electron transport.

#### *14.6 Macro Monte Carlo (MMC)*

The MMC code uses pre-computed kugels (electron histories stored in look-up tables, see 14.1). To handle material interfaces the diameter of the kugels is decreased while approaching a boundary. The MMC method was introduced in a period when it was not yet realistic to perform full Monte Carlo transport in treatment planning systems. However, this system is still used in the treatment planning system of Varian. Varian has benchmarked the Macro MC system (fast eMC) against EGSnrc for heterogeneous phantoms. They state that the accuracy is comparable to standard Monte Carlo codes, but approximately 10 times as fast (Neuenschwander et al 1995).

### *14.7 Dose Engines serving as commissioning tool*

Several groups have introduced dose engines for MCTP that are mainly a commissioning tool for other TP systems. MCV was introduced by Siebers et al. (2000a) primarily as an accurate verification tool. Later ray tracing through the MLC was introduced to speed up calculations (Siebers et al 2002). Leal et al (2003) programmed an automated Monte Carlo system for routine IMRT verification (see figure 14.1). More or less the same was achieved by Spezi et al (2002), Reynaert et al (2004) and Seco et al (2005), although different methods were used.

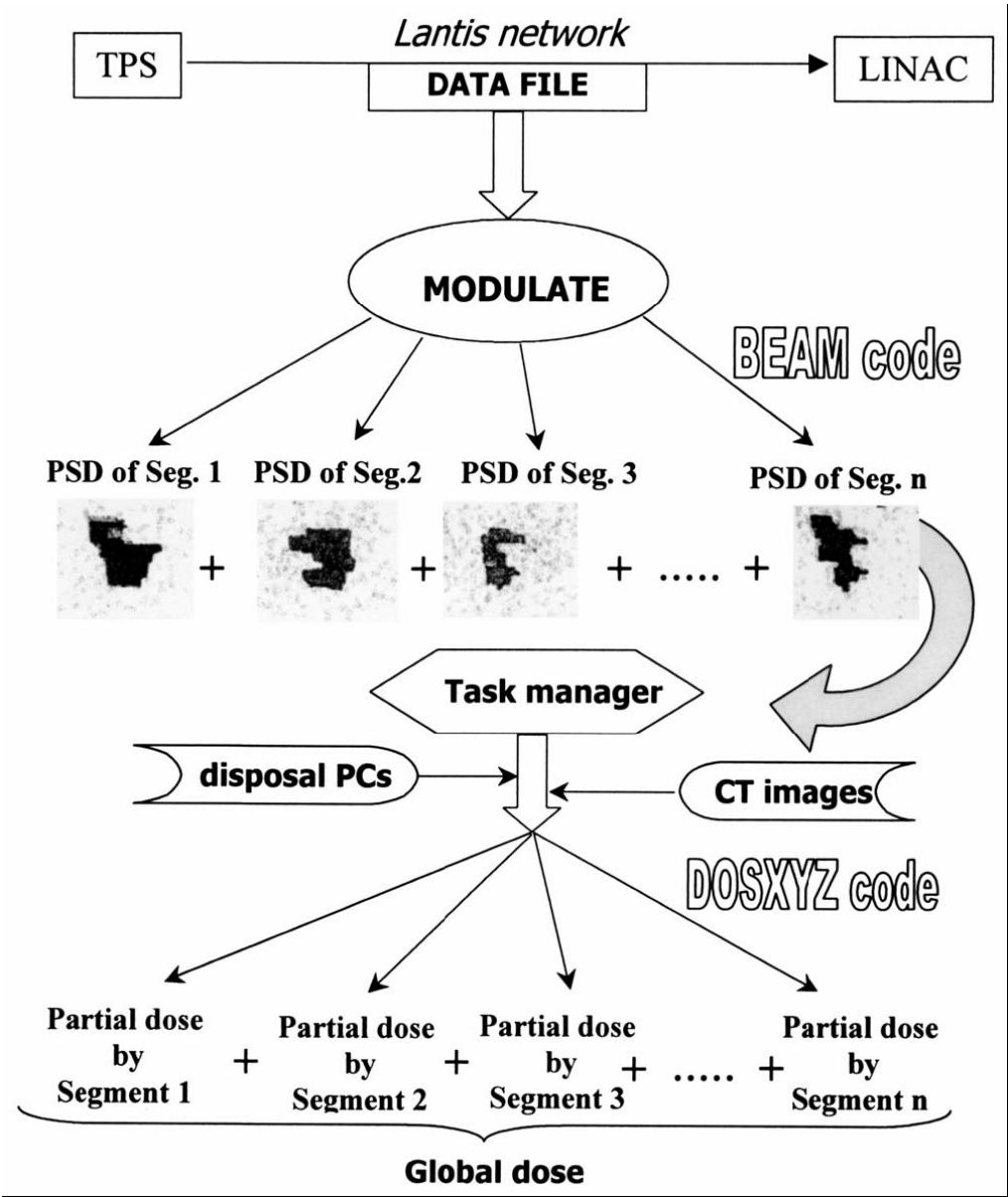


Figure 14.1: Example of using BEAM and DOSXYZ as a Monte Carlo dose engine for treatment planning (reproduced with kind permission of Elsevier from Leal et al (2003)).

## **15 Available commercial MCTP systems**

As mentioned in the Introduction, vendors of clinical treatment planning systems have started to offer Monte Carlo dose calculation engines. An overview of the current state of affairs (dd. 13/12/2004) is presented in Table 15.1. It is realised that some or most of the information in the table is of temporary value only. Nevertheless the table shows how active the various commercial players are in this area.

The information in the table was solicited from all the vendors. All entries, especially the future plans, reflect the information obtained from the vendors as of December 2004.

Table 15.1: Overview of (future) availability of Monte Carlo dose calculation engines in commercial treatment planning systems of vendors who replied to our survey. Status as of 13 December 2004.

Company	Product	Release	Version	Monte Carlo for $\gamma$	Monte Carlo for e $^{-}$	Inverse optimisation / biological models
BrainLab	iPlan RT Dose	Fall 2006	4.0	XVMC	XVMC	Yes
CMS	XiO	June 2005	4.3.0	XVMC	XVMC	Yes
	Monaco	June 2005	4.3.0	XVMC	–	HYPERION
Elekta	Elekta-Plan	2005	1.1	XVMC	–	
		2006	1.2	XVMC	XVMC	
		2007	2.0	XVMC	XVMC	HYPERION
Nucletron	DCM (now OTP)	March 2002	2.0		VMC	
	OTP	2003			VMC++	
		2005	1.4	VMC++	VMC++	Optim. for e $^{-}$
	PLATO	–	–	–	–	–
	TMS	–	–	–	–	–
Philips	Pinnacle <sup>3</sup>	Not available yet	6.9c (beta version)	–	Modified DPM in 6.9 (AMC-Adac MC)	–
Varian	Cadplan	–	–	–	–	–
	Eclipse	Summer 2004	7.2.X	*	Macro MC	–
Siemens	KonRad	July 2003	v2.1	–	–	–
Dosisoft	Isogray	June 2005	–	–	Penelope	–
North American Scientific	Corvus, Peacock	2004	v5	Peregrine	–	Yes

\* Convolution/superposition (Monte Carlo based phase space), release Spring 2005.

## 16 Monte Carlo specific issues of commissioning

### 16.1 Introduction

A commercial MCTP system for IMRT treatments can be benchmarked by measurements, or by an independent accurate Monte Carlo dose engine (preferably a dose engine with only few approximations). Examples of using a MC dose engine for benchmarking are presented by Heath et al (2004), and Reynaert et al (2005), both commissioning the Peregrine system. Benchmark measurements for 3D plans can be performed in heterogeneous phantoms. In the method described by Ma et al (2003), a PMMA phantom with various lung and bone inserts is used for point measurements with an ionisation chamber for the beam setup intended for the patient treatment. The rationale of this approach is the assumption that if the phantom measurements and phantom calculations are in agreement for a specific beam set-up, then the patient calculations will also be correct for the same beam set-up.

In general, commissioning of MCTP systems is hardly different from the conventional (semi-) analytical algorithms. Good practical guide lines on how to commission a 3D TPS were given recently by working parties of the AAPM (AAPM 1995, Fraass et al 1998), the ESTRO (ESTRO 2004), and the NCS (NCS 2006a). These reports not only describe what should be tested, but also define test procedures in considerable detail. However, there are some items, which are specific to MCTP:

- particle source
- segmentation
- normalisation
- variance reduction

The following paragraphs will treat each of these items in more depth.

## 16.2 Particle source and beam modifiers

Particles used in MCTP are generated from a *particle source*. Generally, there are two possible sources representing the output of the upper part (patient independent part) of the linear accelerator (see section 9.1 for more details):

- a phase-space file based on a full simulation of the upper part of the linac.
- a virtual source model, which mimics the radiation from the upper part of the linac head

Both source types are normally tuned by the MCTP system vendor using a set of in-phantom measurements of lateral- and depth-dose distributions, provided by the hospital physicists, and/or on the linac vendor's model specific information (see also section 9.3). A basic measurement set used to configure the MCTP system generally consists of some standard symmetrical fields, and possibly also a set of offset fields and asymmetrical fields, depending on the vendor.

A second aspect is the handling of the transport through the beam modifiers (see section 9.4). If ray-tracing is used it is important to benchmark irregular fields, and also to verify the dose outside the field. It is preferable that the user should be able to switch off the ray-tracing approximation and to alter the cut-off energies in the linac head to perform an evaluation of the applied approximations.

The quality of the final model depends on:

- quality of the basic measurements
- quality of the information provided by the linac vendor
- quality of the Monte Carlo dose engine used

Once the model is provided by the vendor, the user may perform calculations for non-standard set-ups to compare with measurements. If necessary the vendor can be asked to re-tune the source. This situation is not very different from some conventional TP systems.

Periodical accelerator QA should be aimed at keeping the machine performance according to the particle source contained in the MCTP system as it would not be practical to retune the dose engine after each maintenance operation of the linac.

### 16.3 Segmentation

In contrast to most conventional dose calculation algorithms, Monte Carlo dose calculation engines need to know the characteristics (e.g. composition and density) of the irradiated volume. Therefore an important concern in MCTP is the proper segmentation of matter. Thus, the conventional clinical segmentation in *PTV* and *organs at risk* is not sufficient. Even a segmentation based on *electron density* derived from CT-data is generally insufficient. In MCTP dose engines an additional segmentation converting Hounsfield numbers to matter (tissue type) is necessary (section 8.3.2).

Using a CT-phantom with known composition and dimensions, a method to verify the segmentation process could be (Verhaegen and Devic, 2005):

- scan the CT-phantom
- perform an automatic segmentation by the system ( $\Rightarrow$  *segmentation 1*)
- calculate, for a reference setup, the Monte Carlo dose ( $\Rightarrow$  *MC-dose 1*)
- perform a manual segmentation ( $\Rightarrow$  *segmentation 2*)
- calculate, for a reference setup, the Monte Carlo dose ( $\Rightarrow$  *MC-dose 2*)
- compare segmentation (*segmentation 1*, *segmentation 2* and phantom)
- compare dose grids (*MC-dose 1* and *MC-dose 2*)

### 16.4 Normalization / MU determination

In MCTP systems the beam can be calibrated directly by calculating the dose at the isocentre for a reference 10 cm x 10 cm field. For this field the dose per primary history is used to define the relationship between the dose (in Gy) and the number of monitor units MU. Some issues are important, however:

- It is advisable to simulate the reference situation with a large number of histories in order to get the best possible statistics (0.3% or better, Ma et al 2005).
- It is advisable to use a high depth resolution to avoid volume averaging effects

A problem is that the monitor output may depend on the position of the collimating devices due to backscatter of photons from the collimators towards the



monitor. For small fields the backscatter contribution increases. In an Elekta accelerator, the back scatter plate minimises this effect, but for e.g. a Varian machine these corrections are important (see e.g. Liu et al 2000, Verhaegen et al 2000, Hartmann Siantar et al 2001). Nevertheless, normalisation in an MCTP system is rather straightforward, compared to conventional systems where the MUs need to be linked to the particle fluence below the collimating devices (Ahnesjö and Aspradakis 1999).

Just as for conventional systems, MCTP calculations may be checked with a so-called *dose check program*, a program based on a simple formalism to calculate the dose (in Gy) from the MU setting for each segment. This check can be seen as a prolonged commissioning on normalisation and the *Gy-to-MU conversion* (Spezi et al 2002, Ma et al 2004). In Fox Chase Cancer Center, Philadelphia, USA, the MU calculations performed in the Monte Carlo dose engine MCSIM are routinely validated experimentally with a quality assurance phantom (Ma et al 2004).

### 16.5 Variance reduction

Variance reduction is intended to increase the efficiency of a Monte Carlo dose engine, see chapter 11. However, variance reduction techniques are not without risk. Unfortunately, whether a particular type of variance reduction can be applied safely, depends on the problem under study as well as on the Monte Carlo dose engine used. Therefore the only way to find out is to compare dose calculations with and without the use of a particular variance reduction technique. It is therefore desirable that a MCTP system enables the user to switch off variance reduction techniques and approximations.

### 16.6 Literature data on MCTP verification

Benchmarking of MCTP dose engines is as important as for conventional dose calculation algorithms in radiotherapy, as systematic errors in the code and problems with the beam model, CT conversion and the use of variance reduction techniques

and denoising methods may occur. Two possible ways of commissioning a Monte Carlo dose engine exist: comparison with in-phantom measurements and comparison with an independent accurate MC dose engine (such as e.g. BEAM).

Hartmann Siantar et al (2001) have commissioned Peregrine for 6 and 18 MV Photon beams of a Varian linear accelerator. Measurements and BEAM calculations were performed to serve as a reference for the Peregrine results for PDDs, lateral profiles and output factors of 2cm x 2cm to 38cm x 38cm fields. Also wedge fields were investigated and accurate MLC commissioning was performed. Maximum discrepancies were less than 2 %.

Heath et al (2004) also benchmarked the Peregrine code for 6MV photon beams with measurements and EGSnrc calculations. Tests were performed for homogeneous and heterogeneous phantoms (lung and bone equivalent slabs) for 1cm x 1cm, 3cm x 3cm and 10cm x 10cm fields. For the 1cm x 1cm field a deviation of 5 % was obtained that was attributed to the large voxels used in Peregrine, although this assumption was not verified. An MLC experiment was performed as well, which provided results within 2 %. Afterwards Peregrine was used for actual treatment planning for IMRT of head and neck patients.

Reynaert et al (2005) compared the Peregrine system with an accurate dose engine (MCDE) based on BEAMnrc/DOSXYZnrc and measurements for small beam segments in a homogeneous water phantom, illustrating a systematic error in the leaf projection of the Elekta MLC in Peregrine. This led to systematic deviations (up to 10 %) in integral dose in the optical chiasm of IMRT head and neck patients. This example illustrates the importance of commissioning of commercial MCTP dose engines.

Fippel (1999) evaluated the accuracy of XVMC (X-ray Voxel Monte Carlo) by a comparison with DOSXYZnrc in homogeneous and heterogeneous phantoms (bone and lung slabs). For the lung phantom small deviations were obtained (see figure 16.1).

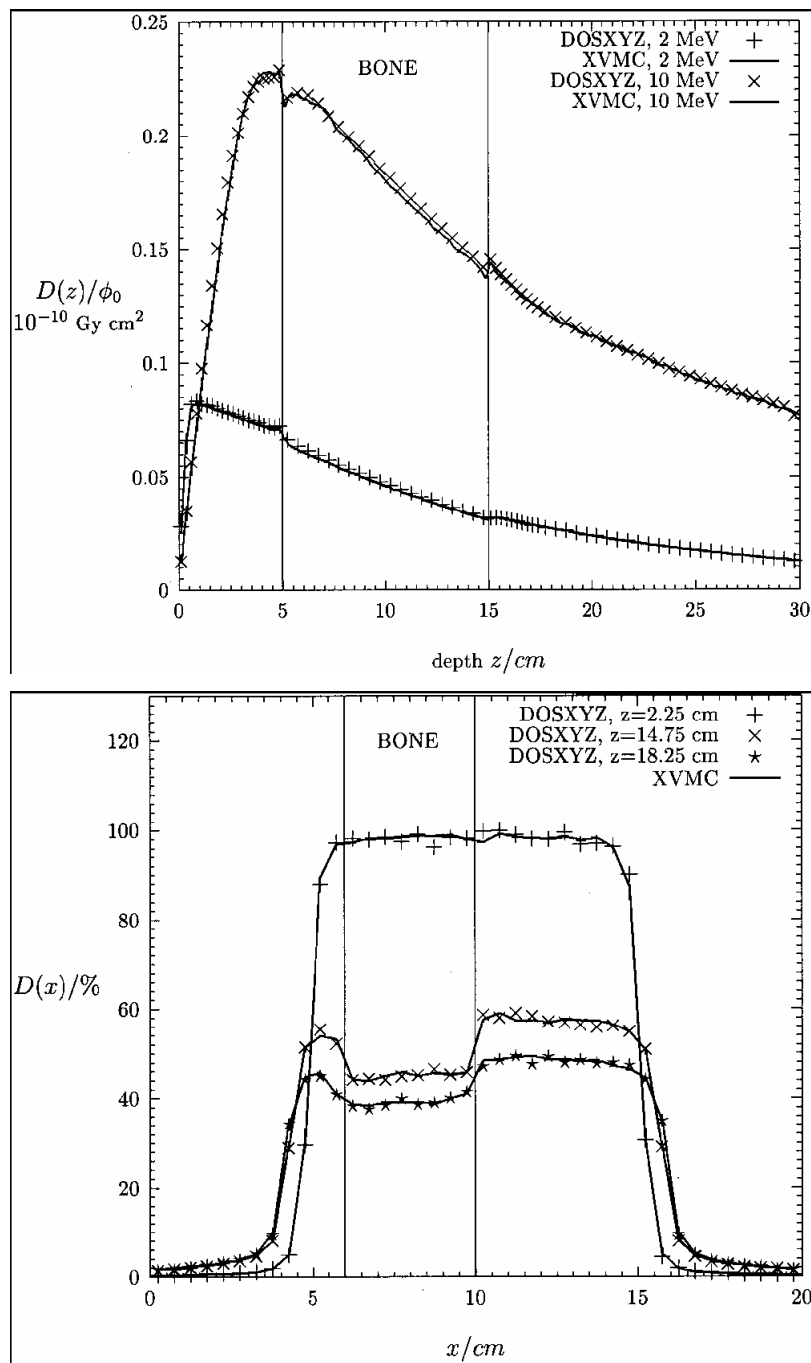


Figure 16.1: Benchmark of XVMC for a phantom containing a bone inhomogeneity (reproduced with kind permission of AAPM from Fippel et al (1999)).

Cygler et al (2004) commissioned the electron beam Monte Carlo treatment planning system of Nucletron. Electron beams in the range of 6 to 20 MeV from a Siemens linear accelerator were investigated. Homogeneous and inhomogeneous phantoms (aluminum slab, hard bone ribs, air cylinder, hard bone cylinder, trachea

and spine) were studied. Monitor unit calculations were compared in homogenous phantoms with independent hand-calculated values. For all cases agreement within 5 % was obtained. Effect of the voxel size in the MC dose engine was illustrated (see figure 16.2).

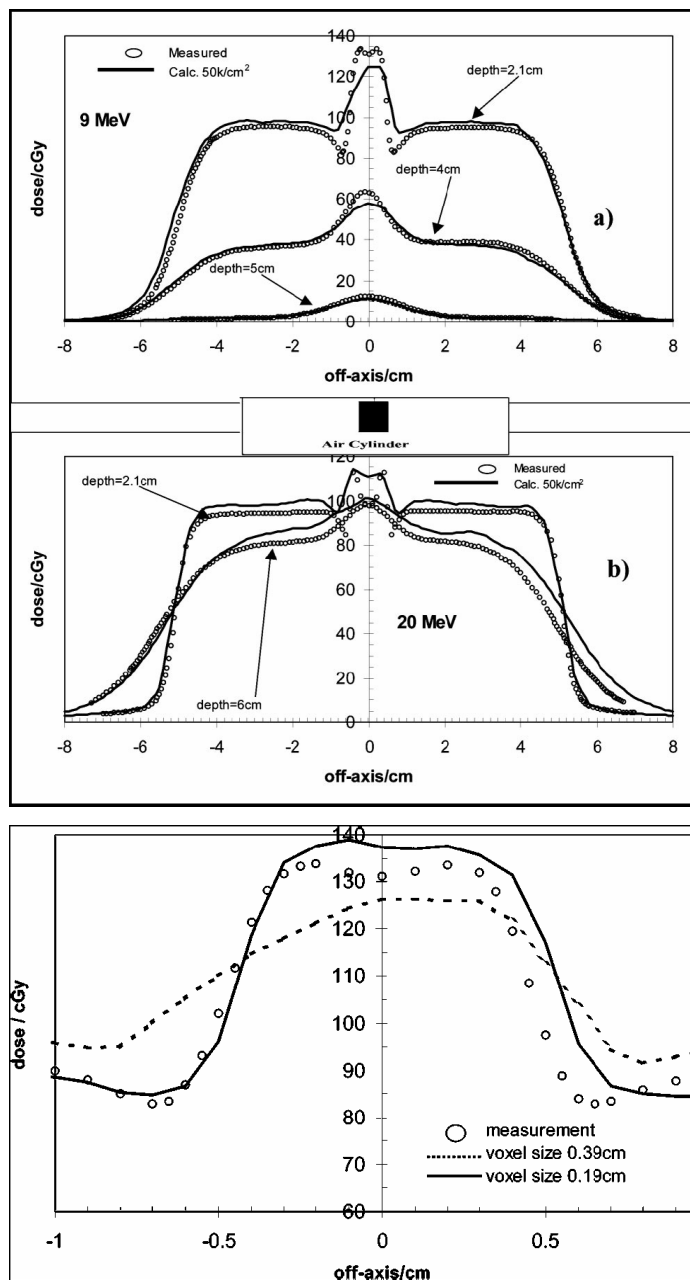


Figure 16.2: Voxel size dependence in the commercial electron MCTP system of Nucletron (reproduced with kind permission of AAPM from Cygler et al (2004)). The figure below is an enlargement of the central part of the figure above.

The voxel size is automatically selected by the system and depends on the field of view. Therefore Cygler et al recommend the vendor to let the user select the voxel dimensions. In the mean time, this system has been used in clinical practice, which has increased the confidence into the results obtained and even had an impact on clinical decisions for certain patients (Cygler et al 2005).

Li et al (2000) commissioned the MCDOSE dose engine with BEAM/DOSXYZ for electron and photon beams in homogeneous and heterogeneous phantoms (lung and bone slabs). Agreement within 1 % was obtained for all cases studied (see figure 16.3).

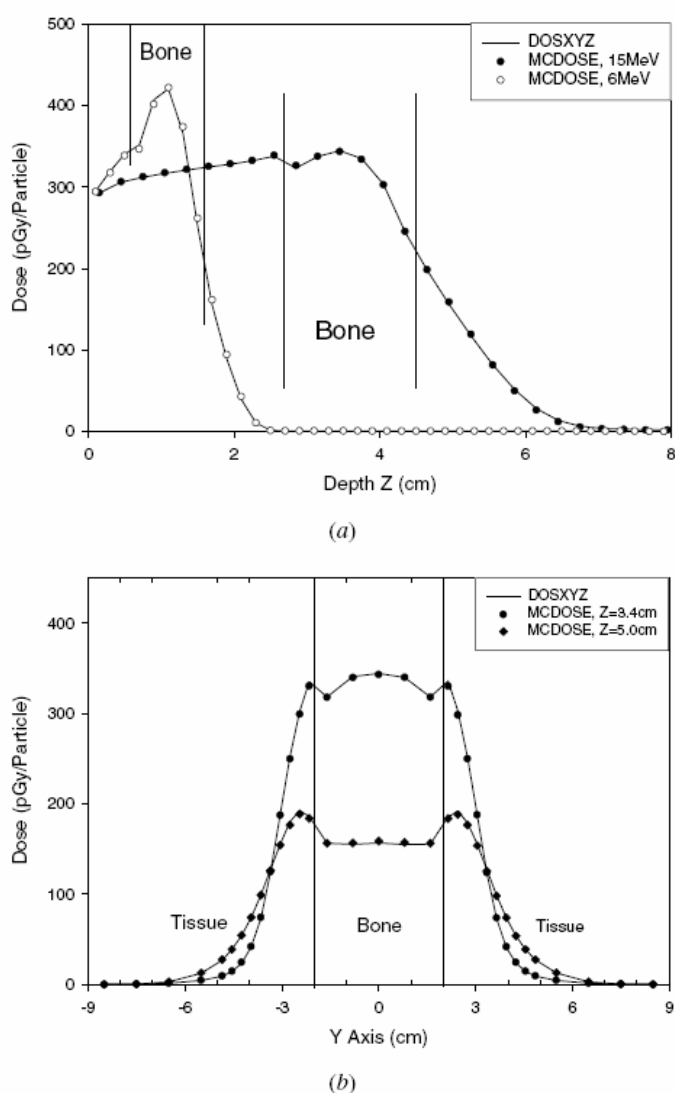


Figure 16.3: Benchmark of MCDOSE against BEAM/DOSXYZ calculations for heterogeneous phantom (reproduced with kind permission from Li et al (2000)).

## *16.7 Conclusion*

Commissioning of Monte Carlo treatment planning systems is, for the larger part, similar to that of conventional treatment planning systems. Some additional tests may be needed and some tests have to be altered. A careful and complete commissioning will, in return, give a good knowledge of the quality of the dose engine itself and of its integration in the planning system. It also provides the physicist with data that can be used to evaluate the quality of Monte Carlo dose calculation engines against conventional dose calculation algorithms.

## 17 Recommendations

The aim of this report is to provide a literature overview on MCTP. In addition, an introduction to Monte Carlo techniques in dosimetry is provided in part 1 to allow the non-initiated reader to understand parts 2 and 3 of the report. The report is not based on practical work conducted by the current NCS sub-group. Therefore it is rather difficult to provide strict guidelines or recommendations, as has been the case in previous NCS reports. For some topics discussions are still evolving and the final conclusion is not known yet.

### *17.1 Comparison of different dose engines*

Further studies comparing the superposition/convolution algorithms with Monte Carlo dose engines are required to determine the clinical relevance of introducing Monte Carlo into the clinic. A few recommendations for such studies are given below:

1. It is necessary to demonstrate that the MC and superposition/convolution programs give good results (compared to measurements) in homogeneous phantoms for single beam irradiations. It is equally important to tune the beam input of a superposition/convolution system as for a Monte Carlo dose engine. The importance of accurate beam modelling is illustrated by Chetty et al (2005) and Reynaert et al (2005). Only for systems that pass this test, a clinical comparison is meaningful.
2. Important parameters in a comparison are the following:
  - technically: integral dose to a structure, differential surface of two DVHs
  - clinical relevance: all quantities that are used for planning and evaluation, e.g.  $D_{\text{mean}}$ ,  $D_{90}$ ,  $D_{\text{iso}}$  for the PTV and  $D_{\text{max}}$ ,  $D_{\text{mean}}$ , integral dose for the critical organs, equivalent uniform dose (EUD), TCP and NTCP and evaluation of clinical outcome post-treatment.
  - It is less relevant to compare volume fractions receiving a certain dose. Especially for DVHs with a large slope (as in the PTV) a small dose error can give rise to large volume errors, which are not really relevant when

evaluating the influence of dose errors. To give an example: if according to dose engine A, 40 % of the volume receives a dose of 50 Gy while in system B, only 20 % receives this dose, but the 20 % difference volume receives a dose of 49.5 Gy instead, then these two DVHs are clinically equivalent. It is also preferable to focus on dose (and not on NTCP or TCP). NTCP differences are always much larger than dose differences and can thus be misleading.

- When a group of patients is investigated, not only the mean values for all patients should be given but also the worst individual cases. From the moment that a clinical important parameter ( $D_{\text{mean}}$  e.g.) differs significantly (say 5 %) in one structure of 1 patient, then the added value of MCTP over superposition/convolution is illustrated for the studied cases (if recommendation 1 is taken into account).

## 17.2 Commissioning

Most commercial MCTP vendors will develop a source model for the customers based on a set of measurements provided by the customer. As for every TP system, careful commissioning of this model is required. This should be performed for an extensive set of measurements that are appropriate for the treatments for which the dose engine will be used. For IMRT e.g. it is important to test small offset fields (regular, but also irregular to test the MLC modelling). If the model does not provide the required accuracy, it should be re-tuned by the vendor.

In addition, it is important to test the algorithm in heterogeneous phantoms in situations where measurements can be performed adequately. Especially in situations of electronic equilibrium the code must be tested. Additionally, benchmarking a treatment plan in a patient-alike phantom is necessary as well. Measurement uncertainties should be taken into account though.



### *17.3 CT conversion*

Taking into account the effects resulting from the conversion from dose to medium to dose to water (see section 10.4) it is important to define a sufficiently large number of material subsets with different chemical compositions (especially for skeletal tissues) and to use a stoichiometric calibration method such as the one described by Schneider *et al* (1996, 2000). Each scanner should be calibrated individually in terms of mass density or electron density. This calibration curve can be used continuously or in discrete subdivisions of certain materials (lung tissue). A Monte Carlo treatment planning system should allow the user to enter his own conversion results.

### *17.4 Conversion of dose to medium to dose to water*

At present the authors do not wish to take a stand on whether dose to water or dose to medium should be used. We do recommend, however, that Monte Carlo treatment planning system developers enable both possibilities so that users can make their own choice. TCP/NTCP based planning systems should preferably convert to dose-to-water. On the other hand the question can be raised if it would be possible to convert dose to water to dose to medium in the TCP/NTCP – dose relations. Conversion is necessary for comparison of Monte Carlo results with conventional dose calculations. Of course, for this purpose the dose obtained by conventional systems can also be converted to dose to medium. Converting dose to medium to dose to water will certainly increase the uncertainty in the final dose distribution.

### *17.5 Variance reduction techniques and approximations*

In theory, variance reduction techniques do not introduce bias in the results as long as care has been taken concerning under-sampling. In the literature some approximations wrongly are considered to be variance reduction techniques. So the reader should always bare this in mind. The effect of the approximations applied in

some fast Monte Carlo dose calculation engines is not clear at the moment. Using ray-tracing through the beam modifiers or using a virtual source model might seem unacceptable, but nobody has demonstrated that these techniques lead to clinically relevant deviations. Future studies should provide more insight. MCTP systems should provide the user the possibility to switch of/on these approximations and variance reduction techniques, to study the corresponding effects.

### *17.6 Denoising*

All methods described above have potential to increase the Monte Carlo calculation speed with factors ranging from 2 to 20. No method is perfect and any applied method should always be validated. Interesting guidance is provided by the acceptance criteria formulated by Kawrakow (Kawrakow, 2002). It seems preferable not to use smoothing, but the simulation of a large number of histories takes a very long time. In inverse planning an interesting compromise is the usage of smoothing in the first steps of an optimisation loop. Once the optimisation is finished a final Monte Carlo calculation without smoothing (but with a sufficiently large number of histories) can be performed (Fippel and Nüsslin, 2003 and Kawrakow, 2002 ). A Monte Carlo treatment planning system should enable the user to switch off the de-noising for evaluation purposes.

## 18 Conclusion

The Monte Carlo technique has the ability to decrease uncertainty in dose calculations for radiotherapy treatment planning. Especially cases of small and highly irregular fields depositing dose in tissue containing significant inhomogeneities are expected to benefit from MCTP. Currently, several Monte Carlo dose calculation engines are being built into commercial treatment planning systems, while others are already available (e.g. Peregrine).

Care should be taken that the approximations and variance reduction techniques applied in current dose engines do not introduce deviations from the result obtained with a Monte Carlo code without significant approximations. Therefore it is important that current fast Monte Carlo dose calculation engines are benchmarked by measurements and/or by Monte Carlo systems that place the emphasis on accuracy. Preferentially MCTP systems should allow the user to switch on/off approximations and variance reduction techniques, so that evaluation of obtained results is possible.

It should be noted that even in a Monte Carlo dose engine without any approximations or variance reduction methods, several sources of uncertainty remain: further work seems necessary on the derivation of material properties obtained from CT data, where discretisation effects can lead to the use of erroneous cross sections. This uncertainty is increased even further when dose to medium is converted to dose to water, a topic which is still under discussion. In addition it is important that the output of the linear accelerator is modelled correctly. This can be done by full Monte Carlo modelling of the linac head or by a virtual source model. The effects of using fluence maps to model the transport through the beam modifiers should be benchmarked thoroughly.

The Monte Carlo technique is able to perform 4D treatment planning calculations in approximately the same calculation time as a 3D calculation. This is for example useful in the case of dynamic MLC movement, but also for respiratory organ movement. In these situations the Monte Carlo technique is able to provide the 4D dose information faster than some conventional systems. Further developments may be expected in this field.

Also in the area of inverse Monte Carlo treatment planning, interesting research is being performed, but much additional work remains to be done.

The Monte Carlo method may eventually become the standard in treatment planning as computer technology and simulation algorithms evolve further. Developments in parallel computing (clusters, grid computing) as well as Moore's law (the empirical observation that the number of transistors on integrated circuits doubles every 18 months) may significantly reduce the remaining problem of calculation time.

## References

AAPM TG-23 1995 Radiation Treatment Planning Dosimetry verification AAPM Report 55

Agostinelli S, Allison J, Amako K, et al. 2003 GEANT4 – a Simulation Toolkit *Nucl Instr Meth Phys Res A* **506** 250-303

Ahnesjö A 1987 Invariance of convolution kernels applied to dose calculations for photon beams *Int. conf. on the Use of Computers in Radiation Therapy IX ICCR (Scheveningen, The Netherlands)* ed I A D Bruinvis, PH van der Giessen, H J van Kleffens and F w Wittkämper (Amsterdam: Elsevier) pp 99-102

Ahnesjö A 1989 Collapsed cone convolution of radiant energy for photon dose calculations in heterogeneous media *Med. Phys.* **16** 577-592

Ahnesjö A and Aspradakis M M 1999 Topical Review: Dose calculations for external photon beams in radiotherapy *Phys. Med. Biol.* **44** R99-R155

Andreo P 1991 Review: Monte Carlo techniques in medical radiation physics *Phys. Med. Biol.* **36** 861-920

Antolak J A, Bieda M R and Hogstrom K R 2002 Using Monte Carlo methods to commission electron beams: a feasibility study *Med Phys* **29** 771-786

Archambault L, Beaulieu L, Carrier J F, Castrovillari F, Chauvie S, Foppiano F, Ghiso G, Guatelli S, Incerti S, Lamanna E, Larsson S, Lopes M C, Peralta L, Pia M G, Rodrigues P, Tremblay V H, and Trindade A 2004 Overview of Geant4 applications in medical physics 2003 *IEEE Nuclear Science-Symposium Conference Record* **3** 1743-1745

Arnfield M R, Siantar C H, Siebers J V, Garmon P, Cox L and Mohan R 2000 The impact of electron transport on the accuracy of computed dose *Med. Phys.* **27** 1266-1274

Attix F H 1986 Introduction to Radiological Physics and Radiation Dosimetry (New York: John Wiley & Sons)

Barca G, Castrovillari F, Chauvie S, Cuce D, Foppiano F, Ghiso G, Guatelli S, Lamanna E, Lopes M C, Peralta L, Pia M G, Rodrigues P, Trindade A and Veltri M A 2003 Powerful simulation tool for medical physics applications: GEANT4 *Nucl Phys B (Proc Suppl)* **125** 80–84

Berger M J 1963 Monte Carlo Calculations of the Penetration and Diffusion of Fast Charged Particles (eds), *Methods in Computational Physics* vol 1 ed B Alder, S Fernbach and M Rotenberg (New York: Academic) pp 135-215

Berger M J and Hubbell J H 1987 *Photon Cross Sections on a Personal Computer* Report NBSIR 87-3597 (Gaithersburg MD: National Institute of Standards and Technology)

Berger M J 1988 Electron stopping powers for transport calculations, in: Jenkins T M, Nelson W R and Rindi A (eds) *Monte Carlo Transport of Electrons and Photons* (New York: Plenum Press) pp 57

Berger M J and Wang R 1988 Multiple-Scattering Angular Deflections and Energy-Loss Straggling, *Monte Carlo Transport of Electrons and Photons* ed T M Jenkins, W R Nelson and A Rindi (New York: Plenum) pp 21-56

Berger M J, Hubbell J H, Seltzer S M, Coursey J S and Zucker D S 1999 *XCOM: Photon Cross Section Database (version 1.2)* Available online: <http://physics.nist.gov/xcom> (Gaithersburg MD: National Institute of Standards and Technology)

Bielajew A and Rogers D W O 1987 PRESTA: The parameter reduced electron-step transport algorithm for electron Monte Carlo transport *Nucl Instrum Methods B* **18** 165-181

Bielajew A and Kawrakow I 1997, High accuracy Monte Carlo calculations, World Congress on Medical Physics and Biomedical Engineering, Nice, September 14-19, abstr. pl096

Biggs F and Lighthill R 1988 *Analytical Approximations for X-Ray Cross Sections III* Report SAND-870070 (Albuquerque NM: Sandia National Laboratories)

Björk P, Knöös T and Nilsson P 2002 Influence of initial electron beam characteristics on Monte Carlo calculated absorbed dose distributions for linear accelerator electron beams *Phys Med Biol* **47** 4019–4041

Bogner L, Scherer J and Herbst M 1999 An inverse Monte Carlo optimisation algorithm for conformal radiotherapy, *Phys. Med.* **15**, 111-119

Boudreau C, Heath E, Seuntjens J, Ballivy O and Parker W 2005 IMRT head and neck treatment planning with a commercially available Monte Carlo based planning system *Phys. Med. Biol.* **50** 879-890

Boyer A L and Mok E C 1984 in Proceedings of the Eight international Conference in Radiation Therapy, Toronto, edited by J.R. Cunningham, D. Ragan and J. Van Dyk (IEEE Computer Society, Toronto, 1984), pp 14

Boyer A L and Li S 1997 Geometric analysis of light-field position of a multileaf collimator with curved ends *Med Phys* **24** 757-762

Bratley P, Fox B L and Schrage E L 1983 A Guide to Simulation.

Briesmeister J F 2000 *MCNP<sup>TM</sup> - A General Monte Carlo N-Particle Transport Code, Version 4C* Technical Report No LA-13709-M Los Alamos National Laboratory

Brooks R A, Mitchell L G, O'Conner C M and Di Chiro G 1981 On the relation between computed tomography numbers and specific gravity *Phys Med Biol* **26** 141-147

Brown F B 2003 MCNP - A General Monte Carlo N-Particle Transport Code, Version 5, Vol. I: Overview and Theory Report LA-UR-03-1987; Vol. II: User's Guide Report LA-CP-03-0245; Vol. III: Developer's guide Report LA-CP-03-0284 Los Alamos National Laboratory

Buffa F M and Nahum A E 2000 Monte Carlo dose calculations and radiobiological modelling: analysis of the effect of the statistical noise of the dose distribution on the probability of tumour control, *Phys. Med. Biol.* **45**, 3009-3023

Carrier J-F, Archambault L and Beaulieu L 2004 Validation of GEANT4, an object-oriented Monte Carlo toolkit for simulations in medical physics, *Med. Phys.* **31** 484-492

Chen Y, Boyer A L and Ma C M 2000 Calculation of x-ray transmission through a multileaf collimator, *Med. Phys.* **27** 1717-1726

Chetty I J, Rosu M, McShan D L, Fraass B A, Ten Haken R K 2005 The influence of beam model differences in the comparison of dose calculation algorithms for lung cancer treatment planning *Phys. Med. Biol.* **50** 802-815

Chibani O and Ma C M 2003, Photonuclear dose calculations for high-energy photon beams from Siemens and Varian Linacs *Med Phys* **30** 1990-2000



Chui C-S 1985 A method for three-dimensional gamma-ray dose calculations in heterogeneous media and its applications in radiation therapy *PhD thesis University of Columbia*

Compte de Buffon G 1777 Essai d'arithmetique morale. Supplement a la Naturelle, Vol. 4

Constantinou C and Harrington J C 1992 An electron density calibration phantom for CT-based treatment planning computers, *Med. Phys.* **19** 325-327

Cooper, N.G. (Editor) 1989 From cardinals to chaos - Reflections on the life and legacy of Stanislaw Ulam (Cambridge University Press, New York, NY, USA)

Crammer-Sargison G, Beckman W A and Popescu J 2004 Modelling an extreme water-lung interface using a single pencil beam algorithm and the Monte Carlo method *Phys. Med. Biol.* **49** 1557-1567

Cullen D E, Chen M H, Hubbell J H, Perkins S T, Plechaty E F, Rathkopf J A and Scofield J H 1989 Tables and Graphs of Photon-Interaction Cross Sections from 10 eV to 100 GeV Derived from the LLNL Evaluated Photon Data Library (EPDL), Part A: Z=1 to 50, Part B: Z=51 to 100 Report UCRL-50400 Vol 6 Rev 4 (Livermore CA: Lawrence Livermore National Laboratory)

Cullen D E, Hubbell J H, Kissel L 1997 *EPDL97: the Evaluated Photon Data Library, '97 Version* Report UCRL-50400 Vol 6 Rev 5 (Livermore CA: Lawrence Livermore National Laboratory)

Cullen D E 2002 *Program EPICSHOW: A Computer Code to Allow Interactive viewing of the EPIC Data Libraries (Version 2002-1)* Report UCRL-ID-126455 Rev 4 Part 5 (Livermore CA: Lawrence Livermore National Laboratory)

Cygler J E, Daskalov G M, Chan G H and Ding G X 2004 Evaluation of the first commercial Monte Carlo dose calculation engine for electron beam treatment planning *Med Phys* **31** 142-153

Cygler J E, Lochrin C, Daskalov G M, Howard M, Zohr R, Esche B, Eapen L, Grimard L and Caudrelier J M 2005 Clinical use of a commercial Monte Carlo treatment planning system for electron beams *Phys. Med. Biol.* **50** 1029-1034

De Kock E A and Schreuder A N 1996 Letter to the Editor: The calibration of CT Hounsfield units for radiotherapy treatment planning *Phys. Med. Biol.* **41** 1524-1527

De Marco J J, Solberg T D, and Smathers J B 1998 A CT-based Monte Carlo simulation tool for dosimetry planning and analysis, *Med. Phys.* **25**, 1-11

De Smedt B, Reynaert N, De Neve W and Thierens H 2004 DOSSCORE: an accelerated DOSXYZnrc code with an efficient stepping algorithm and scoring grid, *Phys. Med. Biol.* **49**, 4623-4635

De Smedt B, Vanderstraeten B, Reynaert N, Thierens H., De Neve W 2005 The influence of geometrical and scoring resolution in MCTP, *Phys. Med. Biol.* **50** 4005-4019

Deasy J O 2000 Denoising of electron beam Monte Carlo dose distributions using digital filtering techniques, *Phys. Med. Biol.* **45**, 1765-1779

Deasy J O, Wickerhauser V M and Picard M 2002 Accelerating Monte Carlo simulations of radiation therapy dose distributions using wavelet threshold de-noising, *Med. Phys.* **29** 2366-2373

De Jaeger K, Hoogeman M S, Engelsman M, Seppenwoolde Y, Damen E M F, Mijnheer B J, Boerma L J, and Lebesque J V 2003 Incorporating an improved dose-

calculation algorithm in conformal radiotherapy of lung cancer: re-evaluation of dose in normal lung tissue, *Radiother. Oncol.* **69** 1-10

DeMarco J J, Solberg T D and Smathers J B 1998 A CT-based Monte Carlo simulation tool for dosimetry planning and analysis, *Med. Phys.* **25** 1-11

Demarco J J, Wallace R E and Boedeker K 2002 An analysis of MCNP cross-section and tally methods for low-energy photon emitters *Phys Med Biol* **47** 1321-1332

Deng J, Jiang S B, Kapur A, Li J, Pawlicki T and Ma C-M 2000 Photon beam characterization and modelling for Monte Carlo treatment planning *Phys. Med. Biol.* **45** 411-427

Deng J, Pawlicki T, Chen Y, Li J, Jiang S B and Ma C M 2001 The MLC tongue-and-groove effect on IMRT dose distributions *Phys Med Biol* **46** 1039-1060

Ding M, Li J, Deng J, Fourkai E and Ma C-M 2003 Dose correlation for thoracic motion in radiation therapy of breast cancer, *Med. Phys.* **30**, 2520-2529

Du Plessis F C P, Willemse C A and Lötter M G 1998 The indirect use of CT numbers to establish material properties needed for Monte Carlo calculations of dose distributions in patients *Med Phys* **25** 1195-1201

Dubi A 1986 Monte Carlo Calculations for Nuclear Reactors, in Y. Ronen (Ed.), "CRC Handbook of Nuclear Reactor Calculations", CRC Press, Florida

Ebert M A and Hoban P W 1995 A model for electron-beam applicator scatter *Med Phys* **22** 1419-1429

El Naqa I, Deasy J and Vicic M 2003 Locally adaptive denoising of MC dose distributions via hybrid median filtering *Proc. IEEE Medical Imaging Conf.* (19-25 October, Portland, OR)

El Naqa I, Kawrakow I, Fippel M, Siebers J V, Lindsay P E, Wickerhauser M V Vicić M, Zakarian K, Kauffmann N and Deasy J O 2005 A comparison of Monte Carlo dose calculation denoising techniques *Phys. Med. Biol.* **50** 909-922

ESTRO, 2004, Quality Assurance of Treatment Planning Systems – Practical examples for Non-IMRT Photon Beams, ESTRO booklet 7, ESTRO, Brussels, Belgium

Feller W 1968 An introduction to probability theory and its applications, Volume I, third edition, John, Wiley & sons, New York, NY, USA

Fippel M 1999 Fast Monte Carlo dose calculations for photon beams based on the VMC electron algorithm *Med Phys* **26** 1466-1475

Fippel M and Nüsslin F 2000 Comments on 'Converting absorbed dose to medium to absorbed dose to water for Monte Carlo based photon beam dose calculation' *Phys Med Biol* **45** L17-L18

Fippel M and Nüsslin F 2003 Smoothing Monte Carlo calculated dose distributions by iterative reduction of noise, *Phys. Med. Biol.* **48**, 1289-1304

Fippel M, Haryanto F, Dohm O, Nüsslin F and Kriesen S 2003 A virtual photon energy fluence model for Monte Carlo dose calculation *Med Phys* **30**, 301-311

Fippel M 2004 Efficient particle transport simulation through beam modulating devices for Monte Carlo treatment planning, *Med. Phys.* **31**, 1235-1241

Fix M K, Stampanoni M, Manser P, Born E J, Mini R and Rügsegger P 2001 A multiple source model for 6 MV photon beam dose calculations using Monte Carlo *Phys. Med. Biol.* **46** 1407-1427

Fix M K, Keall P J, Dawson K and Siebers J V 2004 Monte Carlo source model for photon beam radiotherapy: photon source characteristics *Med. Phys.* **31** 3106-3121

Fraass B, Doppke K, Hunt M, McCullough E, Nüsslin F, Rawlinson A, Svensson G and Svensson H. 1998 American Association of Physicists in Medicine Radiation Therapy Committee Task Group 53: Quality assurance for clinical radiotherapy treatment planning *Med Phys* **25** 1773-1836

Fraass B A, Smathers J and Deye J 2003 Summary and recommendations of a National Cancer Institute workshop on issues limiting the clinical use of Monte Carlo calculation algorithms for megavoltage external beam radiation therapy *Med. Phys.* **30** 3206-3216

Francescon P, Cavedon C, Reccanello S and Cora S 2000 Photon dose calculation of a three-dimensional treatment planning system compared to the Monte Carlo code BEAM *Med. Phys.* **27**, 1579-1587

Francescon P, Cavedon C, Fix M K, Keall P J, Dawson K and Siebers J V 2004 Monte Carlo source model for photon beam radiotherapy: photon source characteristics *Med. Phys.* **31** 3106-3121

Garrett D, Hornstein S M, House R K, Moses E I, Patterson R W, Rathkopf J A and Schach von Wiitenau A 1997 Lawrence Livermore National Laboratory's PEREGRINE project UCRL-JC 126732

GEANT4 2003 <http://geant4.web.cern.ch/geant4/>

Goudsmit S A and Saunderson J L 1940 Multiple scattering of electrons *Phys. Rev.* **57** 24-29

Halbleib J A 1988 Structure and operation of the ITS code system, *Monte Carlo Transport of Electrons and Photons* ed T M Jenkins, W R Nelson and A Rindi (New York: Plenum) 249-262

Hartman Siantar C L, Walling R S, Daly T P, Faddegon B, Albright N, Bergstrom P, Bielajew A F, Chuang C, Garrett D, House R K, Knapp D, Wieczorek D J and Verhey L J 2001 Description and dosimetric verification of the PEREGRINE Monte Carlo dose calculation system for photon beams on a water phantom *Med Phys* **28** 1322–1337

He T T 2003 Implementation of a Monte Carlo based inverse planning model for clinical IMRT with MCNP code, Ph.D. Thesis (Univ. Michigan, USA), *abstract in Med. Phys.* **30**, 482

Heath E, Seuntjens J and Sheikh-Bagheri D 2004 Dosimetric evaluation of the clinical implementation of the first commercial IMRT Monte Carlo treatment planning system at 6MV *Med. Phys.* **31** 2771-2779

Heath E and Seuntjens J 2005 4D Monte Carlo dose calculations in deforming anatomy using direct voxel tracking 8th Biennial ESTRO Meeting on Physics for Clinical Radiotherapy, Lisbon, Portugal, 26-29 September 2005

Henson P W and Fox R A 1984 The electron density of bone for inhomogeneity correction in radiotherapy planning using CT numbers *Phys Med Biol* **29** 351-359

Hubbell J H 1969 Photon Cross Sections, Attenuation Coefficients and Energy Absorption Coefficients from 10 keV to 100 GeV Report NSRDS-NBS 29 (Gaithersburg MD: National Bureau of Standards)

Hubbell J H 1982 Photon Mass Attenuation and Energy-Absorption Coefficients from 1 keV to 20 MeV *Int J Appl Radiat Isotopes* **33** 1269-1290

Hubbell J H and Seltzer S M 1995 Tables of X-Ray Mass Attenuation and Mass Energy-Absorption Coefficients 1 keV to 20 MeV for Elements  $Z = 1$  to 92 and 48 Additional Substances of Dosimetric Interest Report NISTIR 5632 (Gaithersburg MD: National Institute of Standards and Technology)

Hubbel J H 1999 Review of photon interaction cross section data in the medical and biological context *Phys Med Biol* **44** R1-R22

ICRU: Report No. 24 1976 Determination of Absorbed Dose in a patient Irradiated by beams of X or Gamma Rays in Radiotherapy Procedures, Washington D.C., International Commission on Radiation Units and Measurements

International Commission on Radiation Units and Measurements (ICRU) 1984 *Stopping Powers for Electrons and Positrons* ICRU Report 37 (Bethesda: International Commission on Radiation Units and Measurements)

International Commission on Radiation Units and Measurements (ICRU) 2001 ICRU Report 64 Dosimetry of High-Energy Photon Beams based on Standards of Absorbed Dose to Water *Journal of the ICRU* **1(1)** (Kent: Nuclear Technology Publishing)

Issy-les-Moulineaux, France, 7-10 July 2003 (Paris: OECD Publications)

James F 1980 Monte Carlo Theory and Practice, *Rep. Prog. Phys.* **43** 1145-1189

James F 1990, A review of pseudo random number generators, *Comp. Phys. Com.* **60** 329-344

Jan S, Santin G, Strul D 2004 GATE: a Simulation Toolkit for PET and SPECT *Phys Med Biol* **49** 4543-4561

Jeraj R and Keall P 1999 Monte Carlo-based inverse treatment planning, *Phys. Med. Biol.* **44**, 1885-1896

Jeraj R, Keall P J, Ostwald P M 1999 Comparisons between MCNP, EGS4 and experiment for clinical electron beams *Phys Med Biol* **44** 705-717

Jeraj R, Keall P 2000 The effect of statistical uncertainty on inverse treatment planning based on Monte Carlo dose calculation *Phys. Med. Biol.* **45** 3601-3613

Jeraj R, Keall P J and Siebers J V 2002 The effect of dose calculation accuracy on inverse treatment planning *Phys. Med. Biol.* **47** 391-407

Jiang S B, Pawlicki T and Ma C-M 2000 Removing the effect of statistical uncertainty on dose-volume histograms from Monte Carlo dose calculations, *Phys. Med. Biol.* **45**, 2151-2161

Johns H E and Cunningham J R 1983 *The Physics of Radiology* 4th edn (Springfield IL: Charles C Thomas Pub Ltd)

Kawrakow I, Fippel M and Friedrich K 1996 3D electron dose calculations using a Voxel based Monte Carlo algorithm (VMC), *Med. Phys.* **23** 445-457

Kawrakow I 2000a, Accurate condensed history Monte Carlo simulation of electron transport I. Egsnrc, the new EGS4 version *Med Phys* **27** 485-498

Kawrakow I 2000b Accurate condensed history Monte Carlo simulation of electron transport II. Application to ion chamber response simulations, *Med. Phys.* **27(3)**, 499-513

Kawrakow I 2000c VMC++, Electron and photon Monte Carlo calculations optimied for Radiation Treatment Planning in "Advanced Monte Carlo for Radiation Physics, particle transport simulation and applications", Proceedings of the Monte Carlo 2000 conferece, Lisbon, 23-26 October 2000, p229-236



Kawrakow I and Fippel M 2000 Investigation of variance reduction techniques for Monte Carlo photon dose calculations using XVMC *Phys Med Biol* **45** 2163-2183

Kawrakow I and Rogers D W O 2000 The EGSnrc code system: Monte Carlo simulation of electron and photon transport *NRCC Report PIRS-701*, National Research Council of Canada, Ottawa

Kawrakow I 2002 On the de-noising of Monte Carlo calculated dose distributions, *Phys. Med. Biol.* **47**, 3087-3103

Kawrakow I and Rogers D W O 2003 The EGSnrc code system: Monte Carlo simulation of electron and photon transport *NRCC Report PIRS-701*, National Research Council of Canada, Ottawa

Kawrakow I 2004 The effect of Monte Carlo statistical uncertainties on the evaluation of dose distributions in radiation treatment planning *Phys. Med. Biol.* **49** 1549-1556

Kawrakow I, Rogers D W O and Walter B R B 2004 Large efficiency improvements in BEAMnrc using directional bremsstrahlung splitting *Med. Phys.* **31** 2883-2898

Keall P and Hoban P 1995 Accounting for primary electron scatter in x-ray beam convolution calculations *Med. Phys.* **22** 1413-1418

Keall P and Hoban P 1996 Superposition dose calculations incorporating Monte Carlo generated electron track kernels *Med. Phys.* **23** 479-485

Keall P J, Siebers J V and Mohan R 2000 The impact of Monte Carlo dose calculations on treatment outcomes in *The use of computers in radiotherapy*, T. Bortfeld and W. Schlegel eds., Springer Verlag, Heidelberg

Keall P J, Siebers J V, Arnfield M, Kim J O and Mohan R 2001 Monte Carlo dose calculations for dynamic IMRT treatments *Phys Med Biol* **46** 929-941

Keall P J, Siebers J V, Joshi S and Mohan R 2004 Monte Carlo as a four-dimensional radiotherapy treatment-planning tool to account for respiratory motion, *Phys. Med. Biol.* **49**, 3639-3648

Kiiewski P K and Bjarngard B E 1978 The use of computed tomography data for radiotherapy dose calculations *Int J Radiat Oncol Biol Phys* **4** 429-435

Kim J O, Siebers J V, Keall P J, Arnfield M R, and Mohan R 2001 A Monte Carlo study of radiation transport through multileaf collimators *Med. Phys.* **28**, 2497-2506

Knuth D E 1981 The art of computer programming – Volume 2

Krieger T and Sauer O A 2005 Monte Carlo- versus pencil-beam-/collapsed-cone-dose calculation in a heterogeneous multi-layer phantom *Phys. Med. Biol.* **50** 859-868

Landau L 1944 On the Energy Loss of fast Particles by Ionization *J Phys (USSR)* **8** 201

Laub W, Alber M, Birkner M and Nüsslin F 2000 Monte Carlo dose computation for IMRT optimisation, *Phys. Med. Biol.* **45**, 1741-1754

Laub W U, Bakai A and Nüsslin F 2001 Intensity modulated irradiation of a thorax phantom: comparisons between measurements, Monte Carlo calculations and pencil beam calculations *Phys. Med. Biol.* **46** 1695-1706

Leal A, Sanchez-Doblado F, Arrans R, Rosello J, Pavon C E and Lagares J I 2003 Routine IMRT verification by means of an automated Monte Carlo simulation system, *Int J Rad Onc Biol Phys* **56**, 58-68

Li J S, Pawlicki T, Deng J, Jiang S B, Mok E and Ma C-M 2000 Validation of a Monte Carlo dose calculation tool for radiotherapy treatment planning *Phys. Med. Biol.* **45** 2969-2985

Liu H H, Mackie R T, McCullough E C 2000 Modeling photon output caused by backscattered radiation into the monitor chamber from collimator jaws using a Monte Carlo technique *Med. Phys.* **27**, 737-744

Liu H H, Verhaegen F and Dong L 2001 A method of simulating dynamic multileaf collimators using Monte Carlo techniques for intensity-modulated radiation therapy, *Phys. Med. Biol.* **46**, 2283-2289

Liu H H and Keall P 2002  $D_m$  rather than  $D_w$  should be used in Monte Carlo treatment planning, *Med. Phys.* **29**, 922-924

Ma C-M and Nahum A E 1993 Calculation of absorbed dose ratios using correlated Monte Carlo sampling *Med Phys* **20** 1189-1199

Ma C-M, Faddegon B A, Rogers D W O and Mackie T R 1997 Accurate characterization of Monte Carlo calculated electron beams in radio-therapy *Med Phys* **24** 401–416

Ma C-M and Jiang S B 1999 Topical Review: Monte Carlo modelling of electron beams from medical accelerators *Phys. Med. Biol.* **44** R157-R189

Ma C-M, Mok E, Kapur A, Pawlicki T, Findley D, Brain S, Forester K and Boyer A L 1999 Clinical implementation of a Monte Carlo treatment planning system, *Med. Phys.* **26** 2133-2143

Ma C-M, Li J S, Pawlicki T, Jiang S B, Deng J, Lee M C, Koumrian T, Luxton M and Brain S 2002 A Monte Carlo dose calculation tool for radiotherapy treatment planning *Phys Med Biol* **47** 1671-1689

Ma C-M, Jiang S B, Pawlicki T, Chen Y, Li J S, Deng J and Boyer A L 2003 A quality assurance phantom for IMRT dose verification, *Phys. Med. Biol.* **48**, 561-572

Ma C-M, Price R A, Li J S, Chen L, Wang L, Fourkai E, Qin L, Yang J 2004 Monitor unit calculation for Monte Carlo treatment planning *Phys. Med. Biol.* **49** 1671-1687

Ma C-M, Li J S, Jiang S B, Pawlicki T, Xiong W, Qin L H and Yang J 2005 Effect of statistical uncertainties on Monte Carlo treatment planning *Phys. Med. Biol.* **50** 891-907

Mackie T R, Scrimger J W and Battista J J 1985 A convolution method of calculating dose for 15-MV x-rays *Med. Phys.* **12** 188-196

Mackie T R 1989 New developments in radiotherapy dose planning *Proc. 17<sup>th</sup> Int. Cong. Radiology, Paris*, p30

Mackie T R 1990 Applications of the Monte Carlo method in radiotherapy *The Dosimetry of ionizing radiation* vol III ed K R Kase, B E Bjarngard and F H Attix (New York: Academic) pp 541-620

Manfredotti C, Nastasi U, Marchisio R, Ongaro C, Gervino G, Ragona R, Anglesio S and Sannazzari G 1990 Monte Carlo simulations of dose distributions in electron beam radiotherapy treatment planning *Nucl. Instr. Methods A* **291** 646-654

Martens C, Reynaert N, De Wagter C, Nilsson P, Coghe M, Palmans H, Thierens H and De Neve W 2002 Underdosage of the upper-airway mucosa for small fields as used in intensity-modulated radiation therapy: A comparison between radiochromic

film measurements, Monte Carlo simulations and collapsed cone convolution calculations *Med Phys.* **29** 1528 – 1535

McCullough E C and Holmes T W 1985 Acceptance testing computerized radiation therapy treatment planning systems: Direct utilization of CT scan data, *Med. Phys.* **12** 237-242

McGrath E J and Irving D C 1975 Techniques for Efficient Monte Carlo simulation Vols I, II, and III. Rep. ORNL-RSIC-38. Radiation Shielding Information Center, Oak Ridge National Laboratories, Oak Ridge, Tennessee

McMaster W H, Del Grande N K, Mallett J H and Hubbell J H 1969 *Compilation of X-Ray Cross Sections* Report UCRL-50174 (Livermore CA: Lawrence Livermore National Laboratory)

Metropolis N 1987 The beginning of the Monte Carlo Method, *Los Alamos Science* **15**, 125-130

Miao B, Jeraj R, Bao S and Mackie T R 2003 Adaptive anisotropic diffusion filtering of Monte Carlo dose distributions, *Phys. Med. Biol.* **48** 2767-2781

Mijnheer B J, Battermann J J and Wambersie A 1987 What degree of accuracy is required and can be achieved in photon and neutron therapy? *Radiother. Oncol.* **8** 237 – 252

Mohan R 1988 Dose calculations for Radiation Treatment Planning in *Monte Carlo Transport of Electrons and Photons*, edited by T. M. Jenkins, W. R. Nelson, A. Rindi,

Mohan R 1997 Why Monte Carlo? Proc. 12<sup>th</sup> Int. conf. on the Use of Computers in Radiation Therapy (Salt Lake City, UT) pp 16-18

Mohan R, Antolak J, Hendee W R 2001 Monte Carlo techniques should replace analytical methods for estimating dose distributions in radiotherapy treatment planning *Med. Phys.* **28** 123-126

Molière G 1948 Theorie der Streuung schneller geladener Teilchen II Mehrfach- und Vielfachstreuung *Z. Naturf. A* **3** 78-97

Nahum A E 1988 Overview of photon and electron Monte Carlo in *Monte Carlo Transport of Electrons and Photons*, edited by T. M. Jenkins, W. R. Nelson, A. Rindi, A. E. Nahum, and D. W. O. Rogers, Plenum Press, New York, pp 3-20

NCS, 2006a, Quality Assurance in 3D-Treatment Planning Systems, NCS report 15, NCS, Delft, the Netherlands

Nelson W R, Hirayama H and Rogers D W O 1985 The EGS4 code system SLAC report 265, Stanford Linear Accelerator Institute

Neuenschwander H and Born E J 1992 A Macro Monte Carlo code for electron beam dose calculations, *Phys. Med. Biol.* **37**, 107-125

Neuenschwander H, Mackie TR and Reckwerdt PJ. 1995 MMC--a high-performance Monte Carlo code for electron beam treatment planning, *Phys Med Biol.* **40**, 543-74.

Paelinck L, Reynaert N, Thierens H, De Neve W and De Wagter C 2005 Experimental verification of lung dose with radiochromic film: comparison with Monte Carlo simulations and commercially available treatment planning systems *Phys. Med. Biol.* **50** 2055-2069

Paganetti H, Jiang H and Trofimov A 2005 4D Monte Carlo simulation of proton beam scanning: modelling of variations in time and space to study the interplay between scanning pattern and time-dependent patient geometry *Phys. Med. Biol.* **50** 983-990

Papanikolaou N, Battista J, Boyer A, Kappas C, Klein E, Mackie T R, Sharpe M and Van Dyk J 2004 Tissue inhomogeneity corrections for megavoltage photon beams AAPM Report No 85 Task group No 65 of the Radiation Therapy Committee of the American Association of Physicists in Medicine (Madison, WI: Medical Physics Publishing)

Park S K and Miller K W Random 1988 Number Generators: Good ones are hard to find, *Communications of the ACM*, Volume 31, No. 10, pp. 1192-1201

Parker R P, Hobday P A and Cassel K J 1979 The direct use of CT numbers in radiotherapy calculations for inhomogeneous media, *Phys. Med. Biol.* **24**, 802-809

Petti P L, Goodman M S, Gabriel T A and Mohan R 1983a Investigation of buildup dose from electron contamination of clinical photon beams *Med Phys* **10** 18-24

Petti P L, Goodman M S, Sisterson J M, Biggs P J, Gabriel T A and Mohan, R 1983b Sources of electron contamination for the CLinac35 25MV photon beam *Med Phys* **10** 369-373

Poon E and Verhaegen F 2005 Accuracy of the photon and electron physics in GEANT4 for radiotherapy applications *Med. Phys.* **32** 1696-1711

Poon E, Verhaegen F and Seuntjens J 2005 Consistency test of the electron transport algorithm in the GEANT4 Monte Carlo code. *Phys. Med. Biol.* **50** 681-694

Press W H, Teukolsky S A, Vetterling W T and Flannery B P 1988 Numerical Recipes

Raeside D E 1976 Monte Carlo principles and applications *Phys. Med. Biol.* **21** 181-197

Reichl LE, 1980, A modern course in statistical physics, University of Texas Press, Austin, TX, USA

Reynaert N, Palmans H, Thierens H, and Jeraj R 2002 Parameter dependence of the MCNP electron transport in determining dose distributions *Med Phys* **29** 2446-2454

Reynaert N, De Smedt B, Coghe M, Paelinck L, Van Duyse B, De Gersem W, De Wagter C, De Neve W and Thierens H 2004 MCDE: a new Monte Carlo dose engine for IMRT, *Phys. Med. Biol.* **49**, N235-N241

Reynaert N, Coghe M, De Smedt B, Paelinck L, Vanderstraeten B, De Gersem W, Van Duyse B, De Wagter C, De Neve W and Thierens H 2005 The importance of accurate linear accelerator head modelling for IMRT Monte Carlo calculations, *Phys. Med. Biol.* **50**, 831-846

Rodrigues P, Trindade A, Peralta L, Alves C, Chaves A, Lopes M C 2004 Application of GEANT4 radiation transport toolkit to calculations in anthropomorphic phantoms *Applied Radiation and Isotopes* **61** 1451–1461

Rogers D W O and Bielajew A F 1988 A Comparison of EGS and ETRAN Monte Carlo Transport of Electrons and Photons ed T M Jenkins, W R Nelson and A Rindi (New York: Plenum) pp 323-344

Rogers D W O and Bielajew A F 1990 Monte Carlo techniques of electron and photon transport in radiation dosimetry *The Dosimetry of ionizing radiation* vol III ed K R Kase, B E Bjärngård and F H Attix (New York: Academic) pp 427-539

Rogers D W O 1993 How accurately can EGS4/PRESTA calculate ion-chamber response?, *Med Phys* **20** 319-323

Rogers D W O, Faddegon B A, Ding G X, Ma C-M, We J and Mackie T R 1995 BEAM: a Monte Carlo code to simulate radiotherapy treatment units *Med. Phys.* **22** 503-524



Rogers D W O, Ma C-M, Walters B, Ding G X, Sheikh-Bagheri D and Zang G 2002 Beamnrc user manual, National Research Council of Canada

Salvat F, Fernández-Varea J M, and Sempau J 2003 Penelope - A code system for Monte Carlo simulation of electron and photon transport, Workshop Proceedings, Issy-les-Moulineaux, France, 7-10 July 2003

Schaart D R, Jansen J Th M, Zoetelief J and de Leege P F A 2002 A comparison of MCNP4C electron transport with ITS 3.0 and experiment at incident energies between 100 keV and 20 MeV: influence of voxel size, substeps and energy indexing algorithm *Phys Med Biol* **47** 1459-1484

Schach von Wittenau A E, Cox L J, Bergstrom P M Jr, Chandler W P and Hartmann Siantar C L 1999 Correlated histogram representation of Monte Carlo derived medical accelerator photon-output phase space *Med Phys* **26** 1196–1211

Schneider U, Pedroni E and Lomax A 1996 The calibration of CT Hounsfield units for radiotherapy treatment planning *Phys Med Biol* **41** 111-124

Schneider W, Bortfeld T and Schlegel W 2000 Correlation between CT numbers and tissue parameters needed for Monte Carlo simulations of clinical dose distributions *Phys Med Biol* **45** 459-478

Seco J, Adams E, Bidmead M, Partridge M and Verhaegen F 2005 IMRT treatments assessed with a Monte Carlo dose calculation engine, *Phys. Med. Biol.* **50**, 817-830

Seltzer S M 1988 An Overview of ETRAN Monte Carlo Methods *Monte Carlo Transport of Electrons and Photons* ed T M Jenkins, W R Nelson and A Rindi (New York: Plenum) 153-182

Sempau J, Acosta E, Baro J, Fernandez-Varea J M and Salvat F 1997 An algorithm for Monte Carlo simulation of coupled electron-photon transport, *Nucl. Instrum. Methods B* **132** 377-390

Sempau J and Bielajew A F 2000 Towards the elimination of Monte Carlo statistical fluctuation from dose volume histograms for radiotherapy treatment planning *Phys. Med. Biol.* **45** 131-157

Sempau J, Wilderman S J and Alex F Bielajew 2000 DPM, a fast, accurate Monte Carlo code optimized for photon and electron radiotherapy treatment planning dose calculations, *Phys. Med. Biol.* **45** 2263-2291

Sempau J, Sánchez-Reyes A, Salvat F, Oulad ben Tahar H, Jiang S B and Fernández-Varea J M 2001 Monte Carlo simulation of electron beams from an accelerator head using PENELOPE *Phys Med Biol* **46** 1163-1186

Sempau J, Fernández-Varea J M, Acosta E, Salvat F 2003 Experimental benchmarks of the Monte Carlo code PENELOPE *Nucl Instr Methods Phys Res B* **207** 107-123

Seuntjens J, Dai J, Heath E, Al-Yahya K and Parker W 2004 Retrospective Monte Carlo study of conformal lung cancer treatment plans, Advanced workshop on current topics in Monte Carlo Treatment planning, May 3-5, Montreal, Canada, p32

Sheikh-Bagheri D and Rogers D W O 2002 Sensitivity of megavoltage photon beam Monte Carlo simulations to electron beam and other parameters *Med Phys* **29** 379-390

Siebers J V, Keall P J and Mohan R 2000a Performance benchmarks of the MCV Monte Carlo system, XIII Int Conf on the use of computers in radiation therapy (Heidelberg, Germany), 129-131

Siebers J V, Keall P J, Nahum A E and Mohan R 2000b Converting absorbed dose to medium to absorbed dose to water for Monte Carlo based beam dose calculations *Phys Med Biol* **45** 983-995

Siebers J V, Keall P J, Nahum A E and Mohan R 2000c Reply to 'Converting absorbed dose to medium to absorbed dose to water for Monte Carlo based beam dose calculations' *Phys Med Biol* **45** L18-L19

Siebers J V, Keall P J, Kim J O and Mohan R 2002 A method for photon beam Monte Carlo multileaf collimator particle transport *Phys Med Biol* **47** 322-532

Solberg T D, DeMarco J J, Holly F E, Smathers J B and DeSalles A A F, 1998, Monte Carlo treatment planning for stereotactic radiotherapy, *Radioth. Oncol.* **49** 73 - 84

Spezi E, Lewis D G and Smith C W 2002 A DICOM-RT-based toolbox for the evaluation and verification of radiotherapy plans., *Phys Med Biol.* **47** 4223-4232

Sternheimer R M, Seltzer S M and Berger M J 1982 Density effect for the ionization loss of charged particles in various substances *Phys Rev B* **26** 6067

Storm E and Israel H I 1970 Photon Cross Sections from 1 keV to 100 MeV for Elements Z=1 to Z=100 *Nucl Data Tables* **A7** 565–681

Torres J, Buades M J, Almansa J F, Guerrero R, and Lallena A M 2004 Dosimetry characterization of  $^{32}\text{P}$  intravascular brachytherapy source wires using Monte Carlo codes PENELOPE and GEANT4 *Med Phys* **31** 296–304

Tzedakis A, Damilakis J E, Mazonakis M, Stratakis J, Varveris H and Gourtsoyioannis N 2004 Influence of initial electron beam parameters on Monte Carlo calculated absorbed dose distributions for radiotherapy photon beams *Med Phys* **31** 907–913

Udale-Smith M 1992 Monte Carlo calculations of electron beam parameters for three Philips linear accelerators *Phys Med Biol* **37** 85–106

Van Battum L J, van der Zee W and Huizenga H 2003 Scattered radiation from applicators in electron beams *Phys Med Biol* **48** 2493–2507

Van der Marck S C and Hogenbirk A 2004 *ORANGE: a new, fast dose engine for radiotherapy*, Proc. ICRS-10.RPS-2004, Madeira)

Van der Zee W and Welleweerd J 1999 Calculating photon beam characteristics with Monte Carlo techniques *Med Phys* **26** 1883–1892

Van der Zee W, Van der Marck S C and Hogenbirk A 2005 ORANGE: a Monte Carlo dose engine for radiotherapy, *Phys. Med. Biol.* **50**, 625-641

Van de Walle J, Martens C, Reynaert N, Palmans H, Coghe M, De Neve W, De Wagter C, Thierens H 2003 Monte Carlo model of the Elekta SLiplus accelerator: validation of a new MLC component module in BEAM for a 6 MV beam, *Phys. Med. Biol.* **48**, 371-385

Van Dyke J, Barnett R, Cygler J and Schragge P 1993 Commissioning and quality assurance of treatment planning computers, *Int. J. Radiat. Oncol. Biol. Phys.* **26**, 261-273

Verhaegen F 2002 Evaluation of the EGSnrc Monte Carlo code for interface dosimetry near high-Z media exposed to kilovolt and  $^{60}\text{Co}$  photons, *Phys. Med. Biol.* **47** 1691-1705

Verhaegen F and Das I J 1999 Monte Carlo modeling of a virtual wedge *Phys Med Biol* **44** N251–N259

Verhaegen F, Symonds-Tayler R, Liu H H and Nahum A E 2000 Backscatter towards the monitor ion chamber in high-energy photon and electron beams: charge integration versus Monte Carlo simulation *Phys. Med. Biol.* **45** 3159-3170

Verhaegen F and Liu H H 2001 Incorporating dynamic collimator motion in Monte Carlo simulations: an application in modelling a dynamic wedge, *Phys. Med. Biol.* **46**, 287-296

Verhaegen F and Seuntjens J 2003 Monte Carlo modelling of external radiotherapy photon beams *Phys. Med. Biol.* **48** R107-R164

Verhaegen J and Devic S, 2004, Sensitivity study for CT image use in Monte Carlo Treatment Planning, Advanced Workshop on Current Topics in MCTP, May 3-5 2004, Montreal, p52

Verhaegen J and Devic S, 2005, Sensitivity study for CT image use in Monte Carlo treatment planning, *Phys. Med. Biol.* **50** 937-946

VISeD 2004, <http://www.mcnpvised.com/>

Wang L, Chui C-S and Lovelock M 1998 A patient-specific Monte Carlo dose-calculation method for photon beams *Med Phys* **25** 867-878

Wang L, Yorke E, Chui C-S 2002 Monte Carlo evaluation of 6 MV intensity modulated radiotherapy plans for head and neck and lung treatments *Med. Phys.* **29** 2705-2717

Waters L S 2002 *MCNPX - User's Manual Version 2.4.0*, Report LA-CP-02-408, Los Alamos National Laboratory.

Webb S 1979 The absorbed dose in the vicinity of an interface between two media irradiated by a  $^{60}\text{Co}$  source *Brit. J. Radiol.* **52** 962-967

Wood W W 1986 Early history of computer simulations in statistical mechanics and molecular dynamics. International school of physics Enrico Fermi, Varenna, Italy, 1985. Molecular-dynamics simulation of statistical mechanical systems, XCVII corso (Soc. Italiana di Fisica, Bologna, Italy)

Yang J, Li J, Chen L, Price R, McNeeley S, Qin L, Wang L, Xiong W and Ma C-M 2005 Dosimetric verification of IMRT treatment planning using Monte Carlo simulations for prostate cancer *Phys. Med. Biol.* **50** 869-878

Ye S-J, Brezovich I A, Pareek P and Naqvi S A 2004 Benchmark of PENELOPE code for low-energy photon transport : dose comparisons with MCNP4 and EGS4, *Phys. Med. Biol.* 49, 387-397

Yeo IJ, Beiki-Ardakani A, Cho Y, Heydarian M, Zhang T, Islam M 2004 EDR2 film dosimetry for IMRT verification using low-energy photon filters *Med Phys* **31** 1960-1963

Yu C X, Mackie T R and Wong J W 1995 Photon dose calculation incorporating explicit electron transport *Med. Phys.* **22** 1157-1165

## ***Appendices***

## Appendix A. An example to illustrate differences between the Monte Carlo technique and analytical and numerical approaches.

To illustrate the differences, the problem of calculating the area of a circle with a radius  $R=1$  is used.

### A.1 Analytical Technique

When the circle centre is positioned at the origin of a Cartesian coordinate system with axes  $x$  and  $y$ , the circle is defined by:

$$\sqrt{x^2 + y^2} = R \quad (\text{A.1})$$

with  $R=1$ .

To solve the problem analytically, one can express the  $y$ -values of both halves of the circle in terms of  $x$ . Integrating over all contributing values of  $x$  results in:

$$A = \int_{-1}^1 2\sqrt{1-x^2} dx \quad (\text{A.2})$$

This integral can be solved by substituting  $\sin(t)$  for  $x$  and applying goniometric relations, yielding:

$$A = \pi \quad (\text{A.3})$$

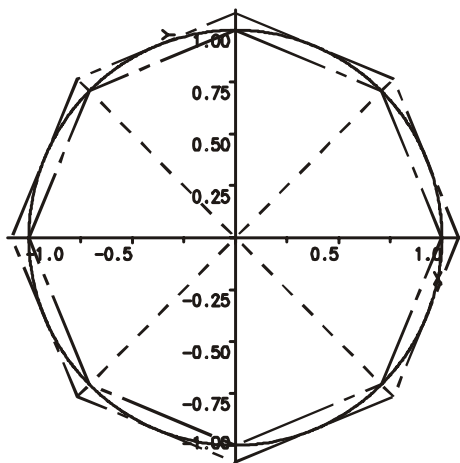


Figure A.1: Numerical solution to the calculation of the area of a circle (solid line) with radius 1. The area of the regular octagon enclosing the circle represents an overestimation of this area. The regular octagon enclosed by the circle provides an underestimation of the area of the circle. In this figure  $n=8$  (see text).



## A.2 Numerical Technique

The problem can also be dealt with by applying a numerical integration technique to solve Equation (A.2). However, for illustration purposes an alternative approach was chosen: The circle can be divided into  $n$  equal sectors (dashed lines in figure A.1). The area of each sector can be approximated by the area of the triangle constructed from the corner points of the sector. This will provide an underestimate of the area of the sector. For an arbitrary integer  $n$  greater than or equal to 4, the area of this triangle is  $\sin(2\pi/n)/2$ . Multiplying this area by  $n$  gives an underestimate of the area of the circle. An overestimation may be derived from the triangles for which the third side is a tangent of the circle, perpendicular to the bisector of the top angle (figure A.1). For an arbitrary integer  $n$  greater than or equal to 4, the area of this triangle is  $\tan(\pi/n)$ . The area of the circle does now obey:

$$\frac{n \sin(\frac{2\pi}{n})}{2} \leq A \leq n \tan(\frac{\pi}{n}) \quad \text{for } n \geq 4 \quad \textbf{(A.4)}$$

Table A.1 shows the over- and underestimates for various integer values  $n$ . As expected, for increasing  $n$ , the difference between the two estimates decreases, becoming less than 0.1% for  $n \approx 100$ .

Table A.1: Calculation of the area of a circle with unit radius, applying a numerical method. The under- and overestimates of the area (equation 6.4) are shown for various values of n.

Integer n	underestimate (n sin(2π/n))/2	overestimate n tan(π/n)
4	2	4
8	2.828427	3.313708
16	3.061467	3.182598
32	3.121445	3.151725
64	3.136548	3.144118
128	3.140331	3.142224
256	3.141277	3.141750
512	3.141514	3.141632
1024	3.141573	3.141603
2048	3.141588	3.141595
4096	3.141591	3.141593
8192	3.141592	3.141593
16384	3.141593	3.141593

### A.3 Monte Carlo Technique

$$Area = 4 \frac{\sum_{i=1}^N f(x_i, y_i)}{N} = 4 \overline{f(x_i, y_i)} \quad (\text{A.6})$$

$$f(x_i, y_i) = \begin{cases} 1 & \text{for } x_i^2 + y_i^2 < 1 \\ 0 & \text{for } x_i^2 + y_i^2 \geq 1 \end{cases} \quad (\text{A.5})$$

To calculate the area of the circle with a Monte Carlo approach, the following considerations are made. By random selection of values for x and y between -1 and 1 the area of the square that encompasses the circle is sampled uniformly. The area of this square equals 4. For a randomly selected point (x<sub>i</sub>, y<sub>i</sub>), the function f(x, y) as defined by equation A.5 may be used to score whether or not the point is within the circle. By counting the total number of selections i (N), and the number of histories yielding a point within the circle (i.e. f(x<sub>i</sub>, y<sub>i</sub>)=1), the area of the circle can be estimated using equation A.6.

According to the central limit theorem, the standard deviation expressing the uncertainty in the Area,  $S_{Area}$ , may be estimated using the equations A.7 and A.8.

$$S_{Area} = \frac{4 S}{\sqrt{N}} \tag{A.7}$$

$$S = \sqrt{\frac{\sum_{i=1}^N f^2(x_i, y_i) - \frac{\{\sum_{j=1}^N f(x_j, y_j)\}^2}{N}}{N - 1}} \tag{A.8}$$

Table A.2 shows some results for the Monte Carlo simulations. To gain a factor

---

Table A.2: Example of the calculation of the area of a circle with unit radius, applying a Monte Carlo method. For various sample sizes (number of histories) the area and the standard deviation are shown.

Sample size	Area	Standard deviation
10	3.2000	0.5060
100	3.1200	0.1657
1000	3.0880	0.0531
10000	3.1420	0.0164
100000	3.1506	0.0052
1000000	3.1423	0.0016
10000000	3.1417	0.0005

---

of 10 in precision the number of histories (sample size) has to be increased by a factor of 100. For a relative standard deviation of 0.1% about 410000 histories have to be included in the calculations. For large sample sizes computer processor time becomes a factor of importance, as it is (nearly) proportional to the sample size. This is in contrast to the numerical method where the increase in n did not result in a significant increase in computer time. An advantage of the Monte Carlo method is the flexibility. To calculate the area of another object, only the test whether a point (x,y) is inside or outside the object and the borders from which the x and y co-ordinates are sampled have to be modified.

#### *A.4 Summary*

Comparing the results for this example, it is concluded that the analytical approach yields an exact solution. The numerical method yields an approximation and, when applied in a more sophisticated way, it may yield an under- and overestimation. The Monte Carlo technique results in an answer with a standard deviation expressing the uncertainty. For the numerical approach the under- and overestimation are absolute (apart from truncation errors). For the Monte Carlo method the results have to be interpreted statistically. It is expected that for every 1 out of 3 calculations the difference between the true value and the calculated value is more than 1 standard deviation. For 1 out of 20 calculations, the difference is more than 2 standard deviations. In Table A.2, 2 out of 7 results were not within 1 standard deviation, but all 7 solutions were well within 2 standard deviations.

## Appendix B: Random numbers in Monte Carlo

### *B.1 Random numbers in computers*

Monte Carlo theory approaches the result by repeatedly calculating a scoring function for randomly varying input variables. It is for these randomly varying input variables that random numbers and random number generators are considered here.

A computer is a deterministic device, and hence incapable of producing truly random numbers. However, a series of pseudo-random numbers can be used to control the calculations. The next number is calculated via a pre-defined relationship, the congruence, from the previous number(s).

An advantage of this method is that it allows for an exact reproduction of the random number sequence, which is valuable for debugging software. However, pseudo-random number sequences have to be used with care. The numbers are never truly random, and it depends on the application whether they are 'random enough'. Problems that may arise include:

The sequence length. Many generators produce random sequences of limited length, and hence may be used only for a limited number of random numbers.

The randomness of specific digits. Generator implementations often generate the higher-order bits more random than the lower-order bits.

The correlation between k-dimensional pairs. It can be shown that for some generators, successive pairs  $(l_1, l_2, \dots, l_k)$  will not fill up the complete k-dimensional space, but will lie on up to  $(k-1)$  'planes'. Dedicated quasi-random number generators may solve this. These generators actually produce no random numbers at all, but the numbers do cover the k-dimensional space very well.

Bad implementations. Many examples are known of good random number algorithms that were implemented badly.

Good references to tests for random number sequences are Knuth (1981) and Bratley et al (1983).

## B.2 Random number generators

The most common way to generate random numbers is by using a linear congruence. The sequence of integers  $I_j, I_{j+1}, I_{j+2}, \dots$  is then defined by

$$I_{j+1} = (a I_j + c) \text{ modulo } m \quad (\text{B.1})$$

Lehmer proposed this relation in 1948. A particular sequence is defined by  $m, a, c$  and  $I_0$ . All are positive integers, and they are referred to as the modulus, multiplier, increment and seed, respectively. The choice of  $m, a$  and  $c$  are very important, and make the distinction between an effective and a useless random number generator.

The sequence has an outcome between 0 and  $m-1$ . Hence, the result should be divided by  $m-1$  to obtain a result between  $[0,1]$ . The formulation in (B.1) and the integer representation facilitates a quick implementation without truncation errors. Obviously, the sequence length can not be greater than  $m$ . As a rule of thumb, the sequence can be used to select up to  $m/1000$  random numbers. Using it for longer sequences introduces unwanted correlations. The future is more and more looking like the past.

A particularly good implementation is the 'Minimal Standard' implementation, proposed by Park and Miller (1988), which uses  $a=16807 (=7^5)$ ,  $c=0$  and  $m=2147483647 (=2^{31}-1)$ . Note that for this 32-bit implementation up to 2 million numbers may be generated before we need to switch to another generator. The equivalent 16-bit implementation may be used for only up to 64 random numbers!

Very useful references to these and other random number generators are Press et al (1988) and James (1990).